FLUID-STRUCTURE INTERACTION WITH APPLICATION TO STRUCTURAL VIBRATION AND BLOOD FLOW IN ARTERIES

A Dissertation

by

HELNAZ SOLTANI

Submitted to the Office of Graduate and Professional Studies of
Texas A&M University
in partial fulfillment of the requirements for the degree of

DOCTOR OF PHILOSOPHY

Chair of Committee,	J.N. Reddy
Committee Members,	Arun R. Srinivasa
	Harry A. Hogan
	Hamn-Ching Chen
Head of Department,	Andreas Polycarpou

May 2016

Major Subject: Mechanical Engineering

ABSTRACT

The problem of interaction between fluids and structures is of practical significance in many fields of engineering. This interaction has to be taken into account in analyzing floating objects, ship sloshing, fluid containers subject to earthquake, flutter of airplane wings, suspended bridge subject to wind, submerged structures such as submarines, dam-reservoir systems, and blood flow through arteries. Such problems are known as the fluid-structure interaction (FSI) problems, where a structural domain interacts with an internal or surrounding fluid. A comprehensive study of these problems still remains a challenging task because of the coupling between the two domains and the existence of strong nonlinearity. For most FSI problems, constructing a complete mathematical model is the most difficult part because of different descriptions of motions used for fluids and solids. Most studies involving FSI embrace many simplifying assumptions to make the problem tractable.

In this dissertation, finite element formulations are presented to study two types of representative FSI problems. First, we investigate the effect of the fluid region on the free vibration of beam and plate structures; in particular, natural frequencies and mode shapes of the beams and plates when they are surrounded by a fluid medium are determined. In these problems, we assume that the strains and rotations are considered to be infinitesimally small. Finite element models are constructed for both structural and fluid domains. To connect these two regions, the solid-fluid interface conditions, using the concept of an added mass, are used to construct a coupled finite element model of the problems. Then, we focus on the transient response of plates in the presence of a fluid medium, wherein we consider the geometric nonlinearity with small strains and moderate rotations.

Second, we study the effect of arterial walls on the blood flow through large arteries. Although we make several assumptions to simplify the development and formulate the finite element model, we obtain a reasonable amount of useful knowledge from this exercise. The problem is nonlinear due to the Navier-Stokes equations governing the fluid domain, even without considering the geometric nonlinearity of the arterial wall. The existence of first derivatives of primary variables, such as volume flow rate, cross-sectional area and pressure, in the obtained system of differential equations allows us to take the advantage of least-squares formulation to construct a corresponding finite element model.

DEDICATION

To my beloved parents and sister,

who offered me unconditional love and encouragement

throughout the course of this study.

ACKNOWLEDGEMENTS

First and foremost, I would like to sincerely thank my academic advisor, Professor J.N. Reddy, for his teaching, advising, and unconditional encouragement and support. He was more than generous with his expertise and precious time. It was definitely an honor for me to work under his supervision.

I am also grateful to Dr. Arun Srinivasa for his time and brilliant comments throughout this study. I also thank my committee members, Dr. Harry A. Hogan and Dr. Hamn-Ching Chen, for their constructive comments and good-natured support.

I have a special feeling of gratitude to my beloved parents for inspiring me, their sacrifice and tolerating my absence. Their words of encouragement and push for tenacity ring in my ears. My sister, Hoonaz, has never left my side and has always given me confidence to achieve my dreams. All of my success and achievements are undoubtedly because of their endless support.

Special thanks goes to my best friend, Navid, for being there throughout the entire period of my doctoral studies. He has been my best cheerleader.

It is my pleasure to appreciate my family and friends who made this dissertation a beginning of my professional journey.

TABLE OF CONTENTS

LIST OF FIGURES

FIGURE Page

LIST OF TABLES

TABLE Page

1. INTRODUCTION

The dynamic analysis of structures, characterized by natural frequencies, mode shapes, and transient response, is of considerable importance in design. In engineering problems in which a structure is in contact with a fluid medium, one needs to deal with a fluid-structure interaction (FSI). The FSI problems include flutter of aerodynamic structures, structural deformation due to explosions, vortex induced vibrations of sub-sea pipelines and risers, inflatable dams, parachute dynamics, blood flow through arteries, to name a few. In these problems it is important, from both theoretical and practical viewpoints, to develop a methodology for studying their dynamic response. For instance, the dynamic response of beams and plates surrounded by a fluid domain and the effect of internal flow on the arterial walls need to be effectively addressed. Generally, finding analytical solutions to FSI problems is made difficult by geometric complexity, nonlinearities, and coupled phenomena. Therefore, researchers have resorted to experimental or numerical simulations.

1.1 Background of the Study

FSI problems are often categorized into loosely-coupled (stagger) and strongly-coupled (in terms of the equations governing the structure and the fluid). In the loosely-coupled FSI problems, typically the interaction of fluid on structure is taken through the forces exerted by the fluid, while in the strongly-coupled ones, the effect of the fluid on the structure and the deformation of the structure on the fluid flow are considered. Thus, the loosely-coupled FSI approach is suitable for cases wherein the structure undergoes infinitesimal deformations (e.g., ship dynamics). On the other hand, a strongly-coupled problem requires the solution of the complete equations of fluid flow and the structure that is in contact (i.e., solve the Navier–Stokes equations

and the equations governing the structure simultaneously).

A significant body of research has been dedicated to loosely-coupled FSI problems, including beams and plates. Shabani *et al.* [1] studied the free vibration of a cantilever micro-beam in contact with bounded incompressible fluid using Fourier-Bessel series formulations. They provided a natural frequency comparison between wet and dry conditions. Jones [2] suggested a damping model in order to approximate the dynamic behavior of a beam surrounded by a fluid medium. Aureli and Porfiri [3] pursued the nonlinear vibration of a cantilever beam submerged in viscous fluids. However, their results are limited to low frequency and large amplitude oscillations. The research of Sedlar *et al.* [4] is focused on the experimental modal analysis of cantilever beams in the air as a fluid. A vibrational analysis of FSI Timoshenko beams has been carried out by Lee and Schultz [5]. Lamb [6] investigated the first bending mode shape of a circular plate by calculating the kinetic energy of the fluid using Rayleigh's method. This result is verified experimentally by Powell [7] and [8]. Muthuveerappan *et al.* [9] simulated the dynamic behavior of a submerged cantilever plate using the finite element approach. Lindholm and Chu [10] calculated the first six resonance frequencies of a cantilever plate as functions of plate thickness, width, and immersion depth. Zhou and Cheung [11] considered the vibration of a vertical plate on a rigid wall in contact with water from only one side. Facci and Porfiri [12] studied the flow dynamics induced by the vibration of a submerged cantilever plate. Liew *et al.* [13] obtained the natural frequencies of a simply supported thick rectangular plate using the three-dimensional elasticity equations and the Ritz method. The dynamic behavior of thick rectangular plates were addressed by Ferreira *et al.* [14] using the first-order shear deformation plate theory and a meshless method. Robinson and Palmer [15] performed a modal analysis of a thin flat horizontal plate floating on an incompressible fluid; however, their studies were limited to normal

modes only. Fu and Price [16] discussed dynamic characteristics of vertical and horizontal cantilever plates with a semi-finite fluid medium interaction. Volcy *et al.* [17] conducted an experimental research on the fundamental natural frequencies of plates immersed in a fluid medium. Kerboua *et al.* [18] developed a method to analyze the FSI problem of rectangular plates based on the Sander's shell theory and the Ritz approach. Haddara and Cao [19] derived an approximate expression for dynamic response of a rectangular plate interacting with a fluid medium. Hosseini-Hashemia *et al.* [20] investigated the dynamic analysis of a moderately thick rectangular plate in contact with a fluid medium using the first-order shear deformation (Mindlin) plate theory. Ergin and Ugurlu [21] used ANSYS software to characterize the dynamic behavior of vertical cantilever plates submerged partially in fluid, and they compared the results with the case of vacuo-interaction. Yadykin *et al.* [22] considered a low aspect ratio for cantilever plates oscillating in a stationary fluid using the airfoil theory.

In all of the above studies, it is verified that the presence of fluid medium decreases the natural frequencies of the structure significantly. One of the most common techniques in evaluating the dynamic behavior of an FSI problem is to introduce the concept of "added mass". The term "added mass" is defined as an external force applied to the submerged structure representing the effect of fluid pressure. There are several studies available in the literature using this concept. Liang *et al.* [23] used the empirical added mass formulation along with the Ritz method to study the dynamic behavior of an FSI plate problem. Kwak [24] found a dimensionless added mass for the vibration of rectangular plates interacting with fluid, and proposed a formula approximating the natural frequencies of a wet plate as functions of corresponding natural frequencies for the vacuum case, assuming that the mode shapes for both wet and vacuum cases are almost the same. Brugo and Minak [25] developed an empirical

method by considering the added mass in order to analyze the relationship between the resonance frequencies and the plate width and immersion depth, for a vertical cantilever plate which is partially or completely immersed in water. Muthuveerappan *et al.* [26] also analyzed the dynamic behavior of a submerged cantilever plate using the concept of added mass.

The transient analysis of FSI problems is also carried out in the literature. Qiu [27] analyzed the transient behavior of a flexible beam floating in an unboundad water domain. Qiu and Liu [28] adopted a finite element procedure to study the hydroelastic transient response of floating plates subjected to dynamic loads. Sturova [29] and [30] considered the unsteady behavior of an elastic beam and a circular elastic plate in shallow water, as well as the case in which an elastic beam is floating on the surface of an infinitely deep fluid. Korobkin [31] solved a two-dimensional unsteady problem of a plate floating on a finite depth water; however, this solution does not include the effect of gravity. Meylan and Sturova [32] determined the time-dependent solution of an elastic plate floating on water surface, but the solution is limited to very large floating structures. Jin and Xing [33] presented the transient dynamic analysis of a beam in contact with water affected by a landing beam.

In studies involving blood flow through arteries, it has been shown that the prediction of blood pressure variations plays an important role in characterizing the dynamic behavior. A large number of methods are proposed to analyze the pressure propagation phenomena in arterial systems. Konig *et al.* [34] analyzed the fluid domain in FSI problems using moving boundaries for different levels of viscosity. Their model was particularly suitable for high viscosity regimes. Stergiopulos *et al.* [35] constructed a computer model for simulating the pressure and flow propagation in the human arterial system. Bathe and Kamm [36] performed an FSI finite element analysis on unsteady blood flows using the ADINA commercial code. Sherwin *et*

al. [37] proposed a finite element method based on the discontinuous Galerkin and Taylor-Galerkin formulations to develop a one-dimensional model for the blood flow in arteries. Wan *et al.* [38] conducted a finite element analysis to solve unsteady blood flows in elastic vessels. Their method is based on the space-time finite element method using the discontinuous Galerkin method. Larrabide *et al.* [39] presented a simulation tool called Hemodynamics Modeling Laboratory (HeMoLab) to model the human cardiovascular system. Porenta *et al.* [40] provided a nonlinear mathematical model for arterial blood flow, taking into account the tapering, branching, and presence of stenosed segments. Gijsen *et al.* [41] presented a three-dimensional finite element simulation for a steady flow to study the influence of non-Newtonian properties of blood on the velocity distribution. Perktold *et al.* [42] compared the Newtonian and non-Newtonian results for pulsatile flows in a three-dimensional human carotid arteries. Perktold *et al.* [43] analyzed the flow and stress patterns in human carotid artery bifurcation models. They approximated the governing Navier–Stokes equations by means of a pressure correction finite element method. Avolio [44] studied the multi-branched model of the human arterial system by dividing the arteries into uniform thin-walled elastic tethered segments with realistic arterial dimensions and wall properties. Holzapfel *et al.* [45] conducted a finite element analysis for structural models considering the viscoelastic behavior of arterial walls.

1.2 Objectives of the Present Study

The methods discussed in the literature concerning the loosely-coupled (staggered) FSI problems are limited to certain structural geometries, such as cantilevered beams and plates. The present study is an attempt to understand the influence of the fluid medium on the dynamic response of beam and plate structures, where the influence of shear deformation is considered through a higher-order theories (e.g.,

the Reddy third-order shear deformation beam and plate theories [46, 47, 48]), and carry out a simple study to determine the response of arteries with internal blood flow. Various finite element models are developed to represent the dynamic response of elastic structures in the presence of an inviscid fluid medium. In addition, a nonlinear finite element formulation is presented to investigate the effect of fluid medium on the transient response of elastic plates. Such formulation is developed based on well-known theories in the literature, enabling the developed methodology to be suitable for all beam and plate problems independent of geometric and material properties and boundary conditions. It is worth mentioning that there exist no studies of the FSI problems using the Reddy third-order shear deformation beam and plate theories.

The approaches used in the literature for the study of blood flow through large arteries are based on several assumptions, which result in simplicity and reduction in the computational cost. However, the behavior of blood flow considering the arterial walls as a rigid structure is substantially different from the case where the blood vessels are assumed to be deformable. This dissertation provides a simple, one-dimensional FSI least-squares-based finite element formulation to predict the pressure variation of the blood flow through the arteries with a low computational cost.

The rest of the dissertation is organized as follows. In Section 2, the effect of the fluid presence on the vibrations of structures, including beams and plates, is investigated. In particular, we study the free vibration of these structures assuming small strains and rotations resulting in the construction of linear finite element models. The proposed method employs the three well-known beam and plate theories [47, 48], and corresponding numerical results are provided for all three theories.

In Section 3, the transient response of plates in contact with a fluid domain is

studied through reformulating the method presented in Section 2 for the nonlinear case. Specifically, we consider small strains and moderate rotations in analyzing the transient response of these FSI problems; the nonlinear forms of the three plate theories discussed in Section 2 are utilized. This nonlinear formulation may be used for a broad range of applications.

In Section 4, a finite element formulation is presented to solve the FSI problem of blood flow through large arteries. Since the Navier–Stokes equations involve nonlinear terms, the resulting finite element model includes nonlinear terms as well, even without considering the geometric nonlinearity. The nature of the derived system of partial differential equations suggests the use of a least-squares formulation [49] in our approach.

Finally, some concluding remarks are provided in Section 5.

2. VIBRATION OF ELASTIC STRUCTURES IN THE PRESENCE OF AN INVISCID FLUID MEDUIM*

2.1 Introduction

The main aim of this section is to study the influence of the presence of fluid in contact with a structure on its dynamic response. In general, the fluid pressure affects the structure deflections and correspondingly the structure deflections change the fluid boundary conditions. So we are dealing with a two-way coupling, and this coupling is intensified when high-speed flows and/or geometrically complex structures are involved. In order to examine our method, we make a number of simplifications throughout this section. For instance, we consider the structural deflections to be small, the fluid to be inviscid, the flow to be low velocity and acceleration, and the surrounding temperature of the fluid to be at environment temperature.

A good understanding of the influence of fluid on the structural response is of great importance in many engineering problems. Most structures consist of beams, plates, and shells as structural elements. Therefore, it is of interest to study the effect of fluid on structural response.

Analytical solutions are available only for rigid structures without any interaction. Also several numerical studied have been published in the field of vibrations of structures. So we are looking for a method that can be used in order to make them applicable for FSI problems.

*Part of the data reported in this chapter is reprinted with permission from "Vibration of Elastic Beams in the Presence of an Inviscid Fluid Medium" by H. Soltani, G. S. Payette, and J. N. Reddy, *International Journal of Structural Stability and Dynamics*, Volume 14, Issue 06, 1450022 [29 pages], Copyright @ 2014 World Scientific Publishing Company, and "Free Vibration Analysis of Elastic Plates in Contact with an Inviscid Fluid Medium" by H. Soltani and J. N. Reddy, *International Journal of Applied Mechanics*, Volume 7, Issue 03, 1550041 [20 pages], Copyright @ 2015 Imperial College Press.

In the present section, we evaluate the interaction between an inviscid fluid and a linear elastic structure using the added mass phenomena. The governing equations for the fluid and solid regions are developed using various structural theories including shear deformation beam and plate theories, considering the coupling between these two regimes. The weak-form finite element models of the governing equations in both regions are developed as an eigenvalue problem, and numerical results are presented.

2.2 Theoretical Formulations

In this sub-section, the governing equations of beams and plates in the presence of a fluid medium are presented. Figures 2.1 and 2.2 contain the domain of the FSI problem with the boundary conditions and typical fluid mesh for the beam and plate, respectively. Three different beam theories, namely, the Euler-Bernoulli, Timoshenko and Reddy third-order beam theories are considered in formulating the beam analysis, and for the case of plate analysis, we will study Classical plate theory, first-order, and Reddy third-order shear deformation plate theory (see Reddy [47] and Wang, Lee, and Reddy [46]).

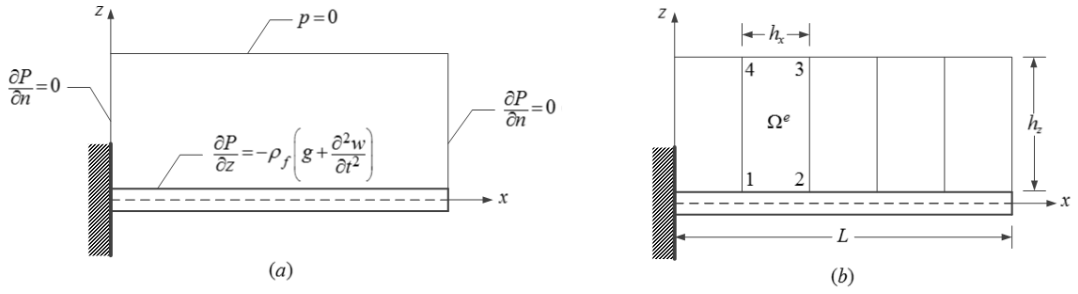

Figure 2.1: Domain of the beam fluid-structure interaction problem with the (a) boundary conditions and (b) typical fluid mesh.

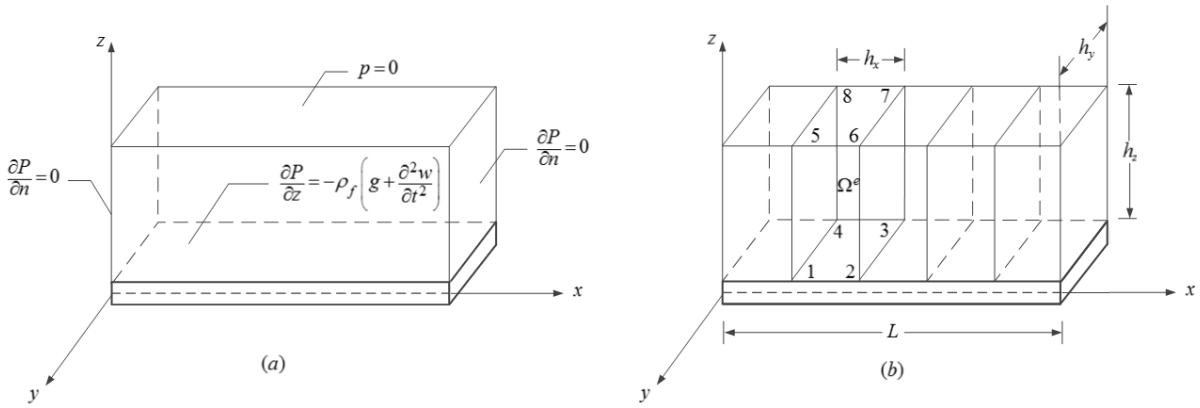

Figure 2.2: Domain of the plate fluid-structure interaction problem with the (a) boundary conditions and (b) typical fluid mesh.

2.2.1 Fluid Mechanics

In the present analysis, we use the continuum hypothesis to formulate an equation governing fluid motion. In general, fluid motion is described by the conservation principles of linear and angular momentum which can be expressed as (see Reddy [50])

$$\nabla \cdot \boldsymbol{\sigma} + \rho_f \mathbf{b} = \rho_f \dot{\mathbf{v}} \tag{2.1}$$

where $\boldsymbol{\sigma}$ is the Cauchy stress tensor, ρ_f is the fluid density, $\mathbf{b}$ is the force vector, which in the present case has only nonzero component due to gravity (per unit mass in the z direction), $\mathbf{v}$ is the velocity vector, and ∇ is the gradient operator with respect to the spatial coordinates $\mathbf{x}$. If we assume the fluid to be inviscid, then the stress tensor can be expressed as

$$\boldsymbol{\sigma} = -p\mathbf{I} \tag{2.2}$$

where $\mathbf{I}$ is the second order identity tensor and p is the pressure. As a result, the momentum equations assume the form

$$-\nabla p + \rho_f \mathbf{b} = \rho_f \dot{\mathbf{v}} \tag{2.3}$$

Taking the divergence of Eq. (2.3) results in the following equation

$$-\nabla^2 p = \rho_f \nabla . \dot{\mathbf{v}} \tag{2.4}$$

where we have used the fact that $\mathbf{b}$ is constant and have also assumed the fluid to be incompressible.

For slowly moving flow, we neglect the right hand side of Eq. (2.4), which results in the following Laplace equation for p

$$-\nabla^2 p = 0 \tag{2.5}$$

For two dimensional flows, Eq. (2.5) can be expressed in the Cartesian coordinate system as

$$-\left(\frac{\partial^2 p}{\partial x^2} + \frac{\partial^2 p}{\partial z^2}\right) = 0 \tag{2.6}$$

And for three dimensional flows, the expression in the Cartesian coordinate system is as follow

$$-\left(\frac{\partial^2 p}{\partial x^2} + \frac{\partial^2 p}{\partial y^2} + \frac{\partial^2 p}{\partial z^2}\right) = 0 \tag{2.7}$$

It is important to note that although time does not appear explicitly in Eqs. (2.5)-

(2.7), it does enter the formulation through the solid-fluid interface. As a result p is, in general, a function of time.

2.2.2 Solid Mechanics

The solid region of the current study is a linearly elastic beam or plate. For our analysis, we will consider Euler-Bernoulli, Timoshenko, and Reddy third-order beam theories for beam structures. For plate structures, our studies will be focused on Classical plate theory, first-order shear deformation plate theory and Reddy third-order shear deformation plate theory.

For beams, the x-axis is taken along the length of the beam, passing through the geometric centroid, and z-coordinate is taken transverse to the length (i.e., the y-coordinate is into the plane of the paper). In the case of plates, the xy-plane is the midplane of the plate with the z-axis transverse to the plane of the plate. The total height of the beam and thickness of the plate are denoted with H.

2.2.2.1 The Euler-Bernoulli Beam Theory (EBT)

The governing equation for the EBT under the assumption of small strains and rotations can be expressed as

$$\frac{\partial^2}{\partial x^2}\left(EI\frac{\partial^2 w}{\partial x^2}\right) + m_s\frac{\partial^2 w}{\partial t^2} - \frac{m_s H^2}{12}\left(\frac{\partial^4 w}{\partial x^2 \partial t^2}\right) = -Wp \tag{2.8}$$

where w is the vertical displacement. In Eq. (2.8) EI denotes the bending stiffness (E is Youngs modulus and I is the second moment of area); $m_s = \rho_s A$ is the mass inertia (ρ_s is the density of the beam material; A is the cross-sectional area of the beam with W being the width and H being the height); and p is the fluid pressure acting normal to the beam. In writing Eq. (2.8), the beam rotary inertia is included [the last term on the left side of Eq. (2.8)]. This term can have a significant effect

upon higher modes of beam vibration.

2.2.2.2 The Timoshenko Beam Theory (TBT)

The effect of transverse shear strains on the beam can be accounted for by using the Timoshenko beam theory. The governing equations of the TBT are

$$\frac{\partial}{\partial x}\left[GAK_s\left(\phi+\frac{\partial w}{\partial x}\right)\right]-Wp=m_s\frac{\partial^2 w}{\partial t^2} \tag{2.9}$$

$$\frac{\partial}{\partial x}\left(EI\frac{\partial \phi}{\partial x}\right)-GAK_s\left(\phi+\frac{\partial w}{\partial x}\right)=\frac{m_s H^2}{12}\frac{\partial^2 \phi}{\partial t^2} \tag{2.10}$$

where w is once again the vertical displacement, ϕ is the rotation of a transverse normal, G is the shear modulus, and K_s is the shear correction factor due to the constant shear strain obtained using this theory. Note that the rotary inertia term is included in Eq. (2.10).

2.2.2.3 The Reddy Beam Theory (RBT)

The RBT is useful because it allows for a parabolic distribution of the shear strain λ_{xz} and shear stress σ_{xz} through the thickness of the beam. As a result, the RBT does not require the shear correction factor [46]. The governing equations for the RBT can be expressed as

$$\frac{\partial \bar{Q}_x}{\partial x}+c_1\frac{\partial^2 P_{xx}}{\partial x^2}-Wp=I_0\frac{\partial^2 w}{\partial t^2}+c_1\left(J_4\frac{\partial^3 \phi}{\partial x\partial t^2}-c_1 I_6\frac{\partial^4 w}{\partial x^2\partial t^2}\right) \tag{2.11}$$

$$\frac{\partial \bar{M}_{xx}}{\partial x}-\bar{Q}_x=K_2\frac{\partial^2 \phi}{\partial t^2}-c_1 J_4\frac{\partial^3 w}{\partial x\partial t^2} \tag{2.12}$$

where the quantities included in Eqs. (2.11) and (2.12) are defined as

$$
\begin{aligned}
&I_0 = \rho_s W H, \quad I_2 = \frac{1}{12}\rho_s W H^3, \quad I_4 = \frac{1}{80}\rho_s W H^5, \quad I_6 = \frac{1}{448}\rho_s W H^7 \\
&\bar{M}_{xx} = M_{xx} - c_1 P_{xx}, \quad \bar{Q}_x = Q_x - 3c_1 R_x \\
&K_2 = I_2 - 2c_1 I_4 + c_1^2 I_6, \quad J_4 = I_4 - c_1 I_6, \quad c_1 = \frac{4}{3H^2}
\end{aligned} \tag{2.13}
$$

and the stress resultants are expressed as

$$
\begin{aligned}
M_{xx} &= E\left[D_2\frac{\partial\phi}{\partial x} - D_4 c_1\left(\frac{\partial\phi}{\partial x} + \frac{\partial^2 w}{\partial x^2}\right)\right] \\
P_{xx} &= E\left[D_4\frac{\partial\phi}{\partial x} - D_6 c_1\left(\frac{\partial\phi}{\partial x} + \frac{\partial^2 w}{\partial x^2}\right)\right] \\
Q_x &= G\left[D_0\frac{\partial w}{\partial x} + D_0\phi - 3D_2 c_1\left(\phi + \frac{\partial w}{\partial x}\right)\right] \\
R_x &= G\left[D_2\frac{\partial w}{\partial x} + D_2\phi - 3D_4 c_1\left(\phi + \frac{\partial w}{\partial x}\right)\right]
\end{aligned} \tag{2.14}
$$

In addition, the geometric parameters D_j are defined as

$$
D_0 = WH, \quad D_2 = \frac{1}{12}WH^3, \quad D_4 = \frac{1}{80}WH^5, \quad D_6 = \frac{1}{448}WH^7 \tag{2.15}
$$

2.2.2.4 The Classical Plate Theory (CPT)

The other structure considered in this study is a rectangular plate. Figure 2.2 shows the dimensions, the boundary conditions, and load on the plate. The plate is assumed to be made of homogeneous, isotropic and linear elastic material. The CPT is governed by the equation

$$
D\left(\frac{\partial^4 w}{\partial x^4} + 2\frac{\partial^4 w}{\partial x^2 \partial y^2} + \frac{\partial^4 w}{\partial y^4}\right) = -m_s\frac{\partial^2 w}{\partial t^2} + \frac{m_s H^2}{12}\frac{\partial^2}{\partial t^2}\left(\frac{\partial^2 w}{\partial x^2} + \frac{\partial^2 w}{\partial y^2}\right) - p \tag{2.16}
$$

where D is the bending rigidity

$$D = \frac{EH^3}{12(1-\nu^2)} \tag{2.17}$$

and all other variables have the same meaning as before.

2.2.2.5 The First-order Shear Deformation Plate Theory (FSDT)

In order to take into account the plate transverse shear deformations in our analysis, we extend the proposed method to the first-order shear deformation plate theory. For the plate at hand, the governing equations of the this theory are of the form

$$\frac{\partial Q_x}{\partial x} + \frac{\partial Q_y}{\partial y} = I_0 \frac{\partial^2 w}{\partial t^2} - p \tag{2.18}$$

$$\frac{\partial M_{xx}}{\partial x} + \frac{\partial M_{xy}}{\partial y} - Q_x = I_2 \frac{\partial^2 \phi_x}{\partial t^2} \tag{2.19}$$

$$\frac{\partial M_{xx}}{\partial x} + \frac{\partial M_{yy}}{\partial y} - Q_y = I_2 \frac{\partial^2 \phi_y}{\partial t^2} \tag{2.20}$$

where w, ϕ_x and ϕ_y are vertical displacement, rotation of a transverse normal about y axis and rotation of a transverse normal about x axis, respectively. The stress resultants in these equations are as follows:

$$Q_x = K_s GH \left(\phi_x + \frac{\partial w}{\partial x} \right)$$

$$Q_y = K_s GH \left(\phi_y + \frac{\partial w}{\partial y} \right)$$

$$M_{xx} = D \left(\frac{\partial \phi_x}{\partial x} + \nu \frac{\partial \phi_y}{\partial y} \right)$$

$$M_{yy} = D \left(\frac{\partial \phi_y}{\partial y} + \nu \frac{\partial \phi_x}{\partial x} \right)$$

$$M_{xy} = \frac{GH^3}{12}\left(\frac{\partial \phi_x}{\partial y} + \nu \frac{\partial \phi_y}{\partial x}\right) \tag{2.21}$$

where D is the bending rigidity defined in Eq. (2.17).

2.2.2.6 Reddy Third-order Shear Deformation Plate Theory (RSDT)

The governing equations of the RSDT are given by the following three equations

$$\begin{aligned} &\frac{\partial \bar{Q}_x}{\partial x} + \frac{\partial \bar{Q}_y}{\partial y} + c\left(\frac{\partial^2 P_{xx}}{\partial x^2} + 2\frac{\partial^2 P_{xy}}{\partial x \partial y} + \frac{\partial^2 P_{yy}}{\partial y^2}\right) + p \\ &= I_0 \frac{\partial^2 w}{\partial t^2} - c^2 I_6 \left(\frac{\partial^4 w}{\partial x^2 \partial t^2} + \frac{\partial^4 w}{\partial y^2 \partial t^2}\right) + cJ\left(\frac{\partial^3 \phi_x}{\partial x \partial t^2} + \frac{\partial^3 \phi_y}{\partial y \partial t^2}\right) \end{aligned} \tag{2.22}$$

$$\frac{\partial \bar{M}_{xx}}{\partial x} + \frac{\partial \bar{M}_{xy}}{\partial y} - \bar{Q}_x = K\frac{\partial^2 \phi_x}{\partial t^2} - cJ\frac{\partial^3 w}{\partial x \partial t^2} \tag{2.23}$$

$$\frac{\partial \bar{M}_{xy}}{\partial x} + \frac{\partial \bar{M}_{yy}}{\partial y} - \bar{Q}_y = K\frac{\partial^2 \phi_y}{\partial t^2} - cJ\frac{\partial^3 w}{\partial y \partial t^2} \tag{2.24}$$

The variables in Eqs. (2.22)-(2.24) are expressed as

$$\begin{aligned} &I_0 = \rho_s H, \quad I_2 = \frac{1}{12}\rho_s H^3, \quad I_4 = \frac{1}{80}\rho_s H^5, \quad I_6 = \frac{1}{448}\rho_s H^7 \\ &\bar{M}_{\alpha\beta} = M_{\alpha\beta} - cP_{\alpha\beta} \quad (\alpha,\beta{=}x,y) \\ &\bar{Q}_\alpha = Q_\alpha - 3cR_\alpha \quad (\alpha{=}x,y) \\ &K = I_2 - 2cI_4 + c^2 I_6, \quad J = I_4 - cI_6, \quad c = \frac{4}{3H^2} \end{aligned} \tag{2.25}$$

The stress resultants, for this theory, are defined as

$$
\begin{aligned}
M_{xx} &= D\left[(1-\alpha)\left(\frac{\partial \phi_x}{\partial x}+\nu\frac{\partial \phi_y}{\partial y}\right)-\alpha\left(\frac{\partial^2 w}{\partial x^2}+\nu\frac{\partial^2 w}{\partial y^2}\right)\right] \\
M_{yy} &= D\left[(1-\alpha)\left(\frac{\partial \phi_y}{\partial y}+\nu\frac{\partial \phi_x}{\partial x}\right)-\alpha\left(\frac{\partial^2 w}{\partial y^2}+\nu\frac{\partial^2 w}{\partial x^2}\right)\right] \\
M_{xy} &= \frac{(1-\nu)\,D}{2}\left[(1-\alpha)\left(\frac{\partial \phi_x}{\partial y}+\frac{\partial \phi_y}{\partial x}\right)-2\alpha\frac{\partial^2 w}{\partial x \partial y}\right] \\
P_{xx} &= D\left[\beta\left(\frac{\partial \phi_x}{\partial x}+\nu\frac{\partial \phi_y}{\partial y}\right)-\gamma\left(\frac{\partial^2 w}{\partial x^2}+\nu\frac{\partial^2 w}{\partial y^2}\right)\right] \\
P_{yy} &= D\left[\beta\left(\frac{\partial \phi_y}{\partial y}+\nu\frac{\partial \phi_x}{\partial x}\right)-\gamma\left(\frac{\partial^2 w}{\partial y^2}+\nu\frac{\partial^2 w}{\partial x^2}\right)\right] \\
P_{xy} &= \frac{(1-\nu)\,D}{2}\left[\beta\left(\frac{\partial \phi_x}{\partial y}+\frac{\partial \phi_y}{\partial x}\right)-2\gamma\frac{\partial^2 w}{\partial x \partial y}\right] \\
Q_x &= (1-\mu)\,GH\left(\phi_x+\frac{\partial w}{\partial x}\right) \\
Q_y &= (1-\mu)\,GH\left(\phi_y+\frac{\partial w}{\partial y}\right) \\
R_x &= \lambda GH\left(\phi_x+\frac{\partial w}{\partial x}\right) \\
R_y &= \lambda GH\left(\phi_y+\frac{\partial w}{\partial y}\right)
\end{aligned}
\tag{2.26}
$$

where

$$
\alpha=\frac{1}{5},\quad \beta=\frac{4H^2}{35},\quad \gamma=\frac{H^2}{28},\quad \lambda=\frac{H^2}{30},\quad \mu=\frac{1}{3} \tag{2.27}
$$

and D is the bending rigidity as in Eq. (2.17).

2.2.3 Solid-Fluid Interface

The interface between the solid and fluid medium requires special attentions. Often an interface between solid and fluid regions are treated by assuming the continuity

of velocity $\mathbf{v}$ and traction $\mathbf{t}$ which can be expressed as

$$\frac{\partial u_s}{\partial t} = v_f \tag{2.28}$$

$$\boldsymbol{\sigma}_s.\mathbf{n} + \boldsymbol{\sigma}_f.\mathbf{n} = 0 \tag{2.29}$$

Evaluating the momentum equation (2.3) at the solid-fluid interface yields the following equation

$$-\frac{\partial p}{\partial z} - \rho_f g = \rho_f \frac{\partial^2 w}{\partial t^2} \tag{2.30}$$

which can be expressed as

$$\frac{\partial p}{\partial z} = -\rho_f \left(g + \frac{\partial^2 w}{\partial t^2} \right) \tag{2.31}$$

Equation (2.31) is therefore the solid-fluid interface condition that will be used in our analysis.

2.3 Finite Element Formulations

In this sub-section, we present finite element formulations for the solid and fluid domains. We also impose the interfacial condition given by Eq. (2.31) to couple the two domains. For details, the reader may consult the textbooks by Reddy [51],[49].

2.3.1 Fluid Medium

Here we consider one row of fluid elements along the beam length (refer to Fig. 2.1). We begin by constructing the weak form of the Eq. (2.5) over a typical fluid element $\Omega^e = (x_a, x_b) \times (z_a, z_b)$. We proceed by multiplying Eq. (2.5) by the first

variation of p

$$0 = -\int_{\Omega_e} \delta p \, \nabla^2 p \, dxdz \tag{2.32}$$

Using the vector identity $\nabla.(\alpha \nabla \phi) = \nabla \alpha . \nabla \phi + \alpha \nabla^2 \phi$ and the divergence theorem, Eq. (2.32) can be expressed as (see Reddy [51])

$$0 = \int_{z_a}^{z_b} \int_{x_a}^{x_b} \left(\frac{\partial \delta p}{\partial x} \frac{\partial p}{\partial x} + \frac{\partial \delta p}{\partial z} \frac{\partial p}{\partial z} \right) dxdz + \int_{x_a}^{x_b} \left[\delta p \frac{\partial p}{\partial z} \right]_{z=0} dx - \oint_{\hat{\Gamma}^e} \delta p \, \nabla p . \hat{\mathbf{n}} \, ds \tag{2.33}$$

where $\hat{\mathbf{n}}$ is the unit normal to the surface with components (n_x, n_z). In Eq. (2.33), $\hat{\Gamma}^e$ denotes the boundary of a fluid element not in contact with the beam. Inserting Eq. (2.31) into Eq. (2.33), we obtain

$$\begin{aligned} 0 = & \int_{z_a}^{z_b} \int_{x_a}^{x_b} \left(\frac{\partial \delta p}{\partial x} \frac{\partial p}{\partial x} + \frac{\partial \delta p}{\partial z} \frac{\partial p}{\partial z} \right) dxdz - \int_{x_a}^{x_b} \left[\delta p \rho_f \left(g + \frac{\partial^2 w}{\partial t^2} \right) \right]_{z=0} dx \\ & - \oint_{\hat{\Gamma}^e} \delta p \left(\frac{\partial p}{\partial x} n_x + \frac{\partial p}{\partial z} n_z \right) ds \end{aligned} \tag{2.34}$$

The finite element model for the fluid domain is obtained by assuming the following approximation of the pressure p over each element (see Reddy [51])

$$p(x, z, t) = \sum_{j=1}^{n} P_j(t) \, \psi_j(x, z) \tag{2.35}$$

where ψ_j are Lagrange family interpolation functions. For the present study, we utilize two dimensional linear rectangular elements (i.e., $n = 4$). The interpolation

functions are of the form

$$\psi_1 = \frac{1}{4}(1-\xi)(1-\eta), \quad \psi_2 = \frac{1}{4}(1+\xi)(1-\eta)$$
$$\psi_3 = \frac{1}{4}(1+\xi)(1+\eta), \quad \psi_4 = \frac{1}{4}(1-\xi)(1+\eta) \tag{2.36}$$

where ξ and η are the element (normalized) coordinates defined as

$$\xi = \frac{2x - x_a - x_b}{h_x}, \quad \eta = \frac{2z - z_a - z_b}{h_z} \tag{2.37}$$

Inserting Eq. (2.35) into Eq. (2.34), we obtain the following set of finite element equations for the fluid medium

$$\mathbf{CP} = \mathbf{f} + \mathbf{Q} \tag{2.38}$$

where

$$C_{ij} = \int_{z_a}^{z_b}\int_{x_a}^{x_b}\left(\frac{\partial\psi_i}{\partial x}\frac{\psi_j}{\partial x} + \frac{\partial\psi_i}{\partial z}\frac{\psi_j}{\partial z}\right)dxdz \tag{2.39}$$
$$f_i = \int_{x_a}^{x_b}\rho_f\psi_i\left(g + \frac{\partial^2 w}{\partial t^2}\right)dx \tag{2.40}$$
$$Q_i = \oint_{\hat{\Gamma}^e}\psi_i\left(\frac{\partial p}{\partial x}n_x + \frac{\partial p}{\partial z}n_z\right)ds \tag{2.41}$$

The matrix $\mathbf{C}$ can be expressed explicitly as

$$\mathbf{C} = \frac{h_z}{6h_x}\begin{bmatrix} 2 & -2 & -1 & 1 \\ -2 & 2 & 1 & -1 \\ -1 & 1 & 2 & -2 \\ 1 & -1 & -2 & 2 \end{bmatrix} + \frac{h_x}{6h_z}\begin{bmatrix} 2 & 1 & -1 & -2 \\ 1 & 2 & -2 & -1 \\ -1 & -2 & 2 & 1 \\ -2 & -1 & 1 & 2 \end{bmatrix} \tag{2.42}$$

where h_x and h_z are the element lengths along the x and z coordinates, respectively. The procedure for the plate problem is the same, except that the fluid element for plate problem is 3D element $\Omega^e = (x_a, x_b) \times (y_a, y_b) \times (z_a, z_b)$

$$\begin{aligned} 0 = & \int_{z_a}^{z_b} \int_{y_a}^{y_b} \int_{x_a}^{x_b} \left(\frac{\partial \delta p}{\partial x} \frac{\partial p}{\partial x} + \frac{\partial \delta p}{\partial y} \frac{\partial p}{\partial y} + \frac{\partial \delta p}{\partial z} \frac{\partial p}{\partial z} \right) dx dy dz \\ & - \int_{y_a}^{y_b} \int_{x_a}^{x_b} \left[\delta p \rho_f \left(g + \frac{\partial^2 w}{\partial t^2} \right) \right]_{z=0} dx dy \\ & - \oint_{\hat{\Gamma}^e} \delta p \left(\frac{\partial p}{\partial x} n_x + \frac{\partial p}{\partial y} n_y + \frac{\partial p}{\partial z} n_z \right) ds \end{aligned} \tag{2.43}$$

All of the variables have the same definition as of the beam problem. We assume the following form of the pressure p for the 3D elements

$$p(x, y, z, t) = \sum_{j=1}^{n} P_j(t) \psi_j(x, y, z) \tag{2.44}$$

where ψ_j^e are Lagrange family interpolation functions in 3D. For the present study, we utilize 8-node brick elements. The interpolation functions are of the form [51]

$$\begin{aligned} \psi_1 &= \frac{1}{8}(1-\xi)(1-\eta)(1-\zeta), \quad \psi_2 = \frac{1}{8}(1+\xi)(1-\eta)(1-\zeta) \\ \psi_3 &= \frac{1}{8}(1+\xi)(1+\eta)(1-\zeta), \quad \psi_4 = \frac{1}{8}(1-\xi)(1+\eta)(1-\zeta) \\ \psi_5 &= \frac{1}{8}(1-\xi)(1-\eta)(1+\zeta), \quad \psi_6 = \frac{1}{8}(1+\xi)(1-\eta)(1+\zeta) \\ \psi_7 &= \frac{1}{8}(1+\xi)(1+\eta)(1+\zeta), \quad \psi_8 = \frac{1}{8}(1-\xi)(1+\eta)(1+\zeta) \end{aligned} \tag{2.45}$$

Substitution of the approximation (2.44) into the weak form (2.43), we obtain

$$\mathbf{CP} = \mathbf{f} + \mathbf{Q} \tag{2.46}$$

where

$$C_{ij} = \int_{z_a}^{z_b} \int_{y_a}^{y_b} \int_{x_a}^{x_b} \left(\frac{\partial \psi_i}{\partial x} \frac{\psi_j}{\partial x} + \frac{\partial \psi_i}{\partial y} \frac{\psi_j}{\partial y} + \frac{\partial \psi_i}{\partial z} \frac{\psi_j}{\partial z} \right) dxdydz \tag{2.47}$$

$$f_i = \int_{y_b}^{y_b} \int_{x_a}^{x_b} \rho_f \psi_i \left(g + \frac{\partial^2 w}{\partial t^2} \right) dxdy \tag{2.48}$$

$$Q_i = \oint_{\hat{\Gamma}} \psi_i \left(\frac{\partial p}{\partial x} n_x + \frac{\partial p}{\partial y} n_y + \frac{\partial p}{\partial z} n_z \right) ds \tag{2.49}$$

2.3.2 Solid Medium

In this sub-section, we formulate finite element models for the solid medium for each beam theory as well as each plate theory.

2.3.2.1 The EBT

The weak form of Eq. (2.8) is given by

$$\begin{aligned} 0 = & \int_{x_a}^{x_b} \left[EI \frac{\partial^2 \delta w}{\partial x^2} \frac{\partial^2 w}{\partial x^2} + \delta w m_s \frac{\partial^2 w}{\partial t^2} + \frac{m_s H^2}{12} \frac{\partial w}{\partial x} \frac{\partial^3 w}{\partial x \partial t^2} + \delta w W p \right] dx \\ & - Q_1 \delta w \left(x_a \right) - Q_2 \left(- \frac{\partial \delta w}{\partial x} \right) \Big|_{x=x_a} - Q_3 \delta w \left(x_b \right) - Q_4 \left(- \frac{\partial \delta w}{\partial x} \right) |_{x=x_b} \end{aligned} \tag{2.50}$$

where the secondary variables Q_j's are defined as

$$\begin{aligned} Q_1 &= - \left[\frac{m_s H^2}{12} \frac{\partial^3 w}{\partial x \partial t^2} - \frac{\partial}{\partial x} \left(EI \frac{\partial^2 w}{\partial x^2} \right) \right] |_{x=x_a} , \quad Q_2 = \left(EI \frac{\partial^2 w}{\partial x^2} \right) |_{x=x_a} \\ Q_3 &= \left[\frac{m_s H^2}{12} \frac{\partial^3 w}{\partial x \partial t^2} - \frac{\partial}{\partial x} \left(EI \frac{\partial^2 w}{\partial x^2} \right) \right] |_{x=x_b} , \quad Q_4 = - \left(EI \frac{\partial^2 w}{\partial x^2} \right) |_{x=x_b} \end{aligned} \tag{2.51}$$

The finite element model for the EBT is obtained by interpolating the transverse displacement w as

$$w \left(x, t \right) = \sum_{j=1}^{4} \Delta_j \left(t \right) \varphi_j \left(x \right) \tag{2.52}$$

where φ_j^e are the Hermite cubic interpolation functions [51]

$$\varphi_1 = 1 - 3\left(\frac{\bar{x}}{h_x}\right)^2 + 2\left(\frac{\bar{x}}{h_x}\right)^3, \quad \varphi_2 = -\bar{x}\left(1 - \frac{\bar{x}}{h_x}\right)^2$$
$$\varphi_3 = 3\left(\frac{\bar{x}}{h_x}\right)^2 - 2\left(\frac{\bar{x}}{h_x}\right)^3, \quad \varphi_4 = -\bar{x}\left[\left(\frac{\bar{x}}{h_x}\right)^2 - \frac{\bar{x}}{h_x}\right] \tag{2.53}$$

where $\bar{x} = x - x_a$, h_x is the length of the element, and Δ the nodal vector consists of the deflection w and the slope $\theta \equiv -(\partial w/\partial x)$ at the nodes as shown in Fig. 2.3. Substituting Eq. (2.52) into Eq. (2.50), we obtain a set of finite element equations for the Euler-Bernoulli beam element

$$m_s \mathbf{M}\ddot{\mathbf{\Delta}} + \mathbf{K}\mathbf{\Delta} = \mathbf{q} + \mathbf{F} \tag{2.54}$$

where

$$M_{ij} = \int_{x_a}^{x_b} \left(\varphi_i \varphi_j + \frac{H^2}{12}\frac{d\varphi_i}{dx}\frac{d\varphi_j}{dx}\right) dx \tag{2.55}$$
$$K_{ij} = \int_{x_a}^{x_b} EI \frac{d^2\varphi_i}{dx^2}\frac{d^2\varphi_j}{dx^2} dx \tag{2.56}$$
$$q_i = \int_{x_a}^{x_b} pW\varphi_i dx \tag{2.57}$$

In addition F^i are the generalized nodal forces and can be defined as

$$\mathbf{F}^1 = \left\{ \begin{array}{cccc} Q_1 & Q_2 & Q_3 & Q_4 \end{array} \right\}^T \tag{2.58}$$

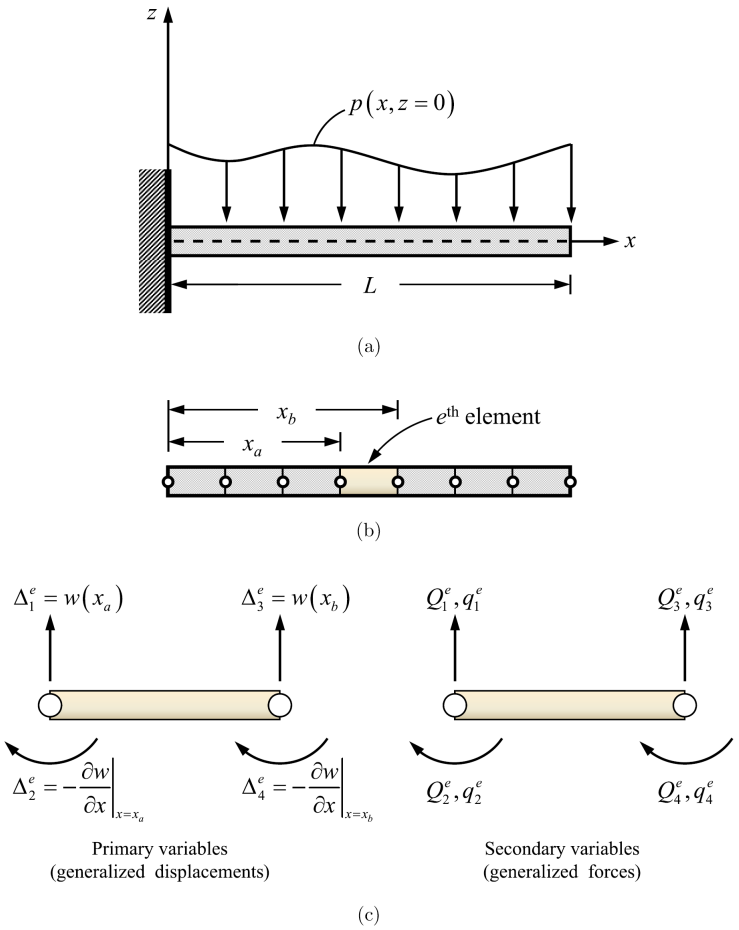

Figure 2.3: (a) Geometry of a cantilever beam and applied load due to fluid pressure, (b) finite element discretization of beam and (c) generalized displacements and generalized forces on a typical Euler-Bernoulli beam element.

The mass matrix $\mathbf{M}$ and stiffness matrix $\mathbf{K}$ can be expressed as

$$\mathbf{M} = \frac{h_x}{420}\begin{bmatrix} 156 & -22h_x & 54 & 13h_x \\ -22h_x & 4h_x^2 & -13h_x & -3h_x^2 \\ 54 & -13h_x & 156 & 22h_x \\ 13h_x & -3h_x^2 & 22h_x & 4h_x^2 \end{bmatrix} + \frac{H^2}{360h_x}\begin{bmatrix} 36 & -3h_x & -36 & -3h_x \\ -3h_x & 4h_x^2 & 3h_x & -h_x^2 \\ -36 & 3h_x & 36 & 3h_x \\ -3h_x & -h_x^2 & 3h_x & 4h_x^2 \end{bmatrix} \tag{2.59}$$

$$\mathbf{K} = \frac{2EI}{h_x^3}\begin{bmatrix} 6 & -3h_x & -6 & -3h_x \\ -3h_x & 2h_x^2 & 3h_x & h_x^2 \\ -6 & 3h_x & 6 & 3h_x \\ -3h_x & h_x^2 & 3h_x & 2h_x^2 \end{bmatrix} \tag{2.60}$$

The general form of q_i will be presented in Sub-section 2.3.4.1.

2.3.2.2 The TBT

The weak forms of Eqs. (2.9) and (2.10) are given by

$$\begin{aligned} 0 = &\int_{x_a}^{x_b} \left[\frac{\partial \delta w}{\partial x} GAK_s \left(\phi + \frac{\partial w}{\partial x} \right) + \delta w m_s \frac{\partial^2 w}{\partial t^2} + \delta w W p \right] dx \\ &- \delta w\left(x_a\right) Q_1 - \delta w\left(x_b\right) Q_3 \end{aligned} \tag{2.61}$$

$$\begin{aligned} 0 = &\int_{x_a}^{x_b} \left[\frac{\partial \delta \phi}{\partial x} EI \frac{\partial \phi}{\partial x} + \delta \phi GAK_s \left(\phi + \frac{\partial w}{\partial x} \right) + \delta \phi \frac{m_s H^2}{12} \frac{\partial^2 \phi}{\partial t^2} \right] dx \\ &- \delta \phi\left(x_a\right) Q_2 - \delta \phi\left(x_b\right) Q_4 \end{aligned} \tag{2.62}$$

where the secondary variables Q_j's are defined as

$$\begin{aligned} Q_1 &= -\left[GAK_s \left(\phi + \frac{\partial w}{\partial x} \right) \right] |_{x=x_a} , \quad Q_2 = -\left(EI \frac{\partial \phi}{\partial x} \right) |_{x=x_a} \\ Q_3 &= \left[GAK_s \left(\phi + \frac{\partial w}{\partial x} \right) \right] |_{x=x_b} , \quad Q_4 = \left(EI \frac{\partial \phi}{\partial x} \right) |_{x=x_b} \end{aligned} \tag{2.63}$$

The finite element model for the TBT is obtained by interpolating the transverse displacement w and beam rotation ϕ as

$$\begin{aligned} w\left(x,t\right) &= \sum_{j=1}^{m} \Delta_j\left(t\right) \psi_j^{(1)}\left(x\right) \\ \phi\left(x,t\right) &= \sum_{j=1}^{m} \Phi_j\left(t\right) \psi_j^{(2)}\left(x\right) \end{aligned} \tag{2.64}$$

where $\psi_j^{(1)}$ and $\psi_j^{(2)}$ are Lagrange interpolation functions, and the generalized displacements (i.e., Δ_j and Φ_j) are depicted in Fig. 2.4.

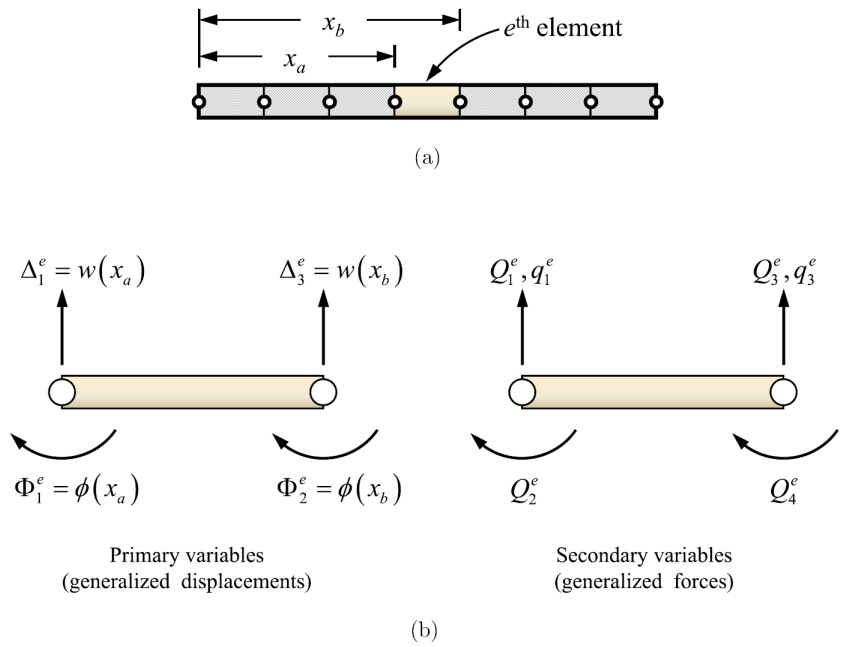

Figure 2.4: (a) Finite element discretization of beam and (b) generalized displacements and generalized forces on a typical Timoshenko beam element.

In the present work, we use linear Lagrange interpolation functions for both $\psi_j^{(1)}$ and $\psi_j^{(2)}$ (i.e., $m = n = 2$) which can be expressed as

$$\begin{aligned} \psi_1^{(1)} &= \psi_1^{(2)} = \frac{x_b - x}{x_b - x_a} \\ \psi_2^{(1)} &= \psi_2^{(2)} = \frac{x - x_a}{x_b - x_a} \end{aligned} \tag{2.65}$$

It is important to note that linear interpolation of both w and ϕ results in shear locking in the thin beam limit. This can be alleviated by using reduced integration of components of the resulting stiffness coefficients involving $\psi_j^{(2)}$. More details can be found in the literature (see Reddy [51], [49]). Inserting Eq. (2.64) into Eq. (2.61) results in the following set of finite element equations

$$m_s \begin{bmatrix} \mathbf{M}^{11} & \mathbf{M}^{12} \\ \mathbf{M}^{21} & \mathbf{M}^{22} \end{bmatrix} \begin{Bmatrix} \ddot{\mathbf{\Delta}}^e \\ \ddot{\mathbf{\Phi}}^e \end{Bmatrix} + \begin{bmatrix} \mathbf{K}^{11} & \mathbf{K}^{12} \\ \mathbf{K}^{21} & \mathbf{K}^{22} \end{bmatrix} \begin{Bmatrix} \mathbf{\Delta}^e \\ \mathbf{\Phi}^e \end{Bmatrix} = \begin{Bmatrix} \mathbf{q}^1 \\ \mathbf{q}^2 \end{Bmatrix} + \begin{Bmatrix} \mathbf{F}^1 \\ \mathbf{F}^2 \end{Bmatrix} \tag{2.66}$$

where the nonzero components of the mass matrices $\mathbf{M}^{\alpha\beta}$, stiffness matrices $\mathbf{K}^{\alpha\beta}$ and force vectors $\mathbf{q}^{\alpha}$ are given as

$$\begin{aligned} M_{ij}^{11} &= \int_{x_a}^{x_b} \psi_i^{(1)} \psi_j^{(1)} dx \\ M_{ij}^{22} &= \frac{H^2}{12} \int_{x_a}^{x_b} \psi_i^{(2)} \psi_j^{(2)} dx \end{aligned} \tag{2.67}$$

$$\begin{aligned} K_{ij}^{11} &= \int_{x_a}^{x_b} GAK_s \frac{d\psi_i^{(1)}}{dx} \frac{d\psi_j^{(1)}}{dx} dx \\ K_{ij}^{12} &= \int_{x_a}^{x_b} GAK_s \frac{d\psi_i^{(1)}}{dx} \psi_j^{(2)} dx \\ K_{ij}^{21} &= \int_{x_a}^{x_b} GAK_s \psi_i^{(2)} \frac{d\psi_j^{(1)}}{dx} dx \\ K_{ij}^{22} &= \int_{x_a}^{x_b} \left(EI \frac{d\psi_i^{(2)}}{dx} \frac{d\psi_j^{(2)}}{dx} + GAK_s \psi_i^{(2)} \psi_j^{(2)} \right) dx \end{aligned} \tag{2.68}$$

$$q_i^1 = -\int_{x_a}^{x_b} pW \psi_i^{(1)} dx \tag{2.69}$$

The mass and stiffness matrices can be expressed explicitly as

$$\mathbf{M}^{11} = \frac{h_x}{6}\begin{bmatrix} 2 & 1 \\ 1 & 2 \end{bmatrix}, \quad \mathbf{M}^{22} = \frac{H^2 h_x}{72}\begin{bmatrix} 2 & 1 \\ 1 & 2 \end{bmatrix} \tag{2.70}$$

$$\mathbf{K}^{11} = \frac{GAK_s}{h_x}\begin{bmatrix} 1 & -1 \\ -1 & 1 \end{bmatrix}, \quad \mathbf{K}^{12} = \frac{GAK_s}{2}\begin{bmatrix} -1 & -1 \\ 1 & 1 \end{bmatrix}$$

$$\mathbf{K}^{21} = \frac{GAK_s}{2}\begin{bmatrix} -1 & 1 \\ -1 & 1 \end{bmatrix}, \quad \mathbf{K}^{22} = \frac{EI}{h_x}\begin{bmatrix} 1 & -1 \\ -1 & 1 \end{bmatrix} + \frac{GAK_s h_x}{4}\begin{bmatrix} 1 & 1 \\ 1 & 1 \end{bmatrix} \tag{2.71}$$

and the generalized force vectors are defined as

$$\mathbf{F}^1 = \begin{Bmatrix} Q_1 & Q_3 \end{Bmatrix}^T$$
$$\mathbf{F}^2 = \begin{Bmatrix} Q_2 & Q_4 \end{Bmatrix}^T \tag{2.72}$$

The second term in $\mathbf{K}^{22}$ expression is obtained using reduced integration of components of the resulting stiffness coefficients involving $\psi_j^{(2)}$. The effect of the fluid pressure as manifested in q_i^1 will be addressed in Sub-section 2.3.4.2.

2.3.2.3 The RBT

The weak forms of the RBT equations can be derived as follows:

$$
\begin{aligned}
0 = \int_{x_a}^{x_b} \{ & I_0 \ddot{w} \delta w + \left[-c_1 J_4 \ddot{\phi} + c_1^2 I_6 \frac{\partial \ddot{w}}{\partial x} + G \left(D_0 - 6 c_1 D_2 + 9 c_1^2 D_4 \right) \left(\phi + \frac{\partial w}{\partial x} \right) \right] \frac{\partial \delta w}{\partial x} \\
& + c_1 E \left(-L_4 \frac{\partial \phi}{\partial x} + c_1 D_6 \frac{\partial^2 w}{\partial x^2} \right) \frac{\partial^2 \delta w}{\partial x^2} + W p \delta w \} dx \\
& - Q_1 \delta w \left(x_a \right) - Q_2 \left(- \frac{\partial \delta w}{\partial x} \right) |_{x=x_a} - Q_5 \delta w \left(x_b \right) - Q_6 \left(- \frac{\partial \delta w}{\partial x} \right) |_{x=x_b}
\end{aligned} \tag{2.73}
$$

$$
\begin{aligned}
0 = \int_{x_a}^{x_b} \{ & \left[K_2 \ddot{\phi} - c_1 J_4 \frac{\partial \ddot{w}}{\partial x} + G \left(D_0 - 6 c_1 D_2 + 9 c_1^2 D_4 \right) \left(\phi + \frac{\partial w}{\partial x} \right) \right] \delta \phi \\
& + E \left(M_2 \frac{\partial \phi}{\partial x} - c_1 L_4 \frac{\partial^2 w}{\partial x^2} \right) \frac{\partial \delta \phi}{\partial x} \} dx - Q_4 \delta \phi \left(x_c \right) - Q_7 \delta \phi \left(x_b \right)
\end{aligned} \tag{2.74}
$$

where the secondary variables Q_j's are defined as

$$
\begin{aligned}
& Q_1 = -Q_x \left|_{x=x_a} \right. , \quad Q_2 = -c_1 P_{xx} \left|_{x=x_a} \right. , \quad Q_3 = -\bar{M}_{xx} \left|_{x=x_a} \right. \\
& Q_5 = Q_x \left|_{x=x_b} \right. , \quad Q_6 = c_1 P_{xx} \left|_{x=x_b} \right. , \quad Q_7 = \bar{M}_{xx} \left|_{x=x_b} \right.
\end{aligned} \tag{2.75}
$$

For sake of brevity, we have also employed the following definitions in Eqs. (2.73) and (2.74)

$$
L_4 = D_4 - c_1 D_6, \quad M_2 = D_2 - 2 c_1 D_4 + c_1^2 D_6 \tag{2.76}
$$

From Eqs. (2.73) and (2.74), it is evident that the primary variables for the RBT are w, dw/dx and ϕ. As a result, ϕ can be interpolated using the Lagrange interpolation functions, while w must be interpolated using the Hermite shape functions. We

therefore interpolate the primary variables as

$$w(x,t) = \sum_{j=1}^{m} \Delta_j(t)\,\varphi_j^e(x)$$
$$\phi(x,t) = \sum_{j=1}^{m} \Phi_j(t)\,\psi_j(x) \tag{2.77}$$

where φ_j and ψ_j are Hermite cubic and Lagrange interpolation functions, respectively. For the present study, we utilize Hermite cubic interpolation functions to

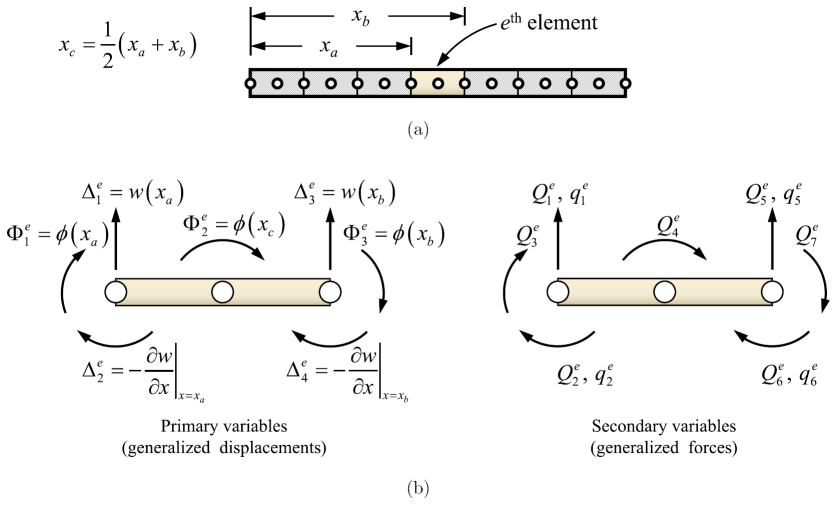

Figure 2.5: (a) Finite element discretization of beam and (b) generalized displacements and generalized forces on a typical third-order beam element.

approximate w and Lagrange quadratic interpolation functions to approximate ϕ (i.e., $m = 4$ and $n = 3$). As a result, the Hermite cubic interpolation functions φ_j are given by Eq. (2.53), and the Lagrange quadratic interpolation functions ψ_j can

be expressed as

$$\begin{aligned}
\psi_1 &= \left(1 - \frac{\bar{x}}{h_x}\right)\left(1 - 2\frac{\bar{x}}{h_x}\right) \\
\psi_2 &= 4\frac{\bar{x}}{h_x}\left(1 - \frac{\bar{x}}{h_x}\right) \\
\psi_3 &= -\frac{\bar{x}}{h_x}\left(1 - 2\frac{\bar{x}}{h_x}\right)
\end{aligned} \tag{2.78}$$

Inserting Eqs. (2.53) and (2.78) into Eqs. (2.73) and (2.74), we obtain the following set of algebraic equation

$$\begin{bmatrix} \mathbf{M}^{11} & \mathbf{M}^{12} \\ \mathbf{M}^{21} & \mathbf{M}^{22} \end{bmatrix} \begin{Bmatrix} \ddot{\mathbf{\Delta}} \\ \ddot{\mathbf{\Phi}} \end{Bmatrix} + \begin{bmatrix} \mathbf{K}^{11} & \mathbf{K}^{12} \\ \mathbf{K}^{21} & \mathbf{K}^{22} \end{bmatrix} \begin{Bmatrix} \mathbf{\Delta} \\ \mathbf{\Phi} \end{Bmatrix} = \begin{Bmatrix} \mathbf{q}^1 \\ \mathbf{q}^2 \end{Bmatrix} + \begin{Bmatrix} \mathbf{F}^1 \\ \mathbf{F}^2 \end{Bmatrix} \tag{2.79}$$

where the nonzero components of the mass matrices $\mathbf{M}^{\alpha\beta}$, stiffness matrices $\mathbf{K}^{\alpha\beta}$ and force vectors $\mathbf{q}^{\alpha}$ are in general given as

$$\begin{aligned}
M_{ij}^{11} &= \int_{x_a}^{x_b} \left(I_0 \varphi_i \varphi_j + c_1^2 I_6 \frac{d\varphi_i}{dx}\frac{d\varphi_j}{dx} \right) dx \\
M_{ij}^{12} &= -\int_{x_a}^{x_b} c_1 J_4 \frac{d\varphi_i}{dx} \psi_j^{(3)} dx \\
M_{ij}^{21} &= -\int_{x_a}^{x_b} c_1 J_4 \psi_i^{(3)} \frac{d\varphi_j}{dx} dx \\
M_{ij}^{22} &= \int_{x_a}^{x_b} K_2 \psi_i^{(3)} \psi_j^{(3)} dx
\end{aligned} \tag{2.80}$$

$$
\begin{aligned}
K_{ij}^{11} &= \int_{x_a}^{x_b} \left[\hat{A}_s \frac{d\varphi_i}{dx} \frac{d\varphi_j}{dx} + c_1^2 E D_6 \frac{d^2\varphi_i}{dx^2} \frac{d^2\varphi_j}{dx^2} \right] dx \\
K_{ij}^{12} &= \int_{x_a}^{x_b} \left[\hat{A}_s \frac{d\varphi_i}{dx} \psi_j^{(3)} - c_1 E L_4 \frac{d^2\varphi_i}{dx^2} \frac{d\psi_j^{(3)}}{dx} \right] dx \\
K_{ij}^{21} &= \int_{x_a}^{x_b} \left[\hat{A}_s \psi_i^{(3)} \frac{d\varphi_j}{dx} - c_1 E L_4 \frac{d\psi_i^{(3)}}{dx} \frac{d^2\varphi_j}{dx^2} \right] dx \\
K_{ij}^{22} &= \int_{x_a}^{x_b} \left[\hat{A}_s \psi_i^{(3)} \psi_j^{(3)} - c_1 M_2 \frac{d\psi_i^{(3)}}{dx} \frac{d\psi_j^{(3)}}{dx} \right] dx
\end{aligned} \tag{2.81}
$$

$$
q_i^1 = -\int_{x_a}^{x_b} W p \varphi_i dx \tag{2.82}
$$

where $\hat{A}_s$ is defined as

$$
\hat{A}_s = G\left(D_0 - 6c_1 D_2 + 9c_1^2 D_4\right) \tag{2.83}
$$

The explicit form of the element matrices is

$$
\mathbf{M}^{11} = \frac{h_x I_0}{420} \begin{bmatrix} 156 & -22h_x & 54 & 13h_x \\ -22h_x & 4h_x^2 & -13h_x & -3h_x^2 \\ 54 & -13h_x & 156 & 22h_x \\ 13h_x & -3h_x^2 & 22h_x & 4h_x^2 \end{bmatrix} + \frac{c_1^2 I_6}{30h_x} \begin{bmatrix} 36 & -3h_x & -36 & -3h_x \\ -3h_x & 4h_x^2 & 3h_x & -h_x^2 \\ -36 & 3h_x & 36 & 3h_x \\ -3h_x & -h_x^2 & 3h_x & 4h_x^2 \end{bmatrix}
$$

$$
\mathbf{M}^{12} = \frac{c_1 J_4}{60} \begin{bmatrix} 6 & 48 & 6 \\ 7h_x & -4h_x & -3h_x \\ -6 & -48 & -6 \\ -3h_x & -4h_x & 7h_x \end{bmatrix}
$$

$$\mathbf{M}^{21} = \frac{c_1 J_4}{60} \begin{bmatrix} 6 & 7h_x & -6 & -3h_x \\ 48 & -4h_x & -48 & -4h_x \\ 6 & -3h_x & -6 & 7h_x \end{bmatrix}$$

$$\mathbf{M}^{22} = \frac{h_x K_2}{30} \begin{bmatrix} 4 & 2 & -1 \\ 2 & 16 & 2 \\ -1 & 2 & 4 \end{bmatrix} \tag{2.84}$$

$$\mathbf{K}^{11} = \frac{\hat{A}_s}{30h_x} \begin{bmatrix} 36 & -3h_x & -36 & -3h_x \\ -3h_x & 4h_x^2 & 3h_x & -h_x^2 \\ -36 & 3h_x & 36 & 3h_x \\ -3h_x & -h_x^2 & 3h_x & 4h_x^2 \end{bmatrix} + \frac{2c_1^2 E D_6}{h_x^3} \begin{bmatrix} 6 & -3h_x & -6 & -3h_x \\ -3h_x & 2h_x^2 & 3h_x & h_x^2 \\ -6 & 3h_x & 6 & 3h_x \\ -3h_x & h_x^2 & 3h_x & 2h_x^2 \end{bmatrix}$$

$$\mathbf{K}^{12} = \frac{\hat{A}_s}{60} \begin{bmatrix} -6 & -48 & -6 \\ -7h_x & 4h_x & 3h_x \\ 6 & 48 & 6 \\ 3h_x & 4h_x & -7h_x \end{bmatrix} - \frac{c_1 E L_4}{h_x^2} \begin{bmatrix} 4 & -8 & 4 \\ -3h_x & 4h_x & -h_x \\ -4 & 8 & -4 \\ -h_x & 4h_x & -3h_x \end{bmatrix}$$

$$\mathbf{K}^{21} = \frac{\hat{A}_s}{60} \begin{bmatrix} -6 & -7h_x & 6 & 3h_x \\ -48 & 4h_x & 48 & 4h_x \\ -6 & 3h_x & 6 & -7h_x \end{bmatrix} - \frac{c_1 E L_4}{h_x^2} \begin{bmatrix} 4 & -3h_x & -4 & -h_x \\ -8 & 4h_x & 8 & 4h_x \\ 4 & -h_x & -4 & -3h_x \end{bmatrix}$$

$$\mathbf{K}^{22} = \frac{h_x \hat{A}_s}{30} \begin{bmatrix} 4 & 2 & -1 \\ 2 & 16 & 2 \\ -1 & 2 & 4 \end{bmatrix} + \frac{EM_2}{3h_x} \begin{bmatrix} 7 & -8 & 1 \\ -8 & 16 & -8 \\ 1 & -8 & 7 \end{bmatrix} \tag{2.85}$$

and the generalized force vectors can be expressed as

$$\begin{aligned} \mathbf{F}_1 &= \left\{ \begin{array}{cccc} \hat{Q}_1 & \hat{Q}_2 & \hat{Q}_5 & \hat{Q}_6 \end{array} \right\}^T \\ \mathbf{F}_2 &= \left\{ \begin{array}{ccc} \hat{Q}_3 & \hat{Q}_4 & \hat{Q}_7 \end{array} \right\}^T \end{aligned} \tag{2.86}$$

The matrices given by Eq. (2.84) can be assembled into the general form given by Eq. (2.79). We will address the specific form of q_i^1 in Sub-section 2.3.4.3.

2.3.2.4 The CPT

In this sub-section, we formulate the finite element formulation for the plate using the CPT, which requires the use of Hermite cubic interpolation of the transverse deflection (see Reddy [51, 49])

$$w(x, y, t) = \sum_{j=1}^{n} \Delta_j(t) \varphi_j(x, y) \tag{2.87}$$

Substituting above shape function in the weak form of the governing differential equation results in the following system of equations (see Reddy [51] for the details):

$$\mathbf{M}\ddot{\mathbf{\Delta}} + \mathbf{K}\mathbf{\Delta} = \mathbf{q} + \mathbf{F} \tag{2.88}$$

where

$$M_{ij} = \int_{\Omega_e} \left[I_0 \varphi_i \varphi_j + I_2 \left(\frac{\partial \varphi_i}{\partial x} \frac{\partial \varphi_j}{\partial x} + \frac{\partial \varphi_i}{\partial y} \frac{\partial \varphi_j}{\partial y} \right) \right] dxdy \tag{2.89}$$

$$\begin{aligned} K_{ij} = \int_{\Omega_e} D \Bigg[& \frac{\partial^2 \varphi_i}{\partial x^2} \frac{\partial^2 \varphi_j}{\partial x^2} + \nu \left(\frac{\partial^2 \varphi_i}{\partial x^2} \frac{\partial^2 \varphi_j}{\partial y^2} + \frac{\partial^2 \varphi_i}{\partial y^2} \frac{\partial^2 \varphi_j}{\partial x^2} \right) \\ & + \frac{\partial^2 \varphi_i}{\partial y^2} \frac{\partial^2 \varphi_j}{\partial y^2} + 4 \frac{\partial^2 \varphi_i}{\partial x \partial y} \frac{\partial^2 \varphi_j}{\partial x \partial y} \Bigg] dxdy \end{aligned} \tag{2.90}$$

$$q_i = \oint_{\Omega_e} p \varphi_i dxdy \tag{2.91}$$

So we have four degrees of freedom ($w, \partial w/\partial x, \partial w/\partial y$, and $\partial^2 w/\partial x \partial y$) at each node. This element is known to be the comforting element, CPT(C). The Hermite cubic interpolation functions of such elements are as follows:

$$\text{with} \quad \xi_1 = -1, \eta_1 = -1 \Rightarrow \begin{cases} \varphi_1 = (1/16)(\xi - 1)^2(-\xi - 2)(\eta - 1)^2(-\eta - 2) \\ \varphi_2 = (1/16)(\xi - 1)^2(-\xi - 1)(\eta - 1)^2(-\eta - 2) \\ \varphi_3 = (1/16)(\xi - 1)^2(-\xi - 2)(\eta - 1)^2(-\eta - 1) \\ \varphi_4 = -(1/16)(\xi - 1)^2(-\xi - 1)(\eta - 1)^2(-\eta - 1) \end{cases}$$

$$\text{with} \quad \xi_2 = +1, \eta_2 = -1 \Rightarrow \begin{cases} \varphi_5 = (1/16)(1 + \xi)^2(\xi - 2)(\eta - 1)^2(-\eta - 2) \\ \varphi_6 = -(1/16)(1 + \xi)^2(\xi - 1)(\eta - 1)^2(-\eta - 2) \\ \varphi_7 = (1/16)(1 + \xi)^2(\xi - 2)(\eta - 1)^2(-\eta - 1) \\ \varphi_8 = (1/16)(1 + \xi)^2(\xi - 1)(\eta - 1)^2(-\eta - 1) \end{cases}$$

$$\text{with} \quad \xi_3 = +1, \eta_3 = +1 \Rightarrow \begin{cases} \varphi_9 = (1/16)(1+\xi)^2(\xi-2)(\eta+1)^2(\eta-2) \\ \varphi_{10} = -(1/16)(1+\xi)^2(\xi-1)(\eta+1)^2(\eta-2) \\ \varphi_{11} = -(1/16)(1+\xi)^2(\xi-2)(\eta+1)^2(\eta-1) \\ \varphi_{12} = (1/16)(1+\xi)^2(\xi-1)(\eta+1)^2(\eta-1) \end{cases}$$

$$\text{with} \quad \xi_4 = -1, \eta_4 = +1 \Rightarrow \begin{cases} \varphi_{13} = (1/16)(\xi-1)^2(-\xi-2)(\eta+1)^2(\eta-2) \\ \varphi_{14} = (1/16)(\xi-1)^2(-\xi-1)(\eta+1)^2(\eta-2) \\ \varphi_{15} = -(1/16)(\xi-1)^2(-\xi-2)(\eta+1)^2(\eta-1) \\ \varphi_{16} = -(1/16)(\xi-1)^2(-\xi-1)(\eta+1)^2(\eta-1) \end{cases} \tag{2.92}$$

2.3.2.5 The FSDT

The finite element model of FSDT is obtained using the following interpolations

$$\begin{aligned} w(x,y,t) &= \sum_{j=1}^{n} \Delta_j(t)\psi_j^{(1)}(x,y) \\ \phi_x(x,y,t) &= \sum_{j=1}^{n} \Phi_j^x(t)\psi_j^{(2)}(x,y) \\ \phi_y(x,y,t) &= \sum_{j=1}^{n} \Phi_j^y(t)\psi_j^{(2)}(x,y) \end{aligned} \tag{2.93}$$

Since there are three degrees of freedom w, ϕ_x and ϕ_y at each node, the Lagrange interpolation of these primary variables will be used. Therefore, the interpolation functions are the same as Eq. (2.36). Inserting Eq. (2.36) into the weak form of the

governing equation, the following system of equations will be obtained.

$$\begin{bmatrix} \mathbf{M}^{11} & 0 & 0 \\ 0 & \mathbf{M}^{22} & 0 \\ 0 & 0 & \mathbf{M}^{33} \end{bmatrix} \begin{Bmatrix} \ddot{\mathbf{\Delta}} \\ \ddot{\mathbf{\Phi}}^x \\ \ddot{\mathbf{\Phi}}^y \end{Bmatrix} + \begin{bmatrix} \mathbf{K}^{11} & \mathbf{K}^{12} & \mathbf{K}^{13} \\ \mathbf{K}^{21} & \mathbf{K}^{22} & \mathbf{K}^{23} \\ \mathbf{K}^{31} & \mathbf{K}^{32} & \mathbf{K}^{33} \end{bmatrix} \begin{Bmatrix} \mathbf{\Delta} \\ \mathbf{\Phi}^x \\ \mathbf{\Phi}^y \end{Bmatrix} = \begin{Bmatrix} \mathbf{q}^1 \\ \mathbf{q}^2 \\ \mathbf{q}^3 \end{Bmatrix} + \begin{Bmatrix} \mathbf{F}^1 \\ \mathbf{F}^2 \\ \mathbf{F}^3 \end{Bmatrix} \tag{2.94}$$

where the nonzero mass matrices $\mathbf{M}^{\alpha\beta}$, stiffness matrices $\mathbf{K}^{\alpha\beta}$, and force vectors $\mathbf{q}^{\alpha}$ will be obtained using the following integrals:

$$\begin{aligned}
M_{ij}^{11} &= \int_{\Omega_e} I_0 \psi_i \psi_j dxdy \\
M_{ij}^{22} &= M_{ij}^{33} = \int_{\Omega_e} I_2 \psi_i \psi_j dxdy \qquad (2.95) \\
K_{ij}^{11} &= \int_{\Omega_e} GHK_s \left(\frac{\partial \psi_i}{\partial x}\frac{\partial \psi_j}{\partial x} + \frac{\partial \psi_i}{\partial y}\frac{\partial \psi_j}{\partial y} \right) dxdy \\
K_{ij}^{12} &= K_{ij}^{21} = \int_{\Omega_e} GHK_s \frac{\partial \psi_i}{\partial x} \psi_j dxdy \\
K_{ij}^{13} &= K_{ij}^{31} = \int_{\Omega_e} GHK_s \frac{\partial \psi_i}{\partial y} \psi_j dxdy \\
K_{ij}^{22} &= \int_{\Omega_e} \left(D\frac{\partial \psi_i}{\partial x}\frac{\partial \psi_j}{\partial x} + \frac{GH^3}{12}\frac{\partial \psi_i}{\partial y}\frac{\partial \psi_j}{\partial y} + GHK_s \psi_i \psi_j \right) dxdy \\
K_{ij}^{23} &= K_{ij}^{32} = \int_{\Omega_e} \left(\nu D\frac{\partial \psi_i}{\partial x}\frac{\partial \psi_j}{\partial y} + \frac{GH^3}{12}\frac{\partial \psi_i}{\partial y}\frac{\partial \psi_j}{\partial x} \right) dxdy \\
K_{ij}^{33} &= \int_{\Omega_e} \left(\frac{GH^3}{12}\frac{\partial \psi_i}{\partial x}\frac{\partial \psi_j}{\partial x} + D\frac{\partial \psi_i}{\partial y}\frac{\partial \psi_j}{\partial y} + GHK_s \psi_i \psi_j \right) dxdy \qquad (2.96) \\
q_i^1 &= \int_{\Omega_e} p \psi_i dxdy \qquad (2.97)
\end{aligned}$$

2.3.2.6 RSDT

In order to formulate the RSDT finite element model, the following interpolations are used for approximating the primary variables

$$\begin{aligned} w(x,y,t) &\approx \sum_{j=1}^{n} \Delta_j(t)\varphi_j(x,y) \\ \phi_x(x,y,t) &\approx \sum_{j=1}^{n} \Phi_j^x(t)\psi_j(x,y) \\ \phi_y(x,y,t) &\approx \sum_{j=1}^{n} \Phi_j^y(t)\psi_j(x,y) \end{aligned} \tag{2.98}$$

where φ_j's are the Hermite cubic interpolation functions of comforting element, RSDT(C), as presented in Eq. (2.92), and ψ_j's are the Lagrange interpolation functions defined in Eq. (2.36). Substituting Eq. (2.98) into the weak form of the RSDT yields

$$\begin{bmatrix} \mathbf{M}^{11} & \mathbf{M}^{12} & \mathbf{M}^{13} \\ \mathbf{M}^{21} & \mathbf{M}^{22} & \mathbf{M}^{23} \\ \mathbf{M}^{31} & \mathbf{M}^{32} & \mathbf{M}^{33} \end{bmatrix} \begin{Bmatrix} \ddot{\boldsymbol{\Delta}} \\ \ddot{\boldsymbol{\Phi}}^x \\ \ddot{\boldsymbol{\Phi}}^y \end{Bmatrix} + \begin{bmatrix} \mathbf{K}^{11} & \mathbf{K}^{12} & \mathbf{K}^{13} \\ \mathbf{K}^{21} & \mathbf{K}^{22} & \mathbf{K}^{23} \\ \mathbf{K}^{31} & \mathbf{K}^{32} & \mathbf{K}^{33} \end{bmatrix} \begin{Bmatrix} \boldsymbol{\Delta} \\ \boldsymbol{\Phi}^x \\ \boldsymbol{\Phi}^y \end{Bmatrix} = \begin{Bmatrix} \mathbf{q}^1 \\ \mathbf{q}^2 \\ \mathbf{q}^3 \end{Bmatrix} + \begin{Bmatrix} \mathbf{F}^1 \\ \mathbf{F}^2 \\ \mathbf{F}^3 \end{Bmatrix} \tag{2.99}$$

where the nonzero mass matrices $\mathbf{M}^{\alpha\beta}$, stiffness matrices $\mathbf{K}^{\alpha\beta}$ and force vectors $\mathbf{q}^{\alpha}$ can be obtained using the following integrals:

$$
\begin{aligned}
M_{ij}^{11} &= \int_{\Omega_e} I_0 \varphi_i \varphi_j + c^2 I_6 \left(\frac{\partial \varphi_i}{\partial x} \frac{\partial \varphi_j}{\partial x} + \frac{\partial \varphi_i}{\partial y} \frac{\partial \varphi_j}{\partial y} \right) dxdy \\
M_{ij}^{12} &= M_{ji}^{21} = \int_{\Omega_e} -cJ \frac{\partial \varphi_i}{\partial x} \psi_j dxdy \\
M_{ij}^{13} &= M_{ji}^{31} = \int_{\Omega_e} -cJ \frac{\partial \varphi_i}{\partial y} \psi_j dxdy \\
M_{ij}^{22} &= M_{ij}^{33} = \int_{\Omega_e} K \psi_i \psi_j dxdy
\end{aligned} \tag{2.100}
$$

$$
\begin{aligned}
K_{ij}^{11} &= \int_{\Omega_e} \left[A \left(\frac{\partial \varphi_i}{\partial x} \frac{\partial \varphi_j}{\partial x} + \frac{\partial \varphi_i}{\partial y} \frac{\partial \varphi_j}{\partial y} \right) + c^2 T \frac{\partial^2 \varphi_i}{\partial x^2} \left(\frac{\partial^2 \varphi_j}{\partial x^2} + \nu \frac{\partial^2 \varphi_j}{\partial y^2} \right) \right. \\
&\quad \left. + 2c^2 (1-\nu) T \frac{\partial^2 \varphi_i}{\partial x \partial y} \frac{\partial^2 \varphi_j}{\partial x \partial y} + c^2 T \frac{\partial^2 \varphi_i}{\partial y^2} \left(\nu \frac{\partial^2 \varphi_j}{\partial x^2} + \frac{\partial^2 \varphi_j}{\partial y^2} \right) \right] dxdy \\
K_{ij}^{12} &= K_{ji}^{21} = \int_{\Omega_e} \left(A \frac{\partial \phi_i}{\partial x} \psi_j - cF \frac{\partial^2 \phi_i}{\partial x^2} \frac{\partial \psi_j}{\partial x} \right. \\
&\quad \left. - c\nu F \frac{\partial^2 \phi_i}{\partial y^2} \frac{\partial \psi_j}{\partial y} - c(1-\nu) F \frac{\partial^2 \phi_i}{\partial x \partial y} \frac{\partial \psi_j}{\partial y} \right) dxdy \\
K_{ij}^{13} &= K_{ji}^{31} = \int_{\Omega_e} \left(A \frac{\partial \phi_i}{\partial y} \psi_j - c\nu F \frac{\partial^2 \phi_i}{\partial x^2} \frac{\partial \psi_j}{\partial x} \right. \\
&\quad \left. - cF \frac{\partial^2 \phi_i}{\partial y^2} \frac{\partial \psi_j}{\partial y} - c(1-\nu) F \frac{\partial^2 \phi_i}{\partial x \partial y} \frac{\partial \psi_j}{\partial x} \right) dxdy \\
K_{ij}^{22} &= \int_{\Omega_e} \left(D \frac{\partial \psi_i}{\partial x} \frac{\partial \psi_j}{\partial x} + \frac{(1-\nu)}{2} D \frac{\partial \psi_i}{\partial y} \frac{\partial \psi_j}{\partial y} + A \psi_i \psi_j \right) dxdy \\
K_{ij}^{23} &= K_{ji}^{32} = \int_{\Omega_e} D \left(\nu \frac{\partial \psi_i}{\partial x} \frac{\partial \psi_j}{\partial y} + \frac{(1-\nu)}{2} \frac{\partial \psi_i}{\partial y} \frac{\partial \psi_j}{\partial x} \right) dxdy \\
K_{ij}^{33} &= \int_{\Omega_e} \left(\frac{(1-\nu)}{2} D \frac{\partial \psi_i}{\partial x} \frac{\partial \psi_j}{\partial x} + D \frac{\partial \psi_i}{\partial y} \frac{\partial \psi_j}{\partial y} + A \psi_i \psi_j \right) dxdy
\end{aligned} \tag{2.101}
$$

$$q_i^1 = \int_{\Omega_e} p\psi_i dxdy \tag{2.102}$$

and the constants are

$$A = \frac{8}{15}GH, \quad D = \frac{17EH^3}{315\,(1-\nu^2)}, \quad F = \frac{EH^5}{105\,(1-\nu^2)}, \quad T = \frac{EH^7}{448\,(1-\nu^2)} \tag{2.103}$$

In Eq. (2.99), $\mathbf{F}^i$ are the generalized nodal force vectors. The general form of q_i^1 in Eq. (2.102) will be presented in Sub-section 2.3.4.6.

2.3.3 Interface Connecting Fluid and Solid Regions

In this sub-section, we address the coupling between the fluid and solid finite element models. At present, we note that the fluid and solid finite element models are coupled in the respective force vectors of each model. There are several approaches that can be used to solve the coupled equations. One approach is to assume a solution for one regime (say the fluid regime) and use this assumed solution as an input for solving the structure equations. The structure solution can then be used as an input for solving the fluid mechanics equations. This process is repeated until adequate convergence of solutions in both fluid and solid regimes is achieved. A more direct approach is to formulate the equations using the appropriate assumed displacements fields [see Eqs. (2.35), (2.44), (2.52), (2.64), (2.77), (2.87), and (2.93)] in the evaluation of $\mathbf{F}$ and $\mathbf{q}$. Using this approach results in the following finite element equations for the fluid region

$$\mathbf{CP} = \hat{\mathbf{f}} + \rho_f \mathbf{S}\ddot{\mathbf{\Delta}} + \mathbf{Q} \tag{2.104}$$

where $\mathbf{S}$ is called the solid-fluid coupling matrix and $\hat{\mathbf{f}}^e$ is a force vector in the fluid medium due to gravity. Equation (2.104) is valid for all three beam models and two

plate models considered in the present study. However, as we will see, the specific form of $\mathbf{S}$ is dictated by the chosen beam theory model; $\mathbf{S}$ and $\hat{\mathbf{f}}$ are therefore defined as

$$S_{ij} = \int_{x_a}^{x_b} \psi_i \chi_j dx, \quad \hat{f}_i = \int_{x_a}^{x_b} \rho_f g \psi_i dx \qquad \text{for beam} \tag{2.105}$$

$$S_{ij} = \int_{y_a}^{y_b} \int_{x_a}^{x_b} \psi_i \chi_j dx dy, \quad \hat{f}_i = \int_{y_a}^{y_b} \int_{x_a}^{x_b} \rho_f g \psi_i dx dy \qquad \text{for plate} \tag{2.106}$$

In Eq. (2.105), $\chi_j = \varphi_j$ for the EBT, RBT, CPT. In the case of the TBT and FSDT, $\chi_j = \psi_j^{(1)}$. $\mathbf{S}$ can be expressed explicitly for the present EBT and RBT formulations as formulations.

$$\mathbf{S} = \frac{h_x}{60} \begin{bmatrix} 21 & -3h_x & 9 & 2h_x \\ 9 & -2h_x & 21 & 3h_x \\ 0 & 0 & 0 & 0 \\ 0 & 0 & 0 & 0 \end{bmatrix} \tag{2.107}$$

For the TBT formulations the solid-fluid coupling matrix is given as

$$\mathbf{S} = \frac{h_x}{6} \begin{bmatrix} 2 & 1 \\ 1 & 2 \\ 0 & 0 \\ 0 & 0 \end{bmatrix} \tag{2.108}$$

2.3.4 Condensing out Pressure Degrees of Freedom

In the most general case, the fluid and structure (beam/plate) equations are coupled such that it is not possible to condense out the pressure degrees of freedom. As a result, the response of one domain cannot be determined independently from

that of the other. In the current study, however, we have formulated our model such that there is one row of fluid elements above the structure. Since the pressure is specified as zero along the top of each fluid element (i.e., $P_3 = P_4 = 0$ for beam problem and $P_5 = P_6 = P_7 = P_8 = 0$ for plate problem), it is possible to condense out the pressure degrees of freedom in the finite element model. The additional pressure degrees of freedom can be condensed out of the formulation by noting that the pressures can be expressed as

$$\mathbf{P} = \bar{\mathbf{C}}^{-1}\left(\hat{\mathbf{f}} + \rho_f \mathbf{S}\ddot{\mathbf{\Delta}} + \mathbf{Q}\right) \tag{2.109}$$

where $\bar{\mathbf{C}}^{-1}$ is defined as

$$\bar{\mathbf{C}}^{-1} = \frac{2\alpha}{4\alpha^2+1}\begin{bmatrix} 2\left(1+\alpha^2\right) & 2\alpha^2-1 & 0 & 0 \\ 2\alpha^2-1 & 2\left(1+\alpha^2\right) & 0 & 0 \\ 0 & 0 & 0 & 0 \\ 0 & 0 & 0 & 0 \end{bmatrix}, \quad \alpha = \frac{h_z}{h_x} \tag{2.110}$$

Equation (2.109) can be utilized in conjunction with the structure models to express the global finite element equations of the system solely in terms of generalized structure displacements.

2.3.4.1 Euler-Bernoulli Formulation

Condensing out pressure degree of freedom, the finite element equations for the EBT can be expressed as

$$m_s \mathbf{M}\ddot{\mathbf{\Delta}} + \mathbf{K}\mathbf{\Delta} = -W\mathbf{S}^T\mathbf{P} + \mathbf{F} \tag{2.111}$$

Using Eq. (2.109) allows Eq. (2.111) to be expressed as

$$\left(m_s\mathbf{M} + m_f\mathbf{S}^T\bar{\mathbf{C}}^{-1}\mathbf{S}\right)\ddot{\mathbf{\Delta}} + \mathbf{K}\mathbf{\Delta} = \mathbf{F} - W\mathbf{S}^T\bar{\mathbf{C}}^{-1}\left(\hat{\mathbf{f}} + \mathbf{Q}\right) \tag{2.112}$$

where $m_f = W\rho_f$ and $m_s = HW\rho_s$. Equation (2.112) can be expressed in compact form as

$$\hat{\mathbf{M}}\ddot{\mathbf{U}} + \hat{\mathbf{K}}\mathbf{U} = \hat{\mathbf{F}} \tag{2.113}$$

The general mass matrix $\hat{\mathbf{M}}$, stiffness matrix $\hat{\mathbf{K}}$, force vector $\hat{\mathbf{F}}$ and displacement $\mathbf{U}$ vector per Eq. (2.113) are defined as

$$\begin{aligned}
\hat{\mathbf{M}} &= m_s\mathbf{M} + m_f\mathbf{S}^T\bar{\mathbf{C}}^{-1}\mathbf{S} \\
\hat{\mathbf{K}} &= \mathbf{K} \\
\hat{\mathbf{F}} &= \mathbf{F} - W\mathbf{S}^T\bar{\mathbf{C}}^{-1}\left(\hat{\mathbf{f}} + \mathbf{Q}\right) \\
\mathbf{U} &= \mathbf{\Delta}
\end{aligned} \tag{2.114}$$

In Eq. (2.114), $\hat{\mathbf{K}}$ is given by Eq. (2.60). Equation (2.113) is the standard form of the element equations of motion, with

$$\mathbf{M}_{\mathrm{a}} = m_f\mathbf{S}^T\bar{\mathbf{C}}^{-1}\mathbf{S} \tag{2.115}$$

being the added mass due to the presence of fluid. Thus, the fluid-structure interaction problem is formulated as one in which the influence of fluid is represented as an added mass to the structural problem. The *added mass* matrix $\hat{\mathbf{M}}_{\mathrm{a}}$ for the

Euler-Bernoulli finite element model is given by

$$\hat{\mathbf{M}}_{\mathrm{a}} = c_0 \begin{bmatrix} 666 + 1800\alpha^2 & -h_x\left(93 + 300\alpha^2\right) & 234 + 1800\alpha^2 & h_x\left(57 + 300\alpha^2\right) \\ -h_x\left(93 + 300\alpha^2\right) & h_x^2\left(14 + 50\alpha^2\right) & -h_x\left(57 + 300\alpha^2\right) & -h_x^2\left(11 + 50\alpha^2\right) \\ 234 + 1800\alpha^2 & -h_x\left(57 + 300\alpha^2\right) & 666 + 1800\alpha^2 & h_x\left(93 + 300\alpha^2\right) \\ h_x\left(57 + 300\alpha^2\right) & -h_x^2\left(11 + 50\alpha^2\right) & h_x\left(93 + 300\alpha^2\right) & h_x^2\left(14 + 50\alpha^2\right) \end{bmatrix} \tag{2.116}$$

$$c_0 = \frac{m_f \alpha h_x^2}{1800\left(1 + 4\alpha^2\right)} \tag{2.117}$$

2.3.4.2 Timoshenko Formulation

To determine the element equations for the TBT, we follow the same procedure employed in the previous sub-section for the EBT. Equation (2.66) can be expressed using the solid-fluid coupling matrix $\mathbf{S}$ as

$$m_s \begin{bmatrix} \mathbf{M}^{11} & \mathbf{M}^{12} \\ \mathbf{M}^{21} & \mathbf{M}^{22} \end{bmatrix} \begin{Bmatrix} \ddot{\boldsymbol{\Delta}} \\ \ddot{\boldsymbol{\Phi}} \end{Bmatrix} + \begin{bmatrix} \mathbf{K}^{11} & \mathbf{K}^{12} \\ \mathbf{K}^{21} & \mathbf{K}^{22} \end{bmatrix} \begin{Bmatrix} \boldsymbol{\Delta} \\ \boldsymbol{\Phi} \end{Bmatrix} = \begin{Bmatrix} -W\mathbf{S}^T\mathbf{P}^e \\ 0 \end{Bmatrix} + \begin{Bmatrix} \mathbf{F}^1 \\ \mathbf{F}^2 \end{Bmatrix} \tag{2.118}$$

Employing Eq. (2.109) allows Eq. (2.118) to be expressed as

$$\begin{aligned} m_s \begin{bmatrix} \bar{\mathbf{M}}^{11} & \mathbf{M}^{12} \\ \mathbf{M}^{21} & \mathbf{M}^{22} \end{bmatrix} \begin{Bmatrix} \ddot{\boldsymbol{\Delta}} \\ \ddot{\boldsymbol{\Phi}} \end{Bmatrix} + \begin{bmatrix} \mathbf{K}^{11} & \mathbf{K}^{12} \\ \mathbf{K}^{21} & \mathbf{K}^{22} \end{bmatrix} \begin{Bmatrix} \boldsymbol{\Delta} \\ \boldsymbol{\Phi} \end{Bmatrix} \\ = \begin{Bmatrix} -W\mathbf{S}^T\bar{\mathbf{C}}^{-1}\left(\hat{\mathbf{f}} + \mathbf{Q}\right) \\ 0 \end{Bmatrix} + \begin{Bmatrix} \mathbf{F}^1 \\ \mathbf{F}^2 \end{Bmatrix} \end{aligned} \tag{2.119}$$

where

$$\bar{\mathbf{M}}^{11} = \mathbf{M}^{11} + \frac{1}{m_s}\mathbf{M}_{\mathrm{a}} \tag{2.120}$$

and as EBT the added mass matrix $\mathbf{M}_{\mathrm{a}}$ is expressed as

$$\mathbf{M}_{\mathrm{a}} = m_f \mathbf{S}^T \bar{\mathbf{C}}^{-1} \mathbf{S} \tag{2.121}$$

It is convenient to rearrange the TBT finite element equations (i.e., Eq. (2.119)) into the general form given by Eq. (2.113). The generalized matrices can be expressed as

$$\begin{aligned}
\hat{\mathbf{K}} &= \frac{2EI}{\mu h_x^3}\begin{bmatrix} 6 & -3h_x & -6 & -3h_x \\ -3h_x & h_x^2(1.5+6\Lambda) & 3h_x & h_x^2(1.5-6\Lambda) \\ -6 & 3h_x & 6 & 3h_x \\ -3h_x & h_x^2(1.5-6\Lambda) & 3h_x & h_x^2(1.5+6\Lambda) \end{bmatrix} \\
\bar{\mathbf{M}} &= \frac{h_x}{6}\begin{bmatrix} 2 & 0 & 1 & 0 \\ 0 & \frac{H^2}{6} & 0 & \frac{H^2}{12} \\ 1 & 0 & 2 & 0 \\ 0 & \frac{H^2}{12} & 0 & \frac{H^2}{6} \end{bmatrix} \\
\bar{\mathbf{M}}_{\mathrm{a}} &= \frac{m_f \alpha h_x^2}{6(1+4\alpha^2)}\begin{bmatrix} 2(1+3\alpha^2) & 0 & 1+6\alpha^2 & 0 \\ 0 & 0 & 0 & 0 \\ 1+6\alpha^2 & 0 & 2(1+3\alpha^2) & 0 \\ 0 & 0 & 0 & 0 \end{bmatrix}
\end{aligned} \tag{2.122}$$

where $\mathbf{U} = \left\{ \begin{array}{cccc} \Delta_1 & \Phi_1 & \Delta_2 & \Phi_2 \end{array} \right\}^T$ and

$$\hat{\mathbf{M}} = \bar{\mathbf{M}} + \bar{\mathbf{M}}_{\mathrm{a}} \tag{2.123}$$

The numerical constants Λ and μ are defined as

$$\Lambda = \frac{EI}{GAK_s h_x^2}, \mu = 12\Lambda \tag{2.124}$$

2.3.4.3 Reddy Third-order Formulation

The element matrices of the RBT are constructed in the same way as for the previous two theories. The element equations for the RBT model can be expressed as

$$\left[\begin{array}{cc} \bar{\mathbf{M}}^{11} & \mathbf{M}^{12} \\ \mathbf{M}^{21} & \mathbf{M}^{22} \end{array} \right] \left\{ \begin{array}{c} \ddot{\boldsymbol{\Delta}} \\ \ddot{\boldsymbol{\Phi}} \end{array} \right\} + \left[\begin{array}{cc} \mathbf{K}^{11} & \mathbf{K}^{12} \\ \mathbf{K}^{21} & \mathbf{K}^{22} \end{array} \right] \left\{ \begin{array}{c} \boldsymbol{\Delta} \\ \boldsymbol{\Phi} \end{array} \right\} = \left\{ \begin{array}{c} -W\mathbf{S}^T\bar{\mathbf{C}}^{-1}\left(\hat{\mathbf{f}} + \mathbf{Q}\right) \\ \mathbf{f}^2 \end{array} \right\} \tag{2.125}$$

where

$$\bar{\mathbf{M}}^{11} = \mathbf{M}^{11} + \mathbf{M}_{\mathrm{a}} \tag{2.126}$$

and the added mass matrix $\mathbf{M}_{\mathrm{a}}$ is again defined as

$$\mathbf{M}_{\mathrm{a}} = m_f \mathbf{S}^T \bar{\mathbf{C}}^{-1} \mathbf{S} \tag{2.127}$$

As in the case of the Timoshenko formulation, it is useful to rearrange the equations of the RBT into the form given by Eq. (2.113). The resulting matrices can be

expressed as

$$\hat{\mathbf{M}} = \bar{\mathbf{M}} + \mathbf{M}_{\mathrm{a}}^{e}, \bar{\mathbf{M}} = \begin{bmatrix} \widehat{\mathbf{M}} & \breve{\mathbf{M}} \end{bmatrix}, \ \hat{\mathbf{K}} = \begin{bmatrix} \widehat{\mathbf{K}} & \breve{\mathbf{K}} \end{bmatrix} \tag{2.128}$$

where $\widehat{\mathbf{M}}$, $\breve{\mathbf{M}}$, $\widehat{\mathbf{K}}$, $\breve{\mathbf{K}}$, and $\mathbf{M}_{\mathrm{a}}$ are expressed as

$$\widehat{\mathbf{M}} = \begin{bmatrix} \frac{13I_0h_x}{35} + \frac{6I_6c_1^2}{5h_x} & -\frac{11I_0h_x^2}{210} - \frac{I_6c_1^2}{10} & \frac{J_4c_1}{10} & \frac{4J_4c_1}{5} \\ -\frac{11I_0h_x^2}{210} - \frac{I_6c_1^2}{10} & \frac{I_0h_x^3}{105} + \frac{2I_6h_xc_1^2}{15} & \frac{7J_4h_xc_1}{60} & -\frac{J_4h_xc_1}{15} \\ \frac{J_4c_1}{10} & \frac{7J_4h_xc_1}{60} & \frac{2K_2h_x}{15} & \frac{K_2h_x}{15} \\ \frac{4J_4c_1}{5} & -\frac{J_4h_xc_1}{15} & \frac{K_2h_x}{15} & \frac{8K_2h_x}{15} \\ \frac{9I_0h_x}{70} - \frac{6I_6c_1^2}{5h_x} & \frac{I_6c_1^2}{10} - \frac{13I_0h_x^2}{420} & -\frac{J_4c_1}{10} & -\frac{4J_4c_1}{5} \\ \frac{13I_0h_x^2}{420} - \frac{I_6c_1^2}{10} & -\frac{I_0h_x^3}{140} - \frac{I_6h_xc_1^2}{30} & \frac{J_4h_xc_1}{20} & -\frac{J_4h_xc_1}{15} \\ \frac{J_4c_1}{10} & -\frac{J_4h_xc_1}{20} & -\frac{K_2h_x}{30} & \frac{K_2h_x}{15} \end{bmatrix} \tag{2.129}$$

$$\breve{\mathbf{M}} = \begin{bmatrix} \frac{9I_0h_x}{70} - \frac{6I_6c_1^2}{5h_x} & \frac{13I_0h_x^2}{420} - \frac{I_6c_1^2}{10} & \frac{J_4c_1}{10} \\ \frac{I_6c_1^2}{10} - \frac{13I_0h_x^2}{420} & -\frac{I_0h_x^3}{140} - \frac{I_6h_xc_1^2}{30} & -\frac{J_4h_xc_1}{20} \\ -\frac{J_4c_1}{10} & \frac{J_4h_xc_1}{20} & \frac{K_2h_x}{30} \\ -\frac{4J_4c_1}{5} & -\frac{J_4h_xc_1}{15} & \frac{K_2h_x}{15} \\ \frac{13I_0h_x}{35} + \frac{6I_6c_1^2}{5h_x} & \frac{11I_0h_x^2}{210} + \frac{I_6c_1^2}{10} & -\frac{J_4c_1}{10} \\ \frac{11I_0h_x^2}{210} + \frac{I_6c_1^2}{10} & \frac{I_0h_x^3}{105} + \frac{2I_6h_xc_1^2}{15} & \frac{7J_4h_xc_1}{60} \\ -\frac{J_4c_1}{10} & \frac{7J_4h_xc_1}{60} & \frac{2K_2h_x}{15} \end{bmatrix} \tag{2.130}$$

$$\widehat{\mathbf{K}} = \begin{bmatrix} \frac{6\hat{A}_s}{5h_x} + \frac{12D_6Ec_1^2}{h_x^3} & -\frac{\hat{A}_s}{10} - \frac{6D_6Ec_1^2}{h_x^2} & -\frac{\hat{A}_s}{10} - \frac{4EL_4c_1}{h_x^2} & \frac{8EL_4c_1}{h_x^2} - \frac{4\hat{A}_s}{5} \\ -\frac{\hat{A}_s}{10} - \frac{6D_6Ec_1^2}{h_x^2} & \frac{2\hat{A}_sh_x}{15} - \frac{4D_6Ec_1^2}{h_x} & \frac{3EL_4c_1}{h_x} - \frac{7\hat{A}_sh_x}{60} & \frac{\hat{A}_sh_x}{15} - \frac{4EL_4c_1}{h_x} \\ -\frac{\hat{A}_s}{10} - \frac{4EL_4c_1}{h_x^2} & \frac{3EL_4c_1}{h_x} - \frac{7\hat{A}_sh_x}{60} & \frac{2\hat{A}_sh_x}{15} + \frac{7EM_2}{3h_x} & \frac{\hat{A}_sh_x}{15} - \frac{8EM_2}{3h_x} \\ \frac{8EL_4c_1}{h_x^2} - \frac{4\hat{A}_s}{5} & \frac{\hat{A}_sh_x}{15} - \frac{4EL_4c_1}{h_x} & \frac{\hat{A}_sh_x}{15} - \frac{8EM_2}{3h_x} & \frac{8\hat{A}_sh_x}{15} + \frac{16EM_2}{3h_x} \\ -\frac{6\hat{A}_s}{5h_x} - \frac{12D_6Ec_1^2}{h_x^3} & \frac{\hat{A}_s}{10} + \frac{6D_6Ec_1^2}{h_x^2} & \frac{\hat{A}_s}{10} + \frac{4EL_4c_1}{h_x^2} & \frac{4\hat{A}_s}{5} - \frac{8EL_4c_1}{h_x^2} \\ -\frac{\hat{A}_s}{10} - \frac{6D_6Ec_1^2}{h_x^2} & \frac{2D_6Ec_1^2}{h_x} - \frac{\hat{A}_sh_x}{30} & \frac{\hat{A}_sh_x}{20} + \frac{EL_4c_1}{h_x} & \frac{\hat{A}_sh_x}{15} - \frac{4EL_4c_1}{h_x} \\ -\frac{\hat{A}_s}{10} - \frac{4EL_4c_1}{h_x^2} & \frac{\hat{A}_sh_x}{20} + \frac{EL_4c_1}{h_x} & \frac{EM_2}{3h_x} - \frac{\hat{A}_sh_x}{30} & \frac{\hat{A}_sh_x}{15} - \frac{8EM_2}{3h_x} \end{bmatrix} \tag{2.131}$$

$$\widecheck{\mathbf{K}} = \begin{bmatrix} -\frac{6\hat{A}_s}{5h_x} - \frac{12D_6Ec_1^2}{h_x^3} & -\frac{\hat{A}_s}{10} - \frac{6D_6Ec_1^2}{h_x^2} & -\frac{\hat{A}_s}{10} - \frac{4EL_4c_1}{h_x^2} \\ \frac{\hat{A}_s}{10} + \frac{6D_6Ec_1^2}{h_x^2} & \frac{2D_6Ec_1^2}{h_x} - \frac{\hat{A}_sh_x}{30} & \frac{\hat{A}_sh_x}{20} + \frac{EL_4c_1}{h_x} \\ \frac{\hat{A}_s}{10} + \frac{4EL_4c_1}{h_x^2} & \frac{\hat{A}_sh_x}{20} + \frac{EL_4c_1}{h_x} & \frac{EM_2}{3h_x} - \frac{\hat{A}_sh_x}{30} \\ \frac{4\hat{A}_s}{5} - \frac{8EL_4c_1}{h_x^2} & \frac{\hat{A}_sh_x}{15} - \frac{4EL_4c_1}{h_x} & \frac{\hat{A}_sh_x}{15} - \frac{8EM_2}{3h_x} \\ \frac{6\hat{A}_s}{5h_x} + \frac{12D_6Ec_1^2}{h_x^3} & \frac{\hat{A}_s}{10} + \frac{6D_6Ec_1^2}{h_x^2} & \frac{\hat{A}_s}{10} + \frac{4EL_4c_1}{h_x^2} \\ \frac{\hat{A}_s}{10} + \frac{6D_6Ec_1^2}{h_x^2} & \frac{2\hat{A}_sh_x}{15} + \frac{4D_6Ec_1^2}{h_x} & \frac{3EL_4c_1}{h_x} - \frac{7\hat{A}_sh_x}{60} \\ \frac{\hat{A}_s}{10} + \frac{4EL_4c_1}{h_x^2} & \frac{3EL_4c_1}{h_x} - \frac{7\hat{A}_sh_x}{60} & \frac{2\hat{A}_sh_x}{15} + \frac{7EM_2}{3h_x} \end{bmatrix} \tag{2.132}$$

$$\mathbf{M}_{\mathrm{a}} = c_0 \begin{bmatrix} 666 + 1800\alpha^2 & -h_x\left(93 + 300\alpha^2\right) & 0 & 0 & 234 + 1800\alpha^2 & h_x\left(57 + 300\alpha^2\right) & 0 \\ -h_x\left(93 + 300\alpha^2\right) & h_x^2\left(14 + 50\alpha^2\right) & 0 & 0 & -h_x\left(57 + 300\alpha^2\right) & -h_x^2\left(11 + 50\alpha^2\right) & 0 \\ 0 & 0 & 0 & 0 & 0 & 0 & 0 \\ 0 & 0 & 0 & 0 & 0 & 0 & 0 \\ 234 + 1800\alpha^2 & -h_x\left(57 + 300\alpha^2\right) & 0 & 0 & 666 + 1800\alpha^2 & h_x\left(93 + 300\alpha^2\right) & 0 \\ h_x\left(57 + 300\alpha^2\right) & -h_x^2\left(11 + 50\alpha^2\right) & 0 & 0 & h_x\left(93 + 300\alpha^2\right) & h_x^2\left(14 + 50\alpha^2\right) & 0 \\ 0 & 0 & 0 & 0 & 0 & 0 & 0 \end{bmatrix} \tag{2.133}$$

$$\mathbf{U} = \left\{ \begin{array}{ccccccc} \Delta_1 & \Delta_2 & \Phi_1 & \Phi_2 & \Delta_3 & \Delta_4 & \Phi_3 \end{array} \right\}^T \tag{2.134}$$

2.3.4.4 Classical Plate Formulation

The finite element equations for the CPT can be expressed as

$$\mathbf{M}\ddot{\boldsymbol{\Delta}} + \mathbf{K}\boldsymbol{\Delta} = -\mathbf{S}^T\mathbf{P} + \mathbf{F} \tag{2.135}$$

Using Eq. (2.109) allows Eq. (2.135) to be expressed as

$$\left(\mathbf{M} + \rho_f \mathbf{S}^T \bar{\mathbf{C}}^{-1}\mathbf{S}\right)\ddot{\boldsymbol{\Delta}} + \mathbf{K}\boldsymbol{\Delta} = \mathbf{F} - \mathbf{S}^T\bar{\mathbf{C}}^{-1}\left(\hat{\mathbf{f}} + \mathbf{Q}\right) \tag{2.136}$$

Equation (2.136) can be expressed in compact form as

$$\hat{\mathbf{M}}\ddot{\mathbf{U}} + \hat{\mathbf{K}}\mathbf{U} = \hat{\mathbf{F}} \tag{2.137}$$

The general mass matrix $\hat{\mathbf{M}}$, stiffness matrix $\hat{\mathbf{K}}$, force vector $\hat{\mathbf{F}}$ and displacement vector $\mathbf{U}$ per Eq. (2.137) are defined as

$$\begin{aligned}
\hat{\mathbf{M}} &= \mathbf{M} + \rho_f \mathbf{S}^T \bar{\mathbf{C}}^{-1}\mathbf{S} \\
\hat{\mathbf{K}} &= \mathbf{K} \\
\hat{\mathbf{F}} &= \mathbf{F} - \mathbf{S}^T\bar{\mathbf{C}}^{-1}\left(\hat{\mathbf{f}} + \mathbf{Q}\right) \\
\mathbf{U} &= \boldsymbol{\Delta}
\end{aligned} \tag{2.138}$$

2.3.4.5 First-order Shear Deformation Formulation

The finite element equations for the FSDT can be expressed as

$$\begin{bmatrix} \mathbf{M}^{11} & 0 & 0 \\ 0 & \mathbf{M}^{22} & 0 \\ 0 & 0 & \mathbf{M}^{33} \end{bmatrix} \begin{Bmatrix} \ddot{\boldsymbol{\Delta}} \\ \ddot{\boldsymbol{\Phi}}^x \\ \ddot{\boldsymbol{\Phi}}^y \end{Bmatrix} + \begin{bmatrix} \mathbf{K}^{11} & \mathbf{K}^{12} & \mathbf{K}^{13} \\ \mathbf{K}^{21} & \mathbf{K}^{22} & \mathbf{K}^{23} \\ \mathbf{K}^{31} & \mathbf{K}^{32} & \mathbf{K}^{33} \end{bmatrix} \begin{Bmatrix} \boldsymbol{\Delta} \\ \boldsymbol{\Phi}^x \\ \boldsymbol{\Phi}^y \end{Bmatrix} = \begin{Bmatrix} -\mathbf{S}^T\mathbf{P} \\ 0 \\ 0 \end{Bmatrix} + \begin{Bmatrix} \mathbf{F}^1 \\ \mathbf{F}^2 \\ \mathbf{F}^3 \end{Bmatrix} \tag{2.139}$$

Using Eq. (2.109) allows Eq. (2.139) to be expressed as

$$\begin{bmatrix} \bar{\mathbf{M}}^{11} & 0 & 0 \\ 0 & \mathbf{M}^{22} & 0 \\ 0 & 0 & \mathbf{M}^{33} \end{bmatrix} \begin{Bmatrix} \ddot{\boldsymbol{\Delta}} \\ \ddot{\boldsymbol{\Phi}}^x \\ \ddot{\boldsymbol{\Phi}}^y \end{Bmatrix} + \begin{bmatrix} \mathbf{K}^{11} & \mathbf{K}^{12} & \mathbf{K}^{13} \\ \mathbf{K}^{21} & \mathbf{K}^{22} & \mathbf{K}^{23} \\ \mathbf{K}^{31} & \mathbf{K}^{32} & \mathbf{K}^{33} \end{bmatrix} \begin{Bmatrix} \boldsymbol{\Delta} \\ \boldsymbol{\Phi}^x \\ \boldsymbol{\Phi}^y \end{Bmatrix} = \begin{Bmatrix} -\mathbf{S}^T\bar{\mathbf{C}}^{-1}\left(\hat{\mathbf{f}}^e + \mathbf{Q}^e\right) \\ 0 \\ 0 \end{Bmatrix} + \begin{Bmatrix} \mathbf{F}^1 \\ \mathbf{F}^2 \\ \mathbf{F}^3 \end{Bmatrix} \tag{2.140}$$

where

$$\bar{\mathbf{M}}^{11} = \mathbf{M}^{11} + \rho_f \mathbf{S}^T\bar{\mathbf{C}}^{-1}\mathbf{S} \tag{2.141}$$

2.3.4.6 Reddy Third-order Shear Deformation Formulation

The finite element equations for the RSDT will be

$$\begin{bmatrix} \mathbf{M}^{11} & \mathbf{M}^{12} & \mathbf{M}^{13} \\ \mathbf{M}^{21} & \mathbf{M}^{22} & 0 \\ \mathbf{M}^{31} & 0 & \mathbf{M}^{33} \end{bmatrix} \begin{Bmatrix} \ddot{\boldsymbol{\Delta}} \\ \ddot{\boldsymbol{\Phi}}^x \\ \ddot{\boldsymbol{\Phi}}^y \end{Bmatrix} + \begin{bmatrix} \mathbf{K}^{11} & \mathbf{K}^{12} & \mathbf{K}^{13} \\ \mathbf{K}^{21} & \mathbf{K}^{22} & \mathbf{K}^{23} \\ \mathbf{K}^{31} & \mathbf{K}^{32} & \mathbf{K}^{33} \end{bmatrix} \begin{Bmatrix} \boldsymbol{\Delta} \\ \boldsymbol{\Phi}^x \\ \boldsymbol{\Phi}^y \end{Bmatrix} = \begin{Bmatrix} -\mathbf{S}^T\mathbf{P} \\ 0 \\ 0 \end{Bmatrix} + \begin{Bmatrix} \mathbf{F}^1 \\ \mathbf{F}^2 \\ \mathbf{F}^3 \end{Bmatrix} \tag{2.142}$$

which becomes

$$\begin{bmatrix} \bar{\mathbf{M}}^{11} & \mathbf{M}^{12} & \mathbf{M}^{13} \\ \mathbf{M}^{21} & \mathbf{M}^{22} & 0 \\ \mathbf{M}^{31} & 0 & \mathbf{M}^{33} \end{bmatrix} \begin{Bmatrix} \ddot{\boldsymbol{\Delta}} \\ \ddot{\boldsymbol{\Phi}}^x \\ \ddot{\boldsymbol{\Phi}}^y \end{Bmatrix} + \begin{bmatrix} \mathbf{K}^{11} & \mathbf{K}^{12} & \mathbf{K}^{13} \\ \mathbf{K}^{21} & \mathbf{K}^{22} & \mathbf{K}^{23} \\ \mathbf{K}^{31} & \mathbf{K}^{32} & \mathbf{K}^{33} \end{bmatrix} \begin{Bmatrix} \boldsymbol{\Delta} \\ \boldsymbol{\Phi}^x \\ \boldsymbol{\Phi}^y \end{Bmatrix} = \begin{Bmatrix} -\mathbf{S}^T\bar{\mathbf{C}}^{-1}\left(\hat{\mathbf{f}} + \mathbf{Q}\right) \\ 0 \\ 0 \end{Bmatrix} + \begin{Bmatrix} \mathbf{F}^1 \\ \mathbf{F}^2 \\ \mathbf{F}^3 \end{Bmatrix} \tag{2.143}$$

using Eq. (2.109). In Eq. (2.143), $\bar{\mathbf{M}}^{11}$ is

$$\bar{\mathbf{M}}^{11} = \mathbf{M}^{11} + \rho_f \mathbf{S}^T\bar{\mathbf{C}}^{-1}\mathbf{S} \tag{2.144}$$

2.3.4.7 Fully Discretized Equations

The global finite element equations can be assembled into the form

$$\mathbf{M}\ddot{\mathbf{\Delta}} + \mathbf{K}\mathbf{\Delta} = \mathbf{F} \tag{2.145}$$

by using the standard global finite element assembly procedure. We note that the eigenvalue problem associated with free vibration of the structure (beam/plate) is given by

$$\left(-\omega^2\mathbf{M} + \mathbf{K}\right)\mathbf{\Delta}_0 = 0 \tag{2.146}$$

The natural frequencies of this problem are expected to be lower than those without influence of the fluid, due to the added mass.

2.4 Numerical Results

In this sub-section, some numerical results for beam and plate structures in contact with a fluid medium are presented to bring out the influence of the fluid-structure interaction on natural frequencies and mode shapes. The effect of the transverse shear deformation is also studied through the use of the first-order and third-order shear deformation theories for beams and plates.

2.4.1 Beam Structure

The following parameters are used in the beam problem:

$$\begin{gathered} E = 200\text{GPa},\ \nu = 0.25,\ \rho_s = 5000\text{kg/m}^3 \\ W = 0.05\text{m},\ H = 0.01\text{m},\ h_z = 0.02\text{m} \end{gathered} \tag{2.147}$$

and we consider L and ρ_f to be varied for different cases. The numerical simulations are performed using the three beam theories EBT, TBT, RBT, and for two different meshes of 20 and 100 elements, for three different boundary conditions; a cantilever beam, a clamped-clamped beam, and a simply supported beam. The corresponding results are presented in Tables 2.1 through 2.6 for a cantilever beam, in Tables 2.7 through 2.12 for a clamped-clamped beam, and in Tables 2.13 through 2.18 for a simply supported beam. The natural frequencies are presented in the following nondimensional form

$$\bar{\omega} = \omega \times L^2 \sqrt{\frac{m_s}{EI}} \tag{2.148}$$

and the results are provided for various density ratios ($\beta = \rho_f/\rho_s$) and beam length-to-height ratios (L/H). We included the rotary inertia term in all simulations. From these results, it can be seen that increasing fluid density ρ_f, or immersion depth h_z, will decrease the natural frequencies for a specified (L/H) ratio and a fixed number of elements. This result can be physically interpreted as follows: since the fluid density ρ_f and the immersion depth h_z serve as an added mass in the mass matrix of the system equations and do not affect the stiffness matrix, increasing either of these parameter decreases the natural frequencies.

Comparing corresponding numerical results of Tables 2.1 through 2.18 indicates that EBT and RBT converge to final values with fewer number of elements compared to TBT which requires more number of elements to converge. Moreover, for a specified L/H ratio and β value, the convergence rate decreases for higher natural frequencies.

As it can be observed, for the thin beam limit all of the three theories converge to the unique solution. However, as L/H ratio decreases, i.e. the beam becomes

Table 2.1: Comparison of nondimonsional natural frequencies of a cantilever beam in contact with a fluid medium using EBT with 20 elements.

		EBT		
L/H	$\bar{\omega}_N$	$\beta = 0$	$\beta = 0.04$	$\beta = 0.08$
100	$\bar{\omega}_1$	3.516	3.383	3.265
	$\bar{\omega}_2$	22.032	21.203	20.462
	$\bar{\omega}_3$	61.678	59.374	57.310
	$\bar{\omega}_4$	120.838	116.362	112.350
	$\bar{\omega}_5$	199.704	192.395	185.833
10	$\bar{\omega}_1$	3.509	3.495	3.482
	$\bar{\omega}_2$	21.743	21.659	21.576
	$\bar{\omega}_3$	59.802	59.581	59.362
	$\bar{\omega}_4$	114.296	113.898	113.503
	$\bar{\omega}_5$	183.245	182.650	182.061

thicker, the EBT is not valid anymore. This statement is exactly consistent with definition.

The mode shapes are also obtained using EBT, TBT and RBT for $L/H = 100$ and a mesh of 100 elements. It is concluded that the corresponding mode shapes of all three beam theories are very similar to each other; and hence, we plotted the first four mode shapes obtained using RBT in Figs. 2.6, 2.8, and 2.9 for three boundary conditions. Now in order to see the effect of fluid-structure interaction on the beam mode shapes for different L/H ratios ($L/H = 10$ and $L/H = 100$), we plotted the first four mode shapes for $\beta = 0$ (without fluid interaction) and for $\beta = 0.04$ (with fluid interaction) in Fig. 2.7 for a cantilever beam. From this figure, it can be realized that by increasing L/H ratio, i.e. making the beam thinner, the fluid medium affects the mode shapes more considerably.

Table 2.2: Comparison of nondimonsional natural frequencies of a cantilever beam in contact with a fluid medium using EBT with 100 elements.

		EBT		
L/H	$\bar{\omega}_N$	$\beta = 0$	$\beta = 0.04$	$\beta = 0.08$
100	$\bar{\omega}_1$	3.516	3.383	3.265
	$\bar{\omega}_2$	22.032	21.203	20.462
	$\bar{\omega}_3$	61.677	59.372	57.308
	$\bar{\omega}_4$	120.830	116.352	112.337
	$\bar{\omega}_5$	199.670	192.349	185.779
10	$\bar{\omega}_1$	3.509	3.495	3.482
	$\bar{\omega}_2$	21.743	21.659	21.576
	$\bar{\omega}_3$	59.801	59.580	59.361
	$\bar{\omega}_4$	114.290	113.891	113.496
	$\bar{\omega}_5$	183.216	182.620	182.030

Table 2.3: Comparison of nondimonsional natural frequencies of a cantilever beam in contact with a fluid medium using TBT with 20 elements.

		TBT		
L/H	$\bar{\omega}_N$	$\beta = 0$	$\beta = 0.04$	$\beta = 0.08$
100	$\bar{\omega}_1$	3.517	3.384	3.265
	$\bar{\omega}_2$	22.158	21.325	20.580
	$\bar{\omega}_3$	62.714	60.371	58.272
	$\bar{\omega}_4$	124.988	120.359	116.209
	$\bar{\omega}_5$	211.405	203.667	196.721
10	$\bar{\omega}_1$	3.490	3.476	3.463
	$\bar{\omega}_2$	21.058	20.976	20.896
	$\bar{\omega}_3$	55.993	55.783	55.575
	$\bar{\omega}_4$	103.048	102.674	102.304
	$\bar{\omega}_5$	159.476	158.915	158.360

Table 2.4: Comparison of nondimonsional natural frequencies of a cantilever beam in contact with a fluid medium using TBT with 100 elements.

		TBT		
L/H	$\bar{\omega}_N$	$\beta = 0$	$\beta = 0.04$	$\beta = 0.08$
100	$\bar{\omega}_1$	3.516	3.383	3.264
	$\bar{\omega}_2$	22.028	21.200	20.459
	$\bar{\omega}_3$	61.661	59.357	57.293
	$\bar{\omega}_4$	120.786	116.309	112.296
	$\bar{\omega}_5$	199.577	192.260	185.692
10	$\bar{\omega}_1$	3.489	3.475	3.462
	$\bar{\omega}_2$	20.942	20.861	20.781
	$\bar{\omega}_3$	55.186	54.979	54.774
	$\bar{\omega}_4$	100.323	99.958	99.597
	$\bar{\omega}_5$	153.044	152.503	151.968

Table 2.5: Comparison of nondimonsional natural frequencies of a cantilever beam in contact with a fluid medium using RBT with 20 elements.

		RBT		
L/H	$\bar{\omega}_N$	$\beta = 0$	$\beta = 0.04$	$\beta = 0.08$
100	$\bar{\omega}_1$	3.516	3.383	3.264
	$\bar{\omega}_2$	22.023	21.195	20.454
	$\bar{\omega}_3$	61.620	59.318	57.255
	$\bar{\omega}_4$	120.627	116.159	112.154
	$\bar{\omega}_5$	199.150	191.861	185.318
10	$\bar{\omega}_1$	3.489	3.476	3.462
	$\bar{\omega}_2$	20.955	20.874	20.794
	$\bar{\omega}_3$	55.269	55.062	54.856
	$\bar{\omega}_4$	100.591	100.225	99.864
	$\bar{\omega}_5$	153.645	153.104	152.568

Table 2.6: Comparison of nondimonsional natural frequencies of a cantilever beam in contact with a fluid medium using RBT with 100 elements.

		RBT		
L/H	$\bar{\omega}_N$	$\beta = 0$	$\beta = 0.04$	$\beta = 0.08$
100	$\bar{\omega}_1$	3.516	3.383	3.264
	$\bar{\omega}_2$	22.023	21.195	20.454
	$\bar{\omega}_3$	61.618	59.315	57.253
	$\bar{\omega}_4$	120.616	116.146	112.138
	$\bar{\omega}_5$	199.107	191.807	185.255
10	$\bar{\omega}_1$	3.489	3.476	3.462
	$\bar{\omega}_2$	20.950	20.869	20.789
	$\bar{\omega}_3$	55.236	55.028	54.823
	$\bar{\omega}_4$	100.485	100.120	99.758
	$\bar{\omega}_5$	153.412	152.871	152.335

Table 2.7: Comparison of nondimonsional natural frequencies of a clamped-clamped beam in contact with a fluid medium using EBT with 20 elements.

		EBT		
L/H	$\bar{\omega}_N$	$\beta = 0$	$\beta = 0.04$	$\beta = 0.08$
100	$\bar{\omega}_1$	22.372	21.529	20.775
	$\bar{\omega}_2$	61.662	59.349	57.278
	$\bar{\omega}_3$	120.861	116.360	112.327
	$\bar{\omega}_4$	199.751	192.389	185.785
	$\bar{\omega}_5$	298.341	287.494	277.750
10	$\bar{\omega}_1$	22.259	22.172	22.086
	$\bar{\omega}_2$	60.523	60.292	60.065
	$\bar{\omega}_3$	116.215	115.793	115.376
	$\bar{\omega}_4$	186.969	186.333	185.704
	$\bar{\omega}_5$	270.397	269.547	268.705

Table 2.8: Comparison of nondimonsional natural frequencies of a clamped-clamped beam in contact with a fluid medium using EBT with 100 elements.

		EBT		
L/H	$\bar{\omega}_N$	$\beta = 0$	$\beta = 0.04$	$\beta = 0.08$
	$\bar{\omega}_1$	22.372	21.529	20.774
	$\bar{\omega}_2$	61.661	59.348	57.276
100	$\bar{\omega}_3$	120.854	116.351	112.316
	$\bar{\omega}_4$	199.717	192.346	185.735
	$\bar{\omega}_5$	298.228	287.352	277.586
	$\bar{\omega}_1$	22.259	22.172	22.086
	$\bar{\omega}_2$	60.522	60.291	60.064
10	$\bar{\omega}_3$	116.207	115.786	115.369
	$\bar{\omega}_4$	186.937	186.300	185.670
	$\bar{\omega}_5$	270.294	269.442	268.598

Table 2.9: Comparison of nondimonsional natural frequencies of a clamped-clamped beam in contact with a fluid medium using TBT with 20 elements.

		TBT		
L/H	$\bar{\omega}_N$	$\beta = 0$	$\beta = 0.04$	$\beta = 0.08$
	$\bar{\omega}_1$	22.532	21.683	20.923
	$\bar{\omega}_2$	62.888	60.529	58.416
100	$\bar{\omega}_3$	125.556	120.879	116.688
	$\bar{\omega}_4$	212.697	204.853	197.817
	$\bar{\omega}_5$	327.719	315.789	305.074
	$\bar{\omega}_1$	21.165	21.081	20.999
	$\bar{\omega}_2$	54.905	54.694	54.484
10	$\bar{\omega}_3$	100.672	100.293	99.918
	$\bar{\omega}_4$	155.336	154.766	154.203
	$\bar{\omega}_5$	217.028	216.251	215.482

Table 2.10: Comparison of nondimonsional natural frequencies of a clamped-clamped beam in contact with a fluid medium using TBT with 100 elements.

		TBT		
L/H	$\bar{\omega}_N$	$\beta = 0$	$\beta = 0.04$	$\beta = 0.08$
100	$\bar{\omega}_1$	22.365	21.522	20.768
	$\bar{\omega}_2$	61.629	59.316	57.246
	$\bar{\omega}_3$	120.765	116.266	112.234
	$\bar{\omega}_4$	199.530	192.166	185.561
	$\bar{\omega}_5$	297.889	287.024	277.268
10	$\bar{\omega}_1$	21.024	20.941	20.859
	$\bar{\omega}_2$	54.005	53.797	53.591
	$\bar{\omega}_3$	97.833	97.465	97.101
	$\bar{\omega}_4$	148.873	148.326	147.785
	$\bar{\omega}_5$	204.826	204.091	203.363

Table 2.11: Comparison of nondimonsional natural frequencies of a clamped-clamped beam in contact with a fluid medium using RBT with 20 elements.

		RBT		
L/H	$\bar{\omega}_N$	$\beta = 0$	$\beta = 0.04$	$\beta = 0.08$
100	$\bar{\omega}_1$	22.359	22.010	21.677
	$\bar{\omega}_2$	61.581	60.624	59.712
	$\bar{\omega}_3$	120.589	118.731	116.956
	$\bar{\omega}_4$	199.069	196.034	193.134
	$\bar{\omega}_5$	296.908	292.445	288.177
10	$\bar{\omega}_1$	21.050	21.046	21.043
	$\bar{\omega}_2$	54.182	54.174	54.166
	$\bar{\omega}_3$	98.393	98.379	98.364
	$\bar{\omega}_4$	150.111	150.089	150.067
	$\bar{\omega}_5$	207.038	207.009	206.979

Table 2.12: Comparison of nondimonsional natural frequencies of a clamped-clamped beam in contact with a fluid medium using RBT with 100 elements.

		RBT		
L/H	$\bar{\omega}_N$	$\beta = 0$	$\beta = 0.04$	$\beta = 0.08$
	$\bar{\omega}_1$	22.358	22.010	21.677
	$\bar{\omega}_2$	61.578	60.622	59.709
100	$\bar{\omega}_3$	120.575	118.716	116.940
	$\bar{\omega}_4$	199.017	195.979	193.075
	$\bar{\omega}_5$	296.757	292.282	288.004
	$\bar{\omega}_1$	21.040	21.037	21.034
	$\bar{\omega}_2$	54.120	54.112	54.103
10	$\bar{\omega}_3$	98.200	98.185	98.170
	$\bar{\omega}_4$	149.690	149.668	149.646
	$\bar{\omega}_5$	206.293	206.264	206.234

Table 2.13: Comparison of nondimonsional natural frequencies of a simply supported beam in contact with a fluid medium using EBT with 20 elements.

		EBT		
L/H	$\bar{\omega}_N$	$\beta = 0$	$\beta = 0.04$	$\beta = 0.08$
	$\bar{\omega}_1$	9.869	9.497	9.164
	$\bar{\omega}_2$	39.472	37.990	36.663
100	$\bar{\omega}_3$	88.797	85.484	82.516
	$\bar{\omega}_4$	157.827	151.993	146.763
	$\bar{\omega}_5$	246.551	237.551	229.470
	$\bar{\omega}_1$	9.829	9.791	9.752
	$\bar{\omega}_2$	38.845	38.696	38.549
10	$\bar{\omega}_3$	85.714	85.400	85.090
	$\bar{\omega}_4$	148.464	147.953	147.447
	$\bar{\omega}_5$	224.775	224.057	223.346

Table 2.14: Comparison of nondimonsional natural frequencies of a simply supported beam in contact with a fluid medium using EBT with 100 elements.

		EBT		
L/H	$\bar{\omega}_N$	$\beta = 0$	$\beta = 0.04$	$\beta = 0.08$
	$\bar{\omega}_1$	9.869	9.497	9.164
	$\bar{\omega}_2$	39.472	37.989	36.662
100	$\bar{\omega}_3$	88.794	85.479	82.511
	$\bar{\omega}_4$	157.810	151.971	146.736
	$\bar{\omega}_5$	246.487	237.468	229.372
	$\bar{\omega}_1$	9.829	9.791	9.752
	$\bar{\omega}_2$	38.845	38.696	38.549
10	$\bar{\omega}_3$	85.711	85.397	85.086
	$\bar{\omega}_4$	148.448	147.936	147.430
	$\bar{\omega}_5$	224.717	223.997	223.285

Table 2.15: Comparison of nondimonsional natural frequencies of a simply supported beam in contact with a fluid medium using TBT with 20 elements.

		TBT		
L/H	$\bar{\omega}_N$	$\beta = 0$	$\beta = 0.04$	$\beta = 0.08$
	$\bar{\omega}_1$	9.898	9.525	9.191
	$\bar{\omega}_2$	39.944	38.443	37.101
100	$\bar{\omega}_3$	91.207	87.804	84.756
	$\bar{\omega}_4$	165.556	159.436	153.949
	$\bar{\omega}_5$	265.777	256.073	247.360
	$\bar{\omega}_1$	9.741	9.703	9.665
	$\bar{\omega}_2$	37.587	37.442	37.299
10	$\bar{\omega}_3$	80.311	80.011	79.714
	$\bar{\omega}_4$	134.481	133.993	133.511
	$\bar{\omega}_5$	197.405	196.707	196.017

Table 2.16: Comparison of nondimonsional natural frequencies of a simply supported beam in contact with a fluid medium using TBT with 100 elements.

		TBT		
L/H	$\bar{\omega}_N$	$\beta = 0$	$\beta = 0.04$	$\beta = 0.08$
	$\bar{\omega}_1$	9.869	9.497	9.164
	$\bar{\omega}_2$	39.472	37.989	36.662
100	$\bar{\omega}_3$	88.794	85.480	82.511
	$\bar{\omega}_4$	157.810	151.971	146.736
	$\bar{\omega}_5$	246.489	237.470	229.374
	$\bar{\omega}_1$	9.713	9.675	9.637
	$\bar{\omega}_2$	37.176	37.033	36.892
10	$\bar{\omega}_3$	78.487	78.193	77.902
	$\bar{\omega}_4$	129.503	129.031	128.565
	$\bar{\omega}_5$	186.940	186.276	185.619

Table 2.17: Comparison of nondimonsional natural frequencies of a simply supported beam in contact with a fluid medium using RBT with 20 elements.

		RBT		
L/H	$\bar{\omega}_N$	$\beta = 0$	$\beta = 0.04$	$\beta = 0.08$
	$\bar{\omega}_1$	9.868	9.714	9.567
	$\bar{\omega}_2$	39.453	38.840	38.254
100	$\bar{\omega}_3$	88.698	87.329	86.021
	$\bar{\omega}_4$	157.517	155.109	152.808
	$\bar{\omega}_5$	245.797	242.087	238.540
	$\bar{\omega}_1$	9.712	9.711	9.709
	$\bar{\omega}_2$	37.161	37.156	37.150
10	$\bar{\omega}_3$	78.430	78.418	78.407
	$\bar{\omega}_4$	129.379	129.360	129.342
	$\bar{\omega}_5$	186.747	186.720	186.693

Table 2.18: Comparison of nondimonsional natural frequencies of a simply supported beam in contact with a fluid medium using RBT with 100 elements.

		RBT		
L/H	$\bar{\omega}_N$	$\beta = 0$	$\beta = 0.04$	$\beta = 0.08$
100	$\bar{\omega}_1$	9.868	9.714	9.567
	$\bar{\omega}_2$	39.452	38.839	38.254
	$\bar{\omega}_3$	88.695	87.326	86.017
	$\bar{\omega}_4$	157.500	155.090	152.786
	$\bar{\omega}_5$	245.733	242.015	238.461
10	$\bar{\omega}_1$	9.712	9.711	9.709
	$\bar{\omega}_2$	37.161	37.155	37.150
	$\bar{\omega}_3$	78.428	78.416	78.404
	$\bar{\omega}_4$	129.369	129.350	129.331
	$\bar{\omega}_5$	186.714	186.687	186.660

2.4.2 Plate Structure

The parameters used for the plate problem are as follows:

$$\begin{aligned} &E = 200 \text{ GPa}, \quad \nu = 0.25, \quad \rho_s = 5000 \text{ kg}/m^3 \\ &L_x = L_y = L = 1 \text{ m}, \quad h_z = 0.02 \text{ m}, \quad \beta = \frac{\rho_f}{\rho_s} \end{aligned} \tag{2.149}$$

and we consider h and ρ_f to be varied for different cases. The natural frequencies are presented in the following nondimensional form

$$\bar{\omega} = \omega \times L_x^2 \sqrt{\frac{\rho_s h}{D}} \tag{2.150}$$

In this sub-section, simulations are performed for three boundary conditions; a plate with one edge clamped and all other edges free (CFFF), a plate with all edges clamped (CCCC), and a plate with all edges simply supported (SSSS), and

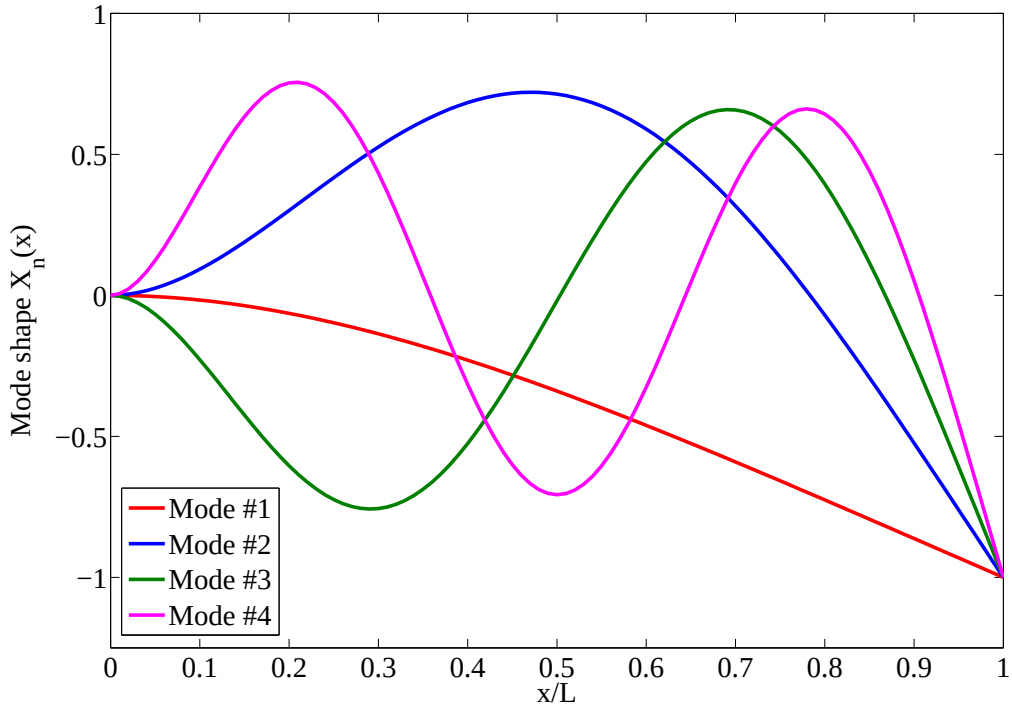

Figure 2.6: The first four mode shapes of a cantilever beam of unit length in an inviscid fluid with $L/H = 100$ and using 100 third-order beam elements.

for three different fluid densities; $\beta = 0$ (corresponding to the case where the plate is not in contact with fluid), $\beta = 0.04$, and $\beta = 0.08$. For each β value, two different plate thickness ratios, $L/H = 10$ and $L/H = 100$, are considered. In all cases, our mesh is 20×20 elements. The dynamic behavior of the plate for the aforementioned cases followed the trend expected from the previous studies; it is influenced by the immersion depth h_z and fluid density ρ_f. For instance, increasing h_z (or correspondingly increasing ρ_f) increases the added mass and consequently decreases the natural frequencies. Moreover, changing L/H ratio results in different variation of natural frequencies to the presence of the fluid medium. The variation of the first six natural frequencies for different β values and L/H ratios are summarized

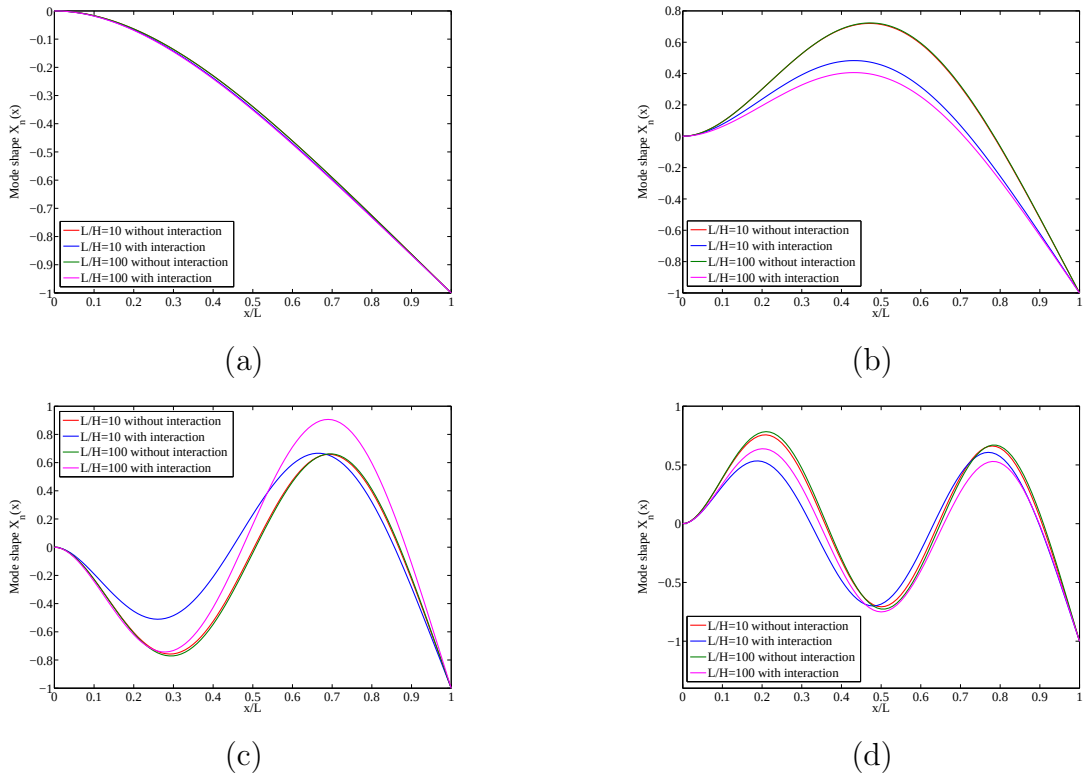

Figure 2.7: The first four mode shape of a cantilever beam of a unit length in an inviscid fluid with $L/H = 100$ and using 100 RBT beam elements, (a) the first mode shape, (b) the second mode shape, (c) the third mode shape and (d) the fourth mode shape.

in Tables 2.19 through 2.21 for CFFF, in Tables 2.22 through 2.24 for CCCC, and in Tables 2.25 through 2.27 for SSSS. It can be concluded that the effect of the added mass for lower natural frequencies is more than for the higher frequencies. Furthermore, increasing β (or h_z) will decrease the natural frequencies. Moreover, for higher β values (more dense fluids), the natural frequencies will be less affected if one changes the fluid density ρ_f.

It can be observed that, at each β value, there is more decrease in the natural frequencies for higher L/H ratios. In addition, the value of this decrease is larger for the higher modes.

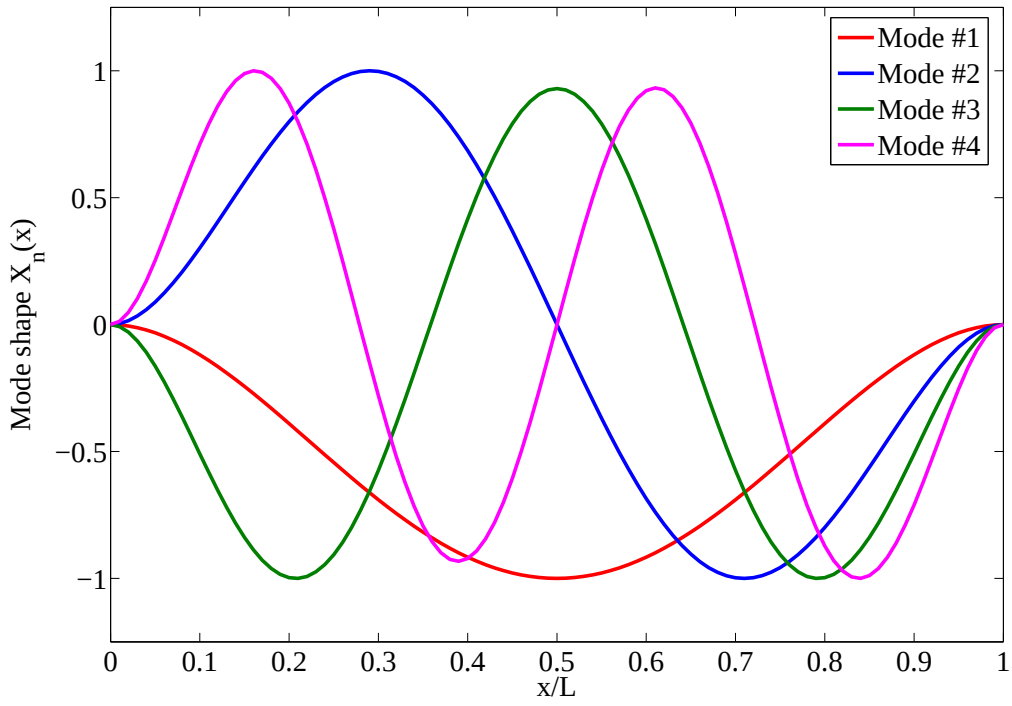

Figure 2.8: The first four mode shapes of a clamped-clamped beam of unit length in an inviscid fluid with $L/H = 100$ and using 100 third-order beam elements.

As shown in Tables 2.19 through 2.27, the results for higher L/H ratios converge for all three plate theories; i.e. in the thin plate limits, we can use any of three plate theories. However, for the lower L/H ratios, since the normality assumption is not valid, CPT overpredicts the natural frequencies.

The mode shapes for CFFF, CCCC and SSSS for the case of $\beta = 0.08$ are depicted in Figs. 2.10, 2.11 and 2.12, respectively. Since the obtained mode shapes for all three theories are exactly the same, we only plotted the mode shapes of the RSDT. These two figures indicate that for small deformations, the presence of the fluid does not affect the mode shapes considerably.

Table 2.19: Comparison of natural frequencies of a CFFF plate in contact with a fluid medium using CPT with 20×20 elements.

		CPT		
L/H	$\bar{\omega}_N$	$\beta = 0$	$\beta = 0.04$	$\beta = 0.08$
100	$\bar{\omega}_1$	1.033	0.910	0.822
	$\bar{\omega}_2$	2.666	2.356	2.134
	$\bar{\omega}_3$	6.380	5.668	5.152
	$\bar{\omega}_4$	8.239	7.356	6.708
	$\bar{\omega}_5$	9.505	8.466	7.707
	$\bar{\omega}_6$	16.714	15.015	13.746
10	$\bar{\omega}_1$	1.031	1.017	1.003
	$\bar{\omega}_2$	2.650	2.614	2.580
	$\bar{\omega}_3$	6.292	6.212	6.135
	$\bar{\omega}_4$	8.074	7.978	7.884
	$\bar{\omega}_5$	9.348	9.232	9.121
	$\bar{\omega}_6$	16.236	16.056	15.882

Table 2.20: Comparison of natural frequencies of a CFFF plate in contact with a fluid medium using FSDT with 20×20 elements.

		FSDT		
L/H	$\bar{\omega}_N$	$\beta = 0$	$\beta = 0.04$	$\beta = 0.08$
100	$\bar{\omega}_1$	1.034	0.921	0.833
	$\bar{\omega}_2$	2.684	2.385	2.212
	$\bar{\omega}_3$	6.422	5.802	5.381
	$\bar{\omega}_4$	8.181	7.872	6.904
	$\bar{\omega}_5$	9.412	8.763	8.102
	$\bar{\omega}_6$	16.463	15.747	14.172
10	$\bar{\omega}_1$	1.029	1.025	1.021
	$\bar{\omega}_2$	2.470	2.461	2.451
	$\bar{\omega}_3$	6.111	6.087	6.064
	$\bar{\omega}_4$	7.696	7.666	7.637
	$\bar{\omega}_5$	8.642	8.609	8.576
	$\bar{\omega}_6$	14.538	14.484	14.430

Table 2.21: Comparison of natural frequencies of a CFFF plate in contact with a fluid medium using RSDT with 20×20 elements.

		RSDT		
L/H	$\bar{\omega}_N$	$\beta = 0$	$\beta = 0.04$	$\beta = 0.08$
100	$\bar{\omega}_1$	1.044	0.919	0.831
	$\bar{\omega}_2$	2.695	2.381	2.157
	$\bar{\omega}_3$	6.509	5.782	5.254
	$\bar{\omega}_4$	8.247	7.365	6.716
	$\bar{\omega}_5$	9.637	8.583	7.813
	$\bar{\omega}_6$	16.829	15.116	13.838
10	$\bar{\omega}_1$	1.031	1.017	1.003
	$\bar{\omega}_2$	2.508	2.474	2.441
	$\bar{\omega}_3$	6.129	6.050	5.974
	$\bar{\omega}_4$	7.684	7.592	7.502
	$\bar{\omega}_5$	8.700	8.592	8.487
	$\bar{\omega}_6$	14.610	14.446	14.287

Table 2.22: Comparison of natural frequencies of a CCCC plate in contact with a fluid medium using CPT with 20×20 elements.

		CPT		
L/H	$\bar{\omega}_N$	$\beta = 0$	$\beta = 0.04$	$\beta = 0.08$
100	$\bar{\omega}_1$	10.828	10.524	10.245
	$\bar{\omega}_2$	22.092	21.474	20.906
	$\bar{\omega}_3$	22.097	21.480	20.911
	$\bar{\omega}_4$	32.772	31.861	31.021
	$\bar{\omega}_5$	39.592	38.495	37.484
	$\bar{\omega}_6$	39.779	38.676	37.660
10	$\bar{\omega}_1$	10.723	10.692	10.661
	$\bar{\omega}_2$	21.587	21.527	21.468
	$\bar{\omega}_3$	21.592	21.533	21.473
	$\bar{\omega}_4$	31.623	31.538	31.453
	$\bar{\omega}_5$	37.896	37.796	37.697
	$\bar{\omega}_6$	38.093	37.992	37.892

Table 2.23: Comparison of natural frequencies of a CCCC plate in contact with a fluid medium using FSDT with 20×20 elements.

		FSDT		
L/H	$\bar{\omega}_N$	$\beta = 0$	$\beta = 0.04$	$\beta = 0.08$
100	$\bar{\omega}_1$	10.787	10.381	10.017
	$\bar{\omega}_2$	22.213	21.381	20.636
	$\bar{\omega}_3$	22.213	21.381	20.636
	$\bar{\omega}_4$	32.747	31.525	30.431
	$\bar{\omega}_5$	40.543	39.035	37.684
	$\bar{\omega}_6$	40.736	39.221	37.863
10	$\bar{\omega}_1$	9.804	9.765	9.727
	$\bar{\omega}_2$	18.898	18.825	18.754
	$\bar{\omega}_3$	18.898	18.825	18.754
	$\bar{\omega}_4$	26.505	26.405	26.306
	$\bar{\omega}_5$	31.680	31.561	31.444
	$\bar{\omega}_6$	31.981	31.861	31.742

Table 2.24: Comparison of natural frequencies of a CCCC plate in contact with a fluid medium using RSDT with 20×20 elements.

		RSDT		
L/H	$\bar{\omega}_N$	$\beta = 0$	$\beta = 0.04$	$\beta = 0.08$
100	$\bar{\omega}_1$	10.776	10.474	10.196
	$\bar{\omega}_2$	21.957	21.344	20.780
	$\bar{\omega}_3$	22.156	21.537	20.968
	$\bar{\omega}_4$	32.559	31.653	30.820
	$\bar{\omega}_5$	39.770	38.668	37.652
	$\bar{\omega}_6$	39.958	38.850	37.829
10	$\bar{\omega}_1$	9.701	9.673	9.645
	$\bar{\omega}_2$	18.495	18.443	18.392
	$\bar{\omega}_3$	18.653	18.601	18.549
	$\bar{\omega}_4$	26.047	25.975	25.903
	$\bar{\omega}_5$	30.834	30.749	30.665
	$\bar{\omega}_6$	31.108	31.022	30.937

Table 2.25: Comparison of natural frequencies of a SSSS plate in contact with a fluid medium using CPT with 20×20 elements.

		CPT		
L/H	$\bar{\omega}_N$	$\beta = 0$	$\beta = 0.04$	$\beta = 0.08$
100	$\bar{\omega}_1$	5.953	5.786	5.632
	$\bar{\omega}_2$	14.831	14.416	14.034
	$\bar{\omega}_3$	14.833	14.418	14.036
	$\bar{\omega}_4$	23.833	23.169	22.558
	$\bar{\omega}_5$	29.598	28.776	28.019
	$\bar{\omega}_6$	29.607	28.784	28.026
10	$\bar{\omega}_1$	5.905	5.888	5.871
	$\bar{\omega}_2$	14.538	14.497	14.457
	$\bar{\omega}_3$	14.540	14.499	14.459
	$\bar{\omega}_4$	23.093	23.031	22.968
	$\bar{\omega}_5$	28.462	28.386	28.310
	$\bar{\omega}_6$	28.470	28.394	28.318

Table 2.26: Comparison of natural frequencies of a SSSS plate in contact with a fluid medium using FSDT with 20×20 elements.

		FSDT		
L/H	$\bar{\omega}_N$	$\beta = 0$	$\beta = 0.04$	$\beta = 0.08$
100	$\bar{\omega}_1$	5.871	5.650	5.452
	$\bar{\omega}_2$	14.802	14.247	13.750
	$\bar{\omega}_3$	14.802	14.247	13.750
	$\bar{\omega}_4$	23.654	22.770	21.979
	$\bar{\omega}_5$	30.061	28.941	27.938
	$\bar{\omega}_6$	30.062	28.942	27.938
10	$\bar{\omega}_1$	5.466	5.444	5.423
	$\bar{\omega}_2$	13.384	13.333	13.282
	$\bar{\omega}_3$	13.384	13.333	13.282
	$\bar{\omega}_4$	20.306	20.230	20.154
	$\bar{\omega}_5$	25.690	25.594	25.500
	$\bar{\omega}_6$	25.740	25.644	25.549

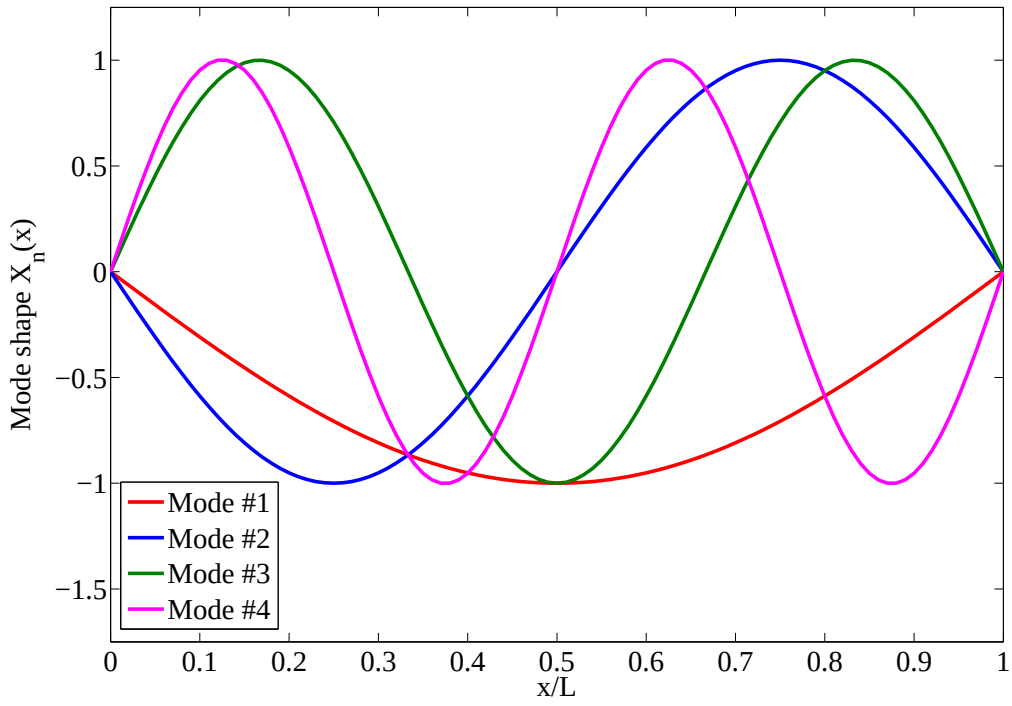

Figure 2.9: The first four mode shapes of a simply supported beam of unit length in an inviscid fluid with $L/H = 100$ and using 100 third-order beam elements.

2.5 Concluding Remarks

In this section, we studied the free vibration problems of fluid-structure interaction for beams and plates, using classical and first-order and Reddy third-order shear deformation theories. We considered the effect of a fluid medium as an added mass incorporated into the mass matrix of the system equations. The effect of various parameters, such as fluid density, structural dimensions, and boundary conditions on the natural frequencies and mode shapes of the structures through numerical simulations.

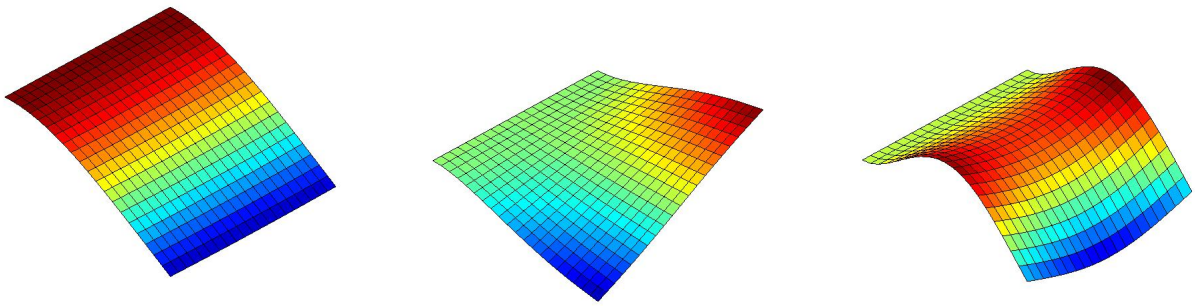

(a) (b) (c)

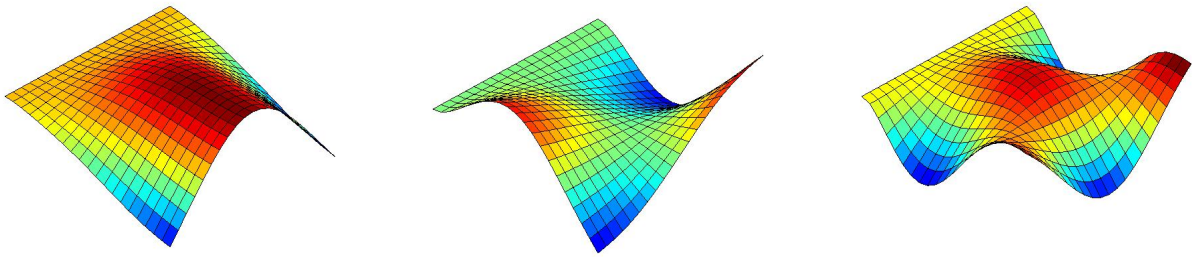

(d) (e) (f)

Figure 2.10: The first six mode shapes of a CFFF plate in an inviscid incompressible fluid medium for $L/H = 10$ and $\beta = 0.08$. (a) The first mode shape, (b) the second mode shape, (c) the third mode shape, (d) the fourth mode shape, (e) the fifth mode shape, and (f) the sixth mode shape.

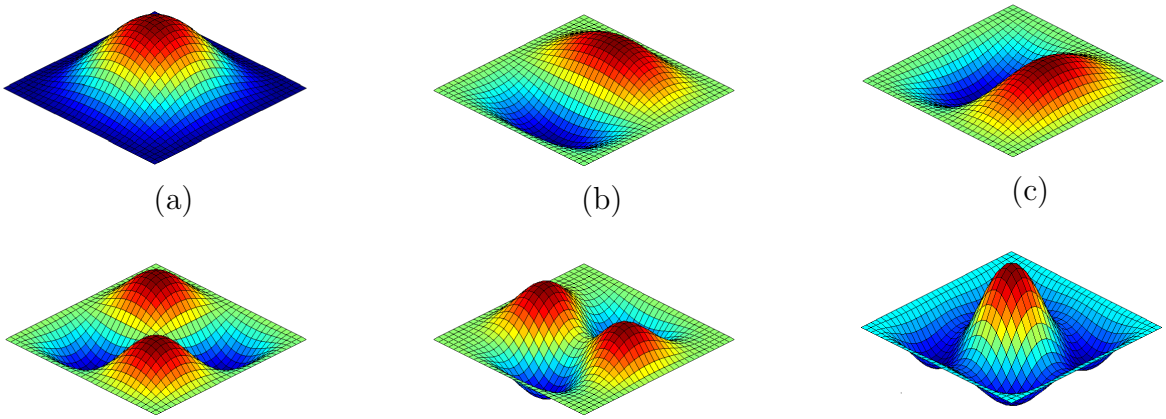

Figure 2.11: The first six mode shapes of a CCCC plate in an inviscid incompressible fluid medium for $L/H = 10$ and $\beta = 0.08$. (a) The first mode shape, (b) the second mode shape, (c) the third mode shape, (d) the fourth mode shape, (e) the fifth mode shape, and (f) the sixth mode shape.

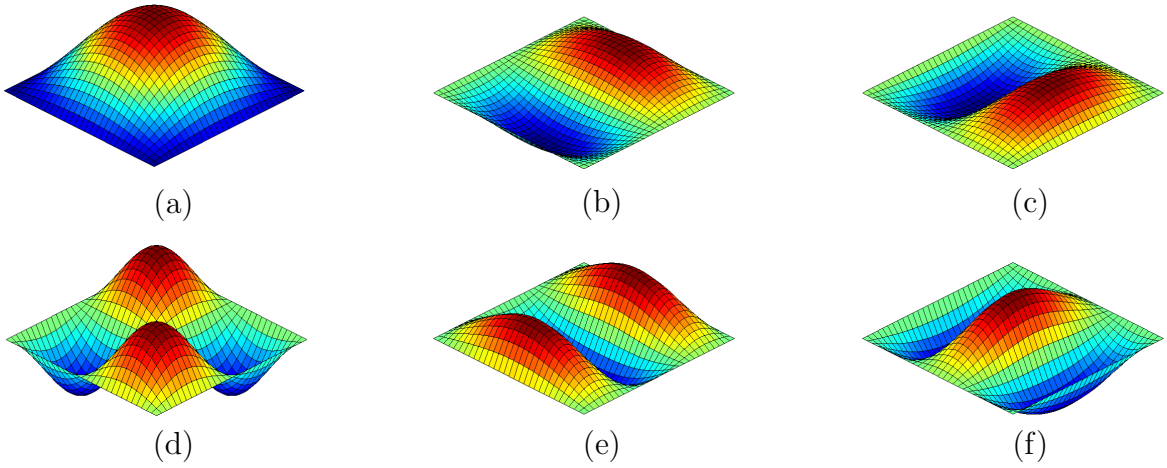

Figure 2.12: The first six mode shapes of a SSSS plate in an inviscid incompressible fluid medium for $L/H = 10$ and $\beta = 0.08$. (a) The first mode shape, (b) the second mode shape, (c) the third mode shape, (d) the fourth mode shape, (e) the fifth mode shape, and (f) the sixth mode shape.

Table 2.27: Comparison of natural frequencies of a SSSS plate in contact with a fluid medium using RSDT with 20×20 elements.

		RSDT		
L/H	$\bar{\omega}_N$	$\beta = 0$	$\beta = 0.04$	$\beta = 0.08$
100	$\bar{\omega}_1$	5.874	5.709	5.558
	$\bar{\omega}_2$	14.639	14.230	13.853
	$\bar{\omega}_3$	14.800	14.386	14.005
	$\bar{\omega}_4$	23.517	22.861	22.258
	$\bar{\omega}_5$	29.555	28.734	27.977
	$\bar{\omega}_6$	29.565	28.744	27.987
10	$\bar{\omega}_1$	5.402	5.386	5.371
	$\bar{\omega}_2$	13.108	13.071	13.035
	$\bar{\omega}_3$	13.237	13.200	13.163
	$\bar{\omega}_4$	19.935	19.880	19.825
	$\bar{\omega}_5$	25.002	24.933	24.865
	$\bar{\omega}_6$	25.048	24.979	24.911

3. NONLINEAR TRANSIENT ANALYSIS OF ELASTIC STRUCTURES IN CONTACT WITH A FLUID DOMAIN

3.1 Introduction

Beams, plates, and shells are considered to be the basic elements of almost any structure. The presence of fluid around a structure can lead to failure of a structure. Most FSI problems arising in aerospace, ship industry, oil and gas industry, and biomedical, require finding a method to investigate the effect of fluid domain on structural response. A coupled finite element formulation of problems involving FSI is considered to be an accurate method to predict the transient response of structures in contact with a fluid medium.

In Section 2, we studied the linear formulation in order to investigate the natural vibration of beams and plates in contact with a fluid medium. In this section, our focus will be on the transient response of structures in the presence of a fluid medium. However, in order to make our approach more applicable, we extend it to the nonlinear formulation results in taking into account the geometric nonlinearity; which in our study, we consider small strains and moderate rotations. Here, three different plate theories; namely Classical Plate Theory (CPT), First-order Shear Deformation Plate Theory (FSDT), and Third-order Shear Deformation Plate Theory (TSDT) with specialization to Reddy Third-order Shear Deformation Plate Theory (RSDT) are considered to model the solid medium, and the Navier-Stokes equation is the theoretical equation governed the fluid medium. The governing equations of the solid domain are based on the classical von-Karman nonlinear strains. The formulation is a combination of the various structure theories and the solid-fluid interface boundary condition, which is used to represent the interaction between the solid

and fluid regimes. The main feature of the proposed methodology is to model the fluid domain as an added mass; the external distributed force due to the presence of the fluid. Then the finite element model of each plate theories will be developed which includes the nonlinear term as expected. The nonlinear solution scheme discussed herein is Newton's method following by the transient response solution of the problem. Since the formulation presented in this study covers several theories in literature, our formulation accounts for any plate geometry.

We will validate the accuracy of such formulation by means of some numerical simulations. We can take the advantage of prescribing the effect of fluid flow on the transient response in order to improve the structural design.

3.2 Theoretical Formulations

As in previous section, here we present theoretical formulation for three different plate theories. The main difference between governing equations presented here with those provided in Section 2 is that herein we do not limit our method to small strains and small rotations. Extending our method to small strains and moderate rotations, we are confronting the nonlinearity in our governing equations for the structural domain. Similar to the previous section, Fig. 3.1 represents the domain of the transient response plate problem and typical fluid mesh.

3.2.1 Fluid Mechanics

The fluid medium governing equation is as described in Section 2, since we are planning to consider the geometric nonlinearity only. Just a quick review of what we have done for deriving the equation governing the fluid domain, this domain assumed to have a density of ρ_f and its motion is fully described by the conservation principles

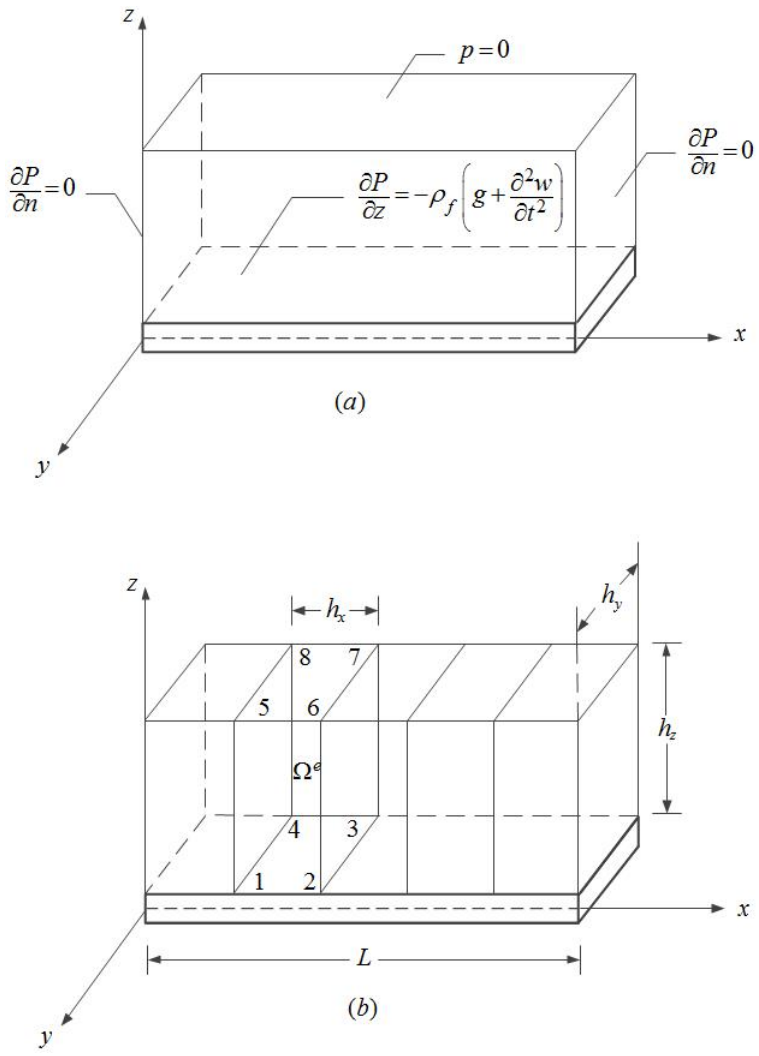

Figure 3.1: Domain of the plate fluid-structure interaction problem with the (a) boundary conditions and (b) typical fluid mesh.

of linear and angular momentum as

$$\nabla \cdot \boldsymbol{\sigma} + \rho_f \mathbf{b} = \rho_f \dot{\mathbf{v}} \tag{3.1}$$

As it can be observed from Fig. 3.1, the force vector has only nonzero components due to gravity and it is measured per unit mass in z direction. For the case of an

inviscid fluid, it is possible to express the stress tensor as a function of the hydrostatic pressure. Taking the divergence of the the obtained equation, taking the advantage of constant incompressible fluid, for the slowly moving flow, we obtain the Laplace equation in terms of p as the governing equation. For the plate problem at hand, we are dealing with three dimensional flows; therefore, the corresponding Laplace expression in the Cartesian coordinate system will be

$$\frac{\partial^2 p}{\partial x^2} + \frac{\partial^2 p}{\partial y^2} + \frac{\partial^2 p}{\partial z^2} = 0 \tag{3.2}$$

In Eq. (3.2), time does not appear explicitly, however, since time enters the formulation through the solid-fluid interface, p is generally a time-dependent variable. It will be presented in Sub-section 3.2.3.

3.2.2 Solid Mechanics

3.2.2.1 The Classical Plate Theory (CPT)

For the CPT, the Kirchhoff hypothesis assumed the following form of the displacement field

$$\begin{aligned} u\left(x, y, , z, t\right) &= u\left(x, y, t\right) - z\frac{\partial w}{\partial x} \\ v\left(x, y, z, t\right) &= v\left(x, y, t\right) - z\frac{\partial w}{\partial y} \\ w\left(x, y, z, t\right) &= w\left(x, y, t\right) \end{aligned} \tag{3.3}$$

The von-Karman strain can be obtained using Green-Lagrange strain tensor. The non-zero terms of the plane strain vector associated with the displacement field in

Eq. (3.3) are calculated as

$$\left\{\begin{array}{c}\varepsilon_{xx}\\ \varepsilon_{yy}\\ \varepsilon_{xy}\end{array}\right\}=\left\{\begin{array}{c}\frac{\partial u}{\partial x}+\frac{1}{2}\left(\frac{\partial w}{\partial x}\right)^2\\ \frac{\partial v}{\partial y}+\frac{1}{2}\left(\frac{\partial w}{\partial y}\right)^2\\ \frac{\partial u}{\partial y}+\frac{\partial v}{\partial x}+\frac{\partial w}{\partial x}\frac{\partial w}{\partial y}\end{array}\right\}-z\left\{\begin{array}{c}\frac{\partial^2 w}{\partial x^2}\\ \frac{\partial^2 w}{\partial y^2}\\ \frac{\partial^2 w}{\partial x\partial y}\end{array}\right\} \tag{3.4}$$

The plane stress can be expressed as

$$\left\{\begin{array}{c}\sigma_{xx}\\ \sigma_{yy}\\ \sigma_{xy}\end{array}\right\}=\left[\begin{array}{ccc}Q_{11} & Q_{12} & 0\\ Q_{12} & Q_{22} & 0\\ 0 & 0 & Q_{66}\end{array}\right]\left\{\begin{array}{c}\varepsilon_{xx}\\ \varepsilon_{yy}\\ \gamma_{xy}\end{array}\right\} \tag{3.5}$$

where Q_{ij} are the elastic stiffnesses defined as

$$\begin{aligned}Q_{11}&=\frac{E_1}{1-\nu_{12}\nu_{21}},\quad Q_2=\frac{E_2}{1-\nu_{12}\nu_{21}}\\ Q_{12}&=\frac{\nu_{21}E_1}{1-\nu_{12}\nu_{21}},\quad Q_{66}=G_{12}\end{aligned} \tag{3.6}$$

Using the above strain and stress fields along with the dynamic version of the principle of virtual displacement, the equilibrium equations for nonlinear CPT are obtained as follows:

$$\begin{aligned}&\frac{\partial N_{xx}}{\partial x}+\frac{\partial N_{xy}}{\partial y}=I_0\frac{\partial^2 u}{\partial t^2}\\ &\frac{\partial N_{xy}}{\partial x}+\frac{\partial N_{yy}}{\partial y}=I_0\frac{\partial^2 v}{\partial t^2}\\ &\frac{\partial}{\partial x}\left(\frac{\partial w}{\partial x}N_{xx}+\frac{\partial w}{\partial y}N_{xy}\right)+\frac{\partial}{\partial y}\left(\frac{\partial w}{\partial x}N_{xy}+\frac{\partial w}{\partial y}N_{yy}\right)+\left(\frac{\partial^2 M_{xx}}{\partial x^2}+2\frac{\partial^2 M_{xy}}{\partial x\partial y}+\frac{\partial^2 M_{yy}}{\partial y^2}\right)\\ &\qquad=-p-I_6\frac{\partial^2}{\partial t^2}\left(\frac{\partial^2 w}{\partial x^2}+\frac{\partial^2 w}{\partial y^2}\right)+I_0\frac{\partial^2 w}{\partial t^2}\end{aligned} \tag{3.7}$$

where I_i is defined as

$$I_i = \int_{-\frac{h}{2}}^{\frac{h}{2}} \rho(z)^i dz \tag{3.8}$$

where the stress resultants have the following definition:

$$\left\{ \begin{array}{c} N_{xx} \\ N_{yy} \\ N_{xy} \end{array} \right\} = \int_{-\frac{h}{2}}^{\frac{h}{2}} \left\{ \begin{array}{c} \sigma_{xx} \\ \sigma_{yy} \\ \sigma_{xy} \end{array} \right\} dz, \quad \left\{ \begin{array}{c} M_{xx} \\ M_{yy} \\ M_{xy} \end{array} \right\} = \int_{-\frac{h}{2}}^{\frac{h}{2}} \left\{ \begin{array}{c} \sigma_{xx} \\ \sigma_{yy} \\ \sigma_{xy} \end{array} \right\} z dz \tag{3.9}$$

3.2.2.2 The First-order Shear Deformation Plate Theory (FSDT)

For the FSDT, the normality condition is relaxed by assuming the following form of the displacements field

$$\begin{aligned} u\left(x, y, , z, t\right) &= u\left(x, y, t\right) + z\phi_x\left(x, y\right) \\ v\left(x, y, , z, t\right) &= v\left(x, y, t\right) + z\phi_y\left(x, y\right) \\ w\left(x, y, , z, t\right) &= w\left(x, y, t\right) \end{aligned} \tag{3.10}$$

The von-Karman nonlinear strain tensor associated with the above displacement field will take the form

$$\begin{aligned} \left\{ \begin{array}{c} \varepsilon_{xx} \\ \varepsilon_{yy} \\ \varepsilon_{xy} \end{array} \right\} &= \left\{ \begin{array}{c} \frac{\partial u}{\partial x} + \frac{1}{2}\left(\frac{\partial w}{\partial x}\right)^2 \\ \frac{\partial v}{\partial y} + \frac{1}{2}\left(\frac{\partial w}{\partial y}\right)^2 \\ \frac{\partial u}{\partial y} + \frac{\partial v}{\partial x} + \frac{\partial w}{\partial x}\frac{\partial w}{\partial y} \end{array} \right\} + z \left\{ \begin{array}{c} \frac{\partial \phi_x}{\partial x} \\ \frac{\partial \phi_y}{\partial y} \\ \frac{\partial \phi_x}{\partial y} + \frac{\partial \phi_y}{\partial x} \end{array} \right\} \\ \left\{ \begin{array}{c} \gamma_{xz} \\ \gamma_{yz} \end{array} \right\} &= \left\{ \begin{array}{c} \phi_x + \frac{\partial w}{\partial x} \\ \phi_y + \frac{\partial w}{\partial y} \end{array} \right\} \end{aligned} \tag{3.11}$$

The plane stress can be expressed as

$$\begin{Bmatrix} \sigma_{xx} \\ \sigma_{yy} \\ \sigma_{xy} \end{Bmatrix} = \begin{bmatrix} Q_{11} & Q_{12} & 0 \\ Q_{12} & Q_{22} & 0 \\ 0 & 0 & Q_{66} \end{bmatrix} \begin{Bmatrix} \varepsilon_{xx} \\ \varepsilon_{yy} \\ \gamma_{xy} \end{Bmatrix}$$
$$\begin{Bmatrix} \sigma_{xz} \\ \sigma_{yz} \end{Bmatrix} = \begin{bmatrix} Q_{44} & 0 \\ 0 & Q_{44} \end{bmatrix} \begin{Bmatrix} \gamma_{xz} \\ \gamma_{yz} \end{Bmatrix} \tag{3.12}$$

Using the above strain and stress field along with the dynamic version of the principle of virtual displacement, the equilibrium equations for nonlinear FSDT are obtained as follows:

$$\begin{aligned}
&\frac{\partial N_{xx}}{\partial x} + \frac{\partial N_{xy}}{\partial y} = I_0 \frac{\partial^2 u}{\partial t^2} \\
&\frac{\partial N_{xy}}{\partial x} + \frac{\partial N_{yy}}{\partial y} = I_0 \frac{\partial^2 v}{\partial t^2} \\
&\frac{\partial}{\partial x}\left(\frac{\partial w}{\partial x} N_{xx} + \frac{\partial w}{\partial y} N_{xy}\right) + \frac{\partial}{\partial y}\left(\frac{\partial w}{\partial x} N_{xy} + \frac{\partial w}{\partial y} N_{yy}\right) + \frac{\partial Q_x}{\partial x} + \frac{\partial Q_y}{\partial y} = -p + I_0 \frac{\partial^2 w}{\partial t^2} \\
&Q_x - \frac{\partial M_{xx}}{\partial x} - \frac{\partial M_{xy}}{\partial y} = I_2 \frac{\partial^2 \phi_x}{\partial t^2} \\
&Q_y - \frac{\partial M_{xy}}{\partial x} - \frac{\partial M_{yy}}{\partial y} = I_2 \frac{\partial^2 \phi_y}{\partial t^2}
\end{aligned} \tag{3.13}$$

where I_i is described by Eq. (3.8) and the stress resultants have the following definition:

$$\begin{Bmatrix} N_{xx} \\ N_{yy} \\ N_{xy} \end{Bmatrix} = \int_{-\frac{h}{2}}^{\frac{h}{2}} \begin{Bmatrix} \sigma_{xx} \\ \sigma_{yy} \\ \sigma_{xy} \end{Bmatrix} dz = \begin{bmatrix} A_{11} & A_{12} & 0 \\ A_{12} & A_{22} & 0 \\ 0 & 0 & A_{66} \end{bmatrix} \begin{Bmatrix} \frac{\partial u}{\partial x} + \frac{1}{2}\left(\frac{\partial w}{\partial x}\right)^2 \\ \frac{\partial v}{\partial y} + \frac{1}{2}\left(\frac{\partial w}{\partial y}\right)^2 \\ \frac{\partial u}{\partial y} + \frac{\partial v}{\partial x} + \frac{\partial w}{\partial x}\frac{\partial w}{\partial y} \end{Bmatrix}$$

$$\begin{Bmatrix} M_{xx} \\ M_{yy} \\ M_{xy} \end{Bmatrix} = \int_{-\frac{h}{2}}^{\frac{h}{2}} \begin{Bmatrix} \sigma_{xx} \\ \sigma_{yy} \\ \sigma_{xy} \end{Bmatrix} z dz = \begin{bmatrix} D_{11} & D_{12} & 0 \\ D_{12} & D_{22} & 0 \\ 0 & 0 & D_{66} \end{bmatrix} \begin{Bmatrix} \frac{\partial \phi_x}{\partial x} \\ \frac{\partial \phi_y}{\partial y} \\ \frac{\partial \phi_x}{\partial y} + \frac{\partial \phi_y}{\partial x} \end{Bmatrix}$$

$$\begin{Bmatrix} Q_x \\ Q_y \end{Bmatrix} = K_s \int_{-\frac{h}{2}}^{\frac{h}{2}} \begin{Bmatrix} \sigma_{xz} \\ \sigma_{yz} \end{Bmatrix} dz = \begin{bmatrix} A_{44} & 0 \\ 0 & A_{44} \end{bmatrix} \begin{Bmatrix} \phi_x + \frac{\partial w}{\partial x} \\ \phi_y + \frac{\partial w}{\partial y} \end{Bmatrix} \tag{3.14}$$

where the coefficients are expressed as

$$\begin{aligned} A_{11} &= \frac{Eh}{1-\nu^2}, \quad A_{12} = \frac{\nu Eh}{1-\nu^2}, \quad A_{44} = A_{66} = Gh = \frac{Eh}{2(1+\nu)} \\ D_{11} &= \frac{Eh^3}{12(1-\nu^2)}, \quad D_{12} = \frac{\nu Eh^3}{12(1-\nu^2)} \end{aligned} \tag{3.15}$$

3.2.2.3 Reddy Third-order Shear Deformation Plate Theory (RSDT)

For the general Third-order Shear Deformation Plate Theory (TSDT), the following form of the displacement field are assumed

$$\begin{aligned} u(x,y,,z,t) &= u(x,y,t) + z\phi_x(x,y) + z^2\theta_x(x,y) + z^3\psi_x(x,y) \\ v(x,y,,z,t) &= v(x,y,t) + z\phi_y(x,y) + z^2\theta_y(x,y) + z^3\psi_y(x,y) \\ w(x,y,,z,t) &= w(x,y,t) + z\phi_z(x,y) + z^2\theta_z(x,y) \end{aligned} \tag{3.16}$$

where we have the following defined variables

$$\begin{aligned}
&\phi_x = \left(\frac{\partial u}{\partial z}\right)_{z=0}, \quad \phi_y = \left(\frac{\partial v}{\partial z}\right)_{z=0}, \quad \phi_z = \left(\frac{\partial w}{\partial z}\right)_{z=0} \\
&\phi_x = \left(\frac{\partial u}{\partial z}\right)_{z=0}, \quad \phi_y = \left(\frac{\partial v}{\partial z}\right)_{z=0}, \quad \phi_z = \left(\frac{\partial w}{\partial z}\right)_{z=0} \\
&\psi_x = \frac{\partial^3 u}{\partial z^3}, \quad \psi_y = \frac{\partial^3 v}{\partial z^3}
\end{aligned} \tag{3.17}$$

RSDT invokes the free shear stress boundary conditions at the top and bottom surface of the plate, i.e. the transverse shear stresses σ_{xz} and σ_{yz} are set to be zero at these two surfaces which result in γ_{xz} and γ_{yz} to be zero. In addition if we set $\phi_z = \theta_z = 0$, the number of generalized displacements reduces from 11 to 5 (u, v, w, ϕ_x, and ϕ_y) which results in the following displacement field

$$\begin{aligned}
u\left(x, y, , z, t\right) &= u\left(x, y, t\right) + z\phi_x - z^3 \frac{4}{3h^2}\left(\phi_x + \frac{\partial w}{\partial x}\right) \\
v\left(x, y, , z, t\right) &= v\left(x, y, t\right) + z\phi_y - z^3 \frac{4}{3h^2}\left(\phi_y + \frac{\partial w}{\partial y}\right) \\
w\left(x, y, , z, t\right) &= w\left(x, y, t\right)
\end{aligned} \tag{3.18}$$

Using the obtained displacement field in the Green-Lagrange strain tensor, the components of the strain tensor take the form

$$\begin{aligned}
\left\{\begin{array}{c} \varepsilon_{xx} \\ \varepsilon_{yy} \\ \gamma_{xy} \end{array}\right\} &= \left\{\begin{array}{c} \varepsilon_{xx}^{(0)} \\ \varepsilon_{yy}^{(0)} \\ \gamma_{xy}^{(0)} \end{array}\right\} + z\left\{\begin{array}{c} \varepsilon_{xx}^{(1)} \\ \varepsilon_{yy}^{(1)} \\ \gamma_{xy}^{(1)} \end{array}\right\} + z^3\left\{\begin{array}{c} \varepsilon_{xx}^{(3)} \\ \varepsilon_{yy}^{(3)} \\ \gamma_{xy}^{(3)} \end{array}\right\} \\
\left\{\begin{array}{c} \gamma_{xz} \\ \gamma_{yz} \end{array}\right\} &= \left\{\begin{array}{c} \gamma_{xz}^{(0)} \\ \gamma_{yz}^{(0)} \end{array}\right\} + z^2\left\{\begin{array}{c} \gamma_{xz}^{(2)} \\ \gamma_{yz}^{(2)} \end{array}\right\}
\end{aligned} \tag{3.19}$$

where $\varepsilon^{(i)}_{\alpha\beta}$ and $\gamma^{(i)}_{\alpha\beta}$ have the following definition based on RSDT

$$
\begin{aligned}
\left\{ \begin{array}{c} \varepsilon^{(0)}_{xx} \\ \varepsilon^{(0)}_{yy} \\ \varepsilon^{(0)}_{xy} \end{array} \right\} &= \left\{ \begin{array}{c} \frac{\partial u}{\partial x} + \frac{1}{2}\left(\frac{\partial w}{\partial x}\right)^2 \\ \frac{\partial v}{\partial y} + \frac{1}{2}\left(\frac{\partial w}{\partial y}\right)^2 \\ \frac{\partial u}{\partial y} + \frac{\partial v}{\partial x} + \frac{\partial w}{\partial x}\frac{\partial w}{\partial y} \end{array} \right\} \\
\left\{ \begin{array}{c} \varepsilon^{(1)}_{xx} \\ \varepsilon^{(1)}_{yy} \\ \varepsilon^{(1)}_{xy} \end{array} \right\} &= \left\{ \begin{array}{c} \frac{\partial \phi_x}{\partial x} \\ \frac{\partial \phi_y}{\partial y} \\ \frac{\partial \phi_x}{\partial y} + \frac{\partial \phi_y}{\partial x} \end{array} \right\} \\
\left\{ \begin{array}{c} \varepsilon^{(3)}_{xx} \\ \varepsilon^{(3)}_{yy} \\ \varepsilon^{(3)}_{xy} \end{array} \right\} &= -c_1 \left\{ \begin{array}{c} \frac{\partial \phi_x}{\partial x} + \frac{\partial^2 w}{\partial x^2} \\ \frac{\partial \phi_y}{\partial y} + \frac{\partial^2 w}{\partial y^2} \\ \frac{\partial \phi_x}{\partial y} + \frac{\partial \phi_y}{\partial x} + 2\frac{\partial^2 w}{\partial x \partial y} \end{array} \right\} \\
\left\{ \begin{array}{c} \gamma^{(0)}_{xz} \\ \gamma^{(0)}_{yz} \end{array} \right\} &= \left\{ \begin{array}{c} \phi_x + \frac{\partial w}{\partial x} \\ \phi_y + \frac{\partial w}{\partial y} \end{array} \right\} \\
\left\{ \begin{array}{c} \gamma^{(2)}_{xz} \\ \gamma^{(2)}_{yz} \end{array} \right\} &= -c_2 \left\{ \begin{array}{c} \phi_x + \frac{\partial w}{\partial x} \\ \phi_y + \frac{\partial w}{\partial y} \end{array} \right\}
\end{aligned}
\tag{3.20}
$$

where the constants are

$$
c_1 = \frac{4}{3h^2}, \quad c_2 = \frac{4}{h^2} \tag{3.21}
$$

Similar to CPT and FSDT, the plane stress are described as

$$\begin{Bmatrix} \sigma_{xx} \\ \sigma_{yy} \\ \sigma_{xy} \end{Bmatrix} = \begin{bmatrix} Q_{11} & Q_{12} & 0 \\ Q_{12} & Q_{22} & 0 \\ 0 & 0 & Q_{66} \end{bmatrix} \begin{Bmatrix} \varepsilon_{xx} \\ \varepsilon_{yy} \\ \gamma_{xy} \end{Bmatrix}$$
$$\begin{Bmatrix} \sigma_{xz} \\ \sigma_{yz} \end{Bmatrix} = \begin{bmatrix} Q_{44} & 0 \\ 0 & Q_{44} \end{bmatrix} \begin{Bmatrix} \gamma_{xz} \\ \gamma_{yz} \end{Bmatrix} \tag{3.22}$$

Using Hamiltons's principle, we can derive the equations of motion of the RSDT

$$\int_0^T (\delta K - \delta U - \delta V_E) dt = 0 \tag{3.23}$$

where δK is the virtual kinetic energy, δU is the virtual strain energy, and δV_E is the virtual work done by external forces. Therefore, the governing equations are as

$$\begin{aligned}
&\frac{\partial M_{xx}^{(0)}}{\partial x} + \frac{\partial M_{xy}^{(0)}}{\partial y} = I_0 \frac{\partial^2 u}{\partial x^2} \\
&\frac{\partial M_{xy}^{(0)}}{\partial x} + \frac{\partial M_{yy}^{(0)}}{\partial y} = I_0 \frac{\partial^2 v}{\partial x^2} \\
&\frac{\partial}{\partial x}\left(\frac{\partial w}{\partial x} M_{xx}^{(0)} + \frac{\partial w}{\partial y} M_{xy}^{(0)}\right) + \frac{\partial}{\partial y}\left(\frac{\partial w}{\partial x} M_{xy}^{(0)} + \frac{\partial w}{\partial y} M_{yy}^{(0)}\right) \\
&\qquad + \frac{\partial \bar{M}_{xz}^{(0)}}{\partial x} + \frac{\partial \bar{M}_{yz}^{(0)}}{\partial y} + c_1\left(\frac{\partial^2 M_{xx}^{(3)}}{\partial x^2} + 2\frac{\partial^2 M_{xy}^{(3)}}{\partial x \partial y} + \frac{\partial^2 M_{yy}^{(3)}}{\partial y^2}\right) + p \\
&\qquad = -c_1^2 I_6 \frac{\partial^2}{\partial t^2}\left(\frac{\partial^2 w}{\partial x^2} + \frac{\partial^2 w}{\partial y^2}\right) + c_2 \bar{I}_4 \frac{\partial^2}{\partial t^2}\left(\frac{\partial \phi_x}{\partial x} + \frac{\partial \phi_y}{\partial y}\right) + I_0 \frac{\partial^2 w}{\partial t^2} \\
&\frac{\partial \bar{M}_{xx}^{(1)}}{\partial x} + \frac{\partial \bar{M}_{xy}^{(1)}}{\partial y} - \bar{M}_{xz}^{(0)} = \hat{I}_2 \frac{\partial^2 \phi_x}{\partial t^2} - c_1 \bar{I}_4 \frac{\partial^3 w}{\partial x \partial t^2} \\
&\frac{\partial \bar{M}_{xy}^{(1)}}{\partial x} + \frac{\partial \bar{M}_{yy}^{(1)}}{\partial y} - \bar{M}_{yz}^{(0)} = \hat{I}_2 \frac{\partial^2 \phi_y}{\partial t^2} - c_1 \bar{I}_4 \frac{\partial^3 w}{\partial y \partial t^2}
\end{aligned} \tag{3.24}$$

where we have

$$\begin{aligned}
\bar{M}_{\alpha\beta}^{(i)} &= M_{\alpha\beta}^{(i)} - c_1 M_{\alpha\beta}^{(i+2)} \\
\bar{M}_{\alpha z}^{(0)} &= M_{\alpha z}^{(0)} - c_2 M_{\alpha z}^{(2)}
\end{aligned} \tag{3.25}$$

and

$$\begin{aligned}
I_i &= \int_{-\frac{h}{2}}^{\frac{h}{2}} \rho(z)^i dz \\
\bar{I}_i &= I_i - c_1 I_{i+2} \\
\hat{I}_i &= \bar{I}_i - c_1 \bar{I}_{i+2}
\end{aligned} \tag{3.26}$$

The following equations relate generalized forces to the generalized displacement field of this theory

$$\begin{Bmatrix} M_{xx}^{(0)} \\ M_{yy}^{(0)} \\ M_{xy}^{(0)} \end{Bmatrix} = \int_{-\frac{h}{2}}^{\frac{h}{2}} \begin{Bmatrix} \sigma_{xx} \\ \sigma_{yy} \\ \sigma_{xy} \end{Bmatrix} dz = \begin{bmatrix} A_{11} & A_{12} & 0 \\ A_{12} & A_{22} & 0 \\ 0 & 0 & A_{66} \end{bmatrix} \begin{Bmatrix} {\varepsilon_{xx}}^{(0)} \\ {\varepsilon_{yy}}^{(0)} \\ {\gamma_{xy}}^{(0)} \end{Bmatrix}$$

$$\begin{Bmatrix} M_{xx}^{(1)} \\ M_{yy}^{(1)} \\ M_{xy}^{(1)} \end{Bmatrix} = \int_{-\frac{h}{2}}^{\frac{h}{2}} \begin{Bmatrix} \sigma_{xx} \\ \sigma_{yy} \\ \sigma_{xy} \end{Bmatrix} z dz$$

$$= \begin{bmatrix} D_{11} & D_{12} & 0 \\ D_{12} & D_{22} & 0 \\ 0 & 0 & D_{66} \end{bmatrix} \begin{Bmatrix} {\varepsilon_{xx}}^{(1)} \\ {\varepsilon_{yy}}^{(1)} \\ {\gamma_{xy}}^{(1)} \end{Bmatrix} + \begin{bmatrix} F_{11} & F_{12} & 0 \\ F_{12} & F_{22} & 0 \\ 0 & 0 & F_{66} \end{bmatrix} \begin{Bmatrix} {\varepsilon_{xx}}^{(3)} \\ {\varepsilon_{yy}}^{(3)} \\ {\gamma_{xy}}^{(3)} \end{Bmatrix}$$

$$\begin{Bmatrix} M_{xx}^{(3)} \\ M_{yy}^{(3)} \\ M_{xy}^{(3)} \end{Bmatrix} = \int_{-\frac{h}{2}}^{\frac{h}{2}} \begin{Bmatrix} \sigma_{xx} \\ \sigma_{yy} \\ \sigma_{xy} \end{Bmatrix} z^3 dz$$

$$= \begin{bmatrix} F_{11} & F_{12} & 0 \\ F_{12} & F_{22} & 0 \\ 0 & 0 & F_{66} \end{bmatrix} \begin{Bmatrix} {\varepsilon_{xx}}^{(1)} \\ {\varepsilon_{yy}}^{(1)} \\ {\gamma_{xy}}^{(1)} \end{Bmatrix} + \begin{bmatrix} H_{11} & H_{12} & 0 \\ H_{12} & H_{22} & 0 \\ 0 & 0 & H_{66} \end{bmatrix} \begin{Bmatrix} {\varepsilon_{xx}}^{(3)} \\ {\varepsilon_{yy}}^{(3)} \\ {\gamma_{xy}}^{(3)} \end{Bmatrix}$$

$$\begin{Bmatrix} M_{xz}^{(0)} \\ M_{yz}^{(0)} \end{Bmatrix} = \int_{-\frac{h}{2}}^{\frac{h}{2}} \begin{Bmatrix} \sigma_{xz} \\ \sigma_{yz} \end{Bmatrix} dz$$

$$= \begin{bmatrix} A_{44} & 0 \\ 0 & A_{44} \end{bmatrix} \begin{Bmatrix} {\gamma_{xz}}^{(0)} \\ {\gamma_{yz}}^{(0)} \end{Bmatrix} + \begin{bmatrix} D_{44} & 0 \\ 0 & D_{44} \end{bmatrix} \begin{Bmatrix} {\gamma_{xz}}^{(2)} \\ {\gamma_{yz}}^{(2)} \end{Bmatrix}$$

$$\begin{Bmatrix} M_{xz}^{(2)} \\ M_{yz}^{(2)} \end{Bmatrix} = \int_{-\frac{h}{2}}^{\frac{h}{2}} \begin{Bmatrix} \sigma_{xz} \\ \sigma_{yz} \end{Bmatrix} z^2 dz$$
$$= \begin{bmatrix} D_{44} & 0 \\ 0 & D_{44} \end{bmatrix} \begin{Bmatrix} {\gamma_{xz}}^{(0)} \\ {\gamma_{yz}}^{(0)} \end{Bmatrix} + \begin{bmatrix} F_{44} & 0 \\ 0 & F_{44} \end{bmatrix} \begin{Bmatrix} {\gamma_{xz}}^{(2)} \\ {\gamma_{yz}}^{(2)} \end{Bmatrix} \tag{3.27}$$

The constants in the above equations are defined as

$$\begin{aligned}
&A_{11} = \frac{Eh}{1-\nu^2}, \quad A_{12} = \frac{\nu Eh}{1-\nu^2}, \quad A_{44} = A_{66} = Gh = \frac{Eh}{2\,(1+\nu)} \\
&D_{11} = \frac{Eh^3}{12\,(1-\nu^2)}, \quad D_{12} = \frac{\nu Eh^3}{12\,(1-\nu^2)}, \quad D_{44} = D_{66} = \frac{Gh^3}{12} = \frac{Eh^3}{24\,(1+\nu)} \\
&F_{11} = \frac{Eh^5}{80\,(1-\nu^2)}, \quad F_{12} = \frac{\nu Eh^5}{80\,(1-\nu^2)}, \quad F_{44} = F_{66} = \frac{Gh^5}{80} = \frac{Eh^5}{160\,(1+\nu)} \\
&H_{11} = \frac{Eh^7}{448\,(1-\nu^2)}, \quad H_{12} = \frac{\nu Eh^7}{448\,(1-\nu^2)}, \quad H_{66} = \frac{Gh^7}{448} = \frac{Eh^7}{996\,(1+\nu)}
\end{aligned} \tag{3.28}$$

3.2.3 Solid-Fluid Interface

The solid-fluid interface boundary conditions can be obtained by considering the fact that structure deflection transfers the momentum to the fluid at the interface which this distributed force in turn, changes the structure deflection. These conditions can be assumed as the continuity of velocity and traction at the interface

$$\frac{\partial u_s}{\partial t} = v_f \tag{3.29}$$

$$\boldsymbol{\sigma}_s.\mathbf{n} + \boldsymbol{\sigma}_f.\mathbf{n} = 0 \tag{3.30}$$

Evaluating the momentum equation at the interface yields the following equation

$$-\frac{\partial p}{\partial z} - \rho_f g = \rho_f \frac{\partial^2 w}{\partial t^2} \tag{3.31}$$

which will be used later as the solid-fluid interface condition.

3.3 Finite Element Formulations

In this sub-section, we present finite element formulations for the solid and fluid domains. We also impose the interfacial condition given by Eq. (3.31) to couple the two domains. For details, the reader may review Section 2.

3.3.1 Fluid Medium Finite Element Model

The weak form of Eq. (3.2) over a typical fluid element $\Omega^e = (x_a, x_b) \times (y_a, y_b) \times (z_a, z_b)$ is constructed by multiplying Eq. (3.2) by the first variation of p as

$$0 = -\int_{\Omega_e} \delta p \left(\frac{\partial^2 p}{\partial x^2} + \frac{\partial^2 p}{\partial y^2} + \frac{\partial^2 p}{\partial z^2} \right) dxdz \tag{3.32}$$

where one row of fluid elements along the plate length is considered (Fig. 3.1). By means of the vector identity $\nabla.(\alpha\nabla\phi) = \nabla\alpha.\nabla\phi + \alpha\nabla^2\phi$ and the divergence theorem, Eq. (3.32) can be expanded as (for details, the reader may consult the textbooks by Reddy [51])

$$\begin{aligned} 0 = & \int_{z_a}^{z_b} \int_{y_a}^{y_b} \int_{x_a}^{x_b} \left(\frac{\partial \delta p}{\partial x}\frac{\partial p}{\partial x} + \frac{\partial \delta p}{\partial y}\frac{\partial p}{\partial y} + \frac{\partial \delta p}{\partial z}\frac{\partial p}{\partial z} \right) dxdydz \\ & - \int_{y_a}^{y_b} \int_{x_a}^{x_b} \left[\delta p \rho_f \left(g + \frac{\partial^2 w}{\partial t^2} \right) \right]_{z=0} dxdy \\ & - \oint_{\hat{\Gamma}^e} \delta p \left(\frac{\partial p}{\partial x} n_x + \frac{\partial p}{\partial y} n_y + \frac{\partial p}{\partial z} n_z \right) ds \end{aligned} \tag{3.33}$$

where (n_x, n_y, n_z) is the unit normal to the surface. In Eq. (3.33), $\hat{\Gamma}^e$ represents the boundary of a fluid element which does not have any interaction with the plate.
In the problem at hand, the last term of Eq. (3.33) is eliminated either by the corresponding term from the adjacent element or by the prescribed boundary conditions.

Substituting Eq. (3.31) into Eq. (3.33), one can obtain

$$\begin{aligned} 0 = & \int_{z_a}^{z_b} \int_{y_a}^{y_b} \int_{x_a}^{x_b} \left(\frac{\partial \delta p}{\partial x} \frac{\partial p}{\partial x} + \frac{\partial \delta p}{\partial y} \frac{\partial p}{\partial y} + \frac{\partial \delta p}{\partial z} \frac{\partial p}{\partial z} \right) dxdydz \\ & - \int_{y_a}^{y_b} \int_{x_a}^{x_b} \left[\delta p \rho_f \left(g + \frac{\partial^2 w}{\partial t^2} \right) \right]_{z=0} dxdy \\ & - \oint_{\hat{\Gamma}^e} \delta p \left(\frac{\partial p}{\partial x} n_x + \frac{\partial p}{\partial y} n_y + \frac{\partial p}{\partial z} n_z \right) ds \end{aligned} \tag{3.34}$$

We assume the following form of the pressure p for the 3D elements

$$p\left(x, y, z, t\right) = \sum_{j=1}^{n} P_j\left(t\right) \psi_j\left(x, y, z\right) \tag{3.35}$$

where ψ_j^e's are 3D Lagrange family interpolation functions. For our study, we consider 8-node brick elements. Therefore, one can utilize the following interpolation functions [51]

$$\begin{aligned} \psi_1 &= \frac{1}{8}\left(1-\xi\right)\left(1-\eta\right)\left(1-\zeta\right), \quad \psi_2 = \frac{1}{8}\left(1+\xi\right)\left(1-\eta\right)\left(1-\zeta\right) \\ \psi_3 &= \frac{1}{8}\left(1+\xi\right)\left(1+\eta\right)\left(1-\zeta\right), \quad \psi_4 = \frac{1}{8}\left(1-\xi\right)\left(1+\eta\right)\left(1-\zeta\right) \\ \psi_5 &= \frac{1}{8}\left(1-\xi\right)\left(1-\eta\right)\left(1+\zeta\right), \quad \psi_6 = \frac{1}{8}\left(1+\xi\right)\left(1-\eta\right)\left(1+\zeta\right) \\ \psi_7 &= \frac{1}{8}\left(1+\xi\right)\left(1+\eta\right)\left(1+\zeta\right), \quad \psi_8 = \frac{1}{8}\left(1-\xi\right)\left(1+\eta\right)\left(1+\zeta\right) \end{aligned} \tag{3.36}$$

Inserting the approximation (2.44) into the weak form (3.34), we have

$$\mathbf{CP} = \mathbf{f} + \mathbf{Q} \tag{3.37}$$

where the element matrices can be calculated by means of the following integrals

$$
\begin{aligned}
C_{ij} &= \int_{z_a}^{z_b}\int_{y_a}^{y_b}\int_{x_a}^{x_b}\left(\frac{\partial\psi_i}{\partial x}\frac{\psi_j}{\partial x}+\frac{\partial\psi_i}{\partial y}\frac{\psi_j}{\partial y}+\frac{\partial\psi_i}{\partial z}\frac{\psi_j}{\partial z}\right)dxdydz \\
f_i &= \int_{y_b}^{y_b}\int_{x_a}^{x_b}\rho_f\psi_i\left(g+\frac{\partial^2 w}{\partial t^2}\right)dxdy \\
Q_i &= \oint_{\hat{\Gamma}^e}\psi_i\left(\frac{\partial p}{\partial x}n_x+\frac{\partial p}{\partial y}n_y+\frac{\partial p}{\partial z}n_z\right)ds
\end{aligned}
\tag{3.38}
$$

3.3.2 Solid Medium

In this sub-section, we formulate finite element models for the solid medium for each plate theory.

3.3.2.1 The CPT

In order to conduct finite element formulation, we use the following approximations for the primary variables of CPT, which are u, v, and w

$$
\begin{aligned}
u(x,y,t) &\approx \sum_{j=1}^{n} U_j(t)\psi_j(x,y) \\
v(x,y,t) &\approx \sum_{j=1}^{n} V_j(t)\psi_j(x,y) \\
w(x,y,t) &\approx \sum_{j=1}^{n} \bar{\Delta}_j(t)\varphi_j(x,y)
\end{aligned}
\tag{3.39}
$$

In the above approximation, u and v are interpolated using Lagrange family of approximation, while we use the Hermite family of approximation in interpolating w. Substituting the approximations in the governing equation results in the following

finite element equations

$$\begin{bmatrix} \mathbf{M^{11}} & \mathbf{M^{12}} & \mathbf{M^{13}} \\ \mathbf{M^{21}} & \mathbf{M^{22}} & \mathbf{M^{23}} \\ \mathbf{M^{31}} & \mathbf{M^{32}} & \mathbf{M^{33}} \end{bmatrix} \begin{Bmatrix} \ddot{\mathbf{U}} \\ \ddot{\mathbf{V}} \\ \ddot{\mathbf{\Delta}} \end{Bmatrix} + \begin{bmatrix} \mathbf{K^{11}} & \mathbf{K^{12}} & \mathbf{K^{13}} \\ \mathbf{K^{21}} & \mathbf{K^{22}} & \mathbf{K^{23}} \\ \mathbf{K^{31}} & \mathbf{K^{32}} & \mathbf{K^{33}} \end{bmatrix} \begin{Bmatrix} \mathbf{U} \\ \mathbf{V} \\ \mathbf{\Delta} \end{Bmatrix}$$
$$= \begin{Bmatrix} \mathbf{q^1} \\ \mathbf{q^2} \\ \mathbf{q^3} \end{Bmatrix} + \begin{Bmatrix} \mathbf{F^1} \\ \mathbf{F^2} \\ \mathbf{F^3} \end{Bmatrix} \tag{3.40}$$

where the nonzero elements of mass matrices $\mathbf{M}^{\alpha\beta}$, stiffness matrices $\mathbf{K}^{\alpha\beta}$ and force vectors $\mathbf{q}^{\alpha}$ can be obtained using the following integrals:

$$M_{ij}^{11} = M_{ji}^{22} = \int_{\Omega_e} I_0 \psi_i \psi_j dxdy$$
$$M_{ij}^{33} = \int_{\Omega_e} I_0 \varphi_i \varphi_j + c^2 I_6 \left(\frac{\partial \varphi_i}{\partial x} \frac{\partial \varphi_j}{\partial x} + \frac{\partial \varphi_i}{\partial y} \frac{\partial \varphi_j}{\partial y} \right) dxdy \tag{3.41}$$

$$
\begin{aligned}
K_{ij}^{11} &= \int_{\Omega^e} \left(A_{11} \frac{\partial \psi_i}{\partial x} \frac{\partial \psi_j}{\partial x} + A_{66} \frac{\partial \psi_i}{\partial y} \frac{\partial \psi_j}{\partial y} \right) dxdy \\
K_{ij}^{12} &= K_{ji}^{21} = \int_{\Omega^e} \left(A_{12} \frac{\partial \psi_i}{\partial x} \frac{\partial \psi_j}{\partial y} + A_{66} \frac{\partial \psi_i}{\partial y} \frac{\partial \psi_j}{\partial x} \right) dxdy \\
K_{ij}^{13} &= \frac{1}{2} \int_{\Omega^e} \left[\frac{\partial \psi_i}{\partial x} \left(A_{11} \frac{\partial w}{\partial x} \frac{\partial \varphi_j}{\partial x} + A_{12} \frac{\partial w}{\partial y} \frac{\partial \varphi_j}{\partial y} \right) \right. \\
&\quad \left. + A_{66} \frac{\partial \psi_i}{\partial y} \left(\frac{\partial w}{\partial x} \frac{\partial \varphi_j}{\partial y} + \frac{\partial w}{\partial y} \frac{\partial \varphi_j}{\partial x} \right) \right] dxdy \\
K_{ij}^{22} &= \int_{\Omega^e} \left(A_{66} \frac{\partial \psi_i}{\partial x} \frac{\partial \psi_j}{\partial x} + A_{22} \frac{\partial \psi_i}{\partial y} \frac{\partial \psi_j}{\partial y} \right) dxdy \\
K_{ij}^{23} &= \frac{1}{2} \int_{\Omega^e} \left[\frac{\partial \psi_i}{\partial y} \left(A_{12} \frac{\partial w}{\partial x} \frac{\partial \varphi_j}{\partial x} + A_{22} \frac{\partial w}{\partial y} \frac{\partial \varphi_j}{\partial y} \right) \right. \\
&\quad \left. + A_{66} \frac{\partial \psi_i}{\partial x} \left(\frac{\partial w}{\partial x} \frac{\partial \varphi_j}{\partial y} + \frac{\partial w}{\partial y} \frac{\partial \varphi_j}{\partial x} \right) \right] dxdy \\
K_{ij}^{31} &= \int_{\Omega^e} \left[\frac{\partial \varphi_i}{\partial x} \left(A_{11} \frac{\partial w}{\partial x} \frac{\partial \psi_j}{\partial x} + A_{66} \frac{\partial w}{\partial y} \frac{\partial \psi_j}{\partial y} \right) \right. \\
&\quad \left. + \frac{\partial \varphi_i}{\partial y} \left(A_{66} \frac{\partial w}{\partial x} \frac{\partial \psi_j}{\partial y} + A_{12} \frac{\partial w}{\partial y} \frac{\psi_j}{\partial x} \right) \right] dxdy \\
K_{ij}^{32} &= \int_{\Omega^e} \left[\frac{\partial \varphi_i}{\partial x} \left(A_{12} \frac{\partial w}{\partial x} \frac{\partial \psi_j}{\partial y} + A_{66} \frac{\partial w}{\partial y} \frac{\partial \psi_j}{\partial x} \right) \right. \\
&\quad \left. + \frac{\partial \varphi_i}{\partial y} \left(A_{66} \frac{\partial w}{\partial x} \frac{\partial \psi_j}{\partial x} + A_{22} \frac{\partial w}{\partial y} \frac{\psi_j}{\partial y} \right) \right] dxdy \\
K_{ij}^{33} &= \int_{\Omega^e} \left[D_{11} \frac{\partial^2 \varphi_i}{\partial x^2} \frac{\partial^2 \varphi_j}{\partial x^2} + D_{12} \left(\frac{\partial^2 \varphi_i}{\partial x^2} \frac{\partial^2 \varphi_j}{\partial y^2} + \frac{\partial^2 \varphi_i}{\partial y^2} \frac{\partial^2 \varphi_j}{\partial x^2} \right) \right. \\
&\quad \left. + D_{22} \frac{\partial^2 \varphi_i}{\partial y^2} \frac{\partial^2 \varphi_j}{\partial y^2} + 4 D_{66} \frac{\partial^2 \varphi_i}{\partial x \partial y} \frac{\partial^2 \varphi_j}{\partial x \partial y} \right] dxdy \\
&\quad + \frac{1}{2} \int_{\Omega^e} \left\{ \left[A_{11} \left(\frac{\partial w}{\partial x} \right)^2 + A_{66} \left(\frac{\partial w}{\partial y} \right)^2 \right] \frac{\partial \varphi_i}{\partial x} \frac{\partial \varphi_j}{\partial x} \right. \\
&\quad + \left[A_{66} \left(\frac{\partial w}{\partial x} \right)^2 + A_{22} \left(\frac{\partial w}{\partial y} \right)^2 \right] \frac{\partial \varphi_i}{\partial y} \frac{\partial \varphi_j}{\partial y} \\
&\quad \left. + \left(A_{12} + A_{66} \right) \frac{\partial w}{\partial x} \frac{\partial w}{\partial y} \left(\frac{\partial \varphi_i}{\partial x} \frac{\partial \varphi_j}{\partial y} + \frac{\partial \varphi_i}{\partial y} \frac{\partial \varphi_j}{\partial x} \right) \right\} dxdy
\end{aligned} \tag{3.42}
$$

$$
q_i^3 = \int_{\Omega_e} p \varphi_i dxdy \tag{3.43}
$$

where the coefficients are expressed as

$$A_{ij} = Q_{ij}h, \quad D_{ij} = Q_{ij}\frac{h^3}{12} \tag{3.44}$$

In Eq. (3.40), $\mathbf{F}^i$ are the generalized nodal force vectors. The general form of q_i^3 in Eq. (3.43) will be presented in Sub-section 3.3.4.1.

3.3.2.2 The FSDT

In order to conduct finite element formulation, we use the following approximations for the primary variables of FSDT, which are u, v, w, ϕ_x, and ϕ_y

$$\begin{aligned}
u(x,y,t) &\approx \sum_{j=1}^{n} U_j(t)\psi_j^{(1)}(x,y) \\
v(x,y,t) &\approx \sum_{j=1}^{n} V_j(t)\psi_j^{(1)}(x,y) \\
w(x,y,t) &\approx \sum_{j=1}^{n} W_j(t)\psi_j^{(2)}(x,y) \\
\phi_x(x,y,t) &\approx \sum_{j=1}^{n} \Phi_j^x(t)\psi_j^{(3)}(x,y) \\
\phi_y(x,y,t) &\approx \sum_{j=1}^{n} \Phi_j^y(t)\psi_j^{(3)}(x,y)
\end{aligned} \tag{3.45}$$

In the above approximation, u, v, w, ϕ_x, and ϕ_y are interpolated using Lagrange family of approximation.

Substituting the approximations in the governing equation results in the following finite element equations

$$\mathbf{M}\ddot{\mathbf{\Delta}} + \mathbf{K}\mathbf{\Delta} = \mathbf{F} \tag{3.46}$$

or in matrix form, we have

$$\begin{bmatrix} \mathbf{M^{11}} & \mathbf{M^{12}} & \mathbf{M^{13}} & \mathbf{M^{14}} & \mathbf{M^{15}} \\ \mathbf{M^{21}} & \mathbf{M^{22}} & \mathbf{M^{23}} & \mathbf{M^{24}} & \mathbf{M^{25}} \\ \mathbf{M^{31}} & \mathbf{M^{32}} & \mathbf{M^{33}} & \mathbf{M^{34}} & \mathbf{M^{35}} \\ \mathbf{M^{41}} & \mathbf{M^{42}} & \mathbf{M^{43}} & \mathbf{M^{44}} & \mathbf{M^{45}} \\ \mathbf{M^{51}} & \mathbf{M^{52}} & \mathbf{M^{53}} & \mathbf{M^{45}} & \mathbf{M^{55}} \end{bmatrix} \begin{Bmatrix} \ddot{\mathbf{U}} \\ \ddot{\mathbf{V}} \\ \ddot{\mathbf{W}} \\ \ddot{\mathbf{\Phi}}_x \\ \ddot{\mathbf{\Phi}}_y \end{Bmatrix}$$

$$+ \begin{bmatrix} \mathbf{K^{11}} & \mathbf{K^{12}} & \mathbf{K^{13}} & \mathbf{K^{14}} & \mathbf{K^{15}} \\ \mathbf{K^{21}} & \mathbf{K^{22}} & \mathbf{K^{23}} & \mathbf{K^{24}} & \mathbf{K^{25}} \\ \mathbf{K^{31}} & \mathbf{K^{32}} & \mathbf{K^{33}} & \mathbf{K^{34}} & \mathbf{K^{35}} \\ \mathbf{K^{41}} & \mathbf{K^{42}} & \mathbf{K^{43}} & \mathbf{K^{44}} & \mathbf{K^{45}} \\ \mathbf{K^{51}} & \mathbf{K^{52}} & \mathbf{K^{53}} & \mathbf{K^{45}} & \mathbf{K^{55}} \end{bmatrix} \begin{Bmatrix} \mathbf{U} \\ \mathbf{V} \\ \mathbf{W} \\ \mathbf{\Phi_x} \\ \mathbf{\Phi_y} \end{Bmatrix} = \begin{Bmatrix} \mathbf{q^1} \\ \mathbf{q^2} \\ \mathbf{q^3} \\ \mathbf{q^4} \\ \mathbf{q^5} \end{Bmatrix} + \begin{Bmatrix} \mathbf{F^1} \\ \mathbf{F^2} \\ \mathbf{F^3} \\ \mathbf{F^4} \\ \mathbf{F^5} \end{Bmatrix} \tag{3.47}$$

where the nonzero elements of mass matrices $\mathbf{M}^{\alpha\beta}$, stiffness matrices $\mathbf{K}^{\alpha\beta}$ and force vectors $\mathbf{q}^{\alpha}$ can be obtained using the following integrals:

$$\begin{aligned} M_{ij}^{11} = M_{ij}^{22} &= \int_{\Omega_e} I_0 \psi_i^{(1)} \psi_j^{(1)} dxdy \\ M_{ij}^{33} &= \int_{\Omega_e} I_0 \psi_i^{(2)} \psi_j^{(2)} dxdy \\ M_{ij}^{44} = M_{ij}^{55} &= \int_{\Omega_e} I_2 \psi_i^{(2)} \psi_j^{(2)} dxdy \end{aligned} \tag{3.48}$$

$$K_{ij}^{11} = \int_{\Omega^e} \left(A_{11} \frac{\partial \psi_i^{(1)}}{\partial x} \frac{\partial \psi_j^{(1)}}{\partial x} + A_{66} \frac{\partial \psi_i^{(1)}}{\partial y} \frac{\partial \psi_j^{(1)}}{\partial y} \right) dxdy$$

$$K_{ij}^{12} = K_{ji}^{21} = \int_{\Omega^e} \left(A_{12} \frac{\partial \psi_i^{(1)}}{\partial x} \frac{\partial \psi_j^{(1)}}{\partial y} + A_{66} \frac{\partial \psi_i^{(1)}}{\partial y} \frac{\partial \psi_j^{(1)}}{\partial x} \right) dxdy$$

$$K_{ij}^{13} = \frac{1}{2} \int_{\Omega^e} \left[\frac{\partial \psi_i^{(1)}}{\partial x} \left(A_{11} \frac{\partial w}{\partial x} \frac{\partial \psi_j^{(2)}}{\partial x} + A_{12} \frac{\partial w}{\partial y} \frac{\partial \psi_j^{(2)}}{\partial y} \right) \right.$$
$$\left. + A_{66} \frac{\partial \psi_i^{(1)}}{\partial y} \left(\frac{\partial w}{\partial x} \frac{\partial \psi_j^{(2)}}{\partial y} + \frac{\partial w}{\partial y} \frac{\partial \psi_j^{(2)}}{\partial x} \right) \right] dxdy$$

$$K_{ij}^{22} = \int_{\Omega^e} \left(A_{66} \frac{\partial \psi_i^{(1)}}{\partial x} \frac{\partial \psi_i^{(1)}}{\partial x} + A_{22} \frac{\partial \psi_i^{(1)}}{\partial y} \frac{\partial \psi_i^{(1)}}{\partial y} \right) dxdy$$

$$K_{ij}^{23} = \frac{1}{2} \int_{\Omega^e} \left[\frac{\partial \psi_i^{(1)}}{\partial y} \left(A_{12} \frac{\partial w}{\partial x} \frac{\partial \psi_j^{(2)}}{\partial x} + A_{22} \frac{\partial w}{\partial y} \frac{\partial \psi_j^{(2)}}{\partial y} \right) \right.$$
$$\left. + A_{66} \frac{\partial \psi_i^{(1)}}{\partial x} \left(\frac{\partial w}{\partial x} \frac{\partial \psi_j^{(2)}}{\partial y} + \frac{\partial w}{\partial y} \frac{\partial \psi_j^{(2)}}{\partial x} \right) \right] dxdy$$

$$K_{ij}^{31} = \int_{\Omega^e} \left[\frac{\partial \psi_i^{(2)}}{\partial x} \left(A_{11} \frac{\partial w}{\partial x} \frac{\partial \psi_j^{(1)}}{\partial x} + A_{66} \frac{\partial w}{\partial y} \frac{\partial \psi_j^{(1)}}{\partial y} \right) \right.$$
$$\left. + \frac{\partial \psi_i^{(2)}}{\partial y} \left(A_{66} \frac{\partial w}{\partial x} \frac{\partial \psi_j^{(1)}}{\partial y} + A_{12} \frac{\partial w}{\partial y} \frac{\psi_j^{(1)}}{\partial x} \right) \right] dxdy$$

$$K_{ij}^{32} = \int_{\Omega^e} \left[\frac{\partial \psi_i^{(2)}}{\partial x} \left(A_{12} \frac{\partial w}{\partial x} \frac{\partial \psi_j^{(1)}}{\partial y} + A_{66} \frac{\partial w}{\partial y} \frac{\partial \psi_j^{(1)}}{\partial x} \right) \right.$$
$$\left. + \frac{\partial \psi_i^{(2)}}{\partial y} \left(A_{66} \frac{\partial w}{\partial x} \frac{\partial \psi_j^{(1)}}{\partial x} + A_{22} \frac{\partial w}{\partial y} \frac{\psi_j^{(1)}}{\partial y} \right) \right] dxdy$$

$$K_{ij}^{33} = \int_{\Omega^e} \left(A_{55} \frac{\partial \psi_i^{(2)}}{\partial x} \frac{\partial \psi_j^{(2)}}{\partial x} + A_{44} \frac{\partial \psi_i^{(2)}}{\partial y} \frac{\partial \psi_j^{(2)}}{\partial y} \right) dxdy$$
$$+ \frac{1}{2} \int_{\Omega^e} \left\{ \left[A_{11} \left(\frac{\partial w}{\partial x} \right)^2 + A_{66} \left(\frac{\partial w}{\partial y} \right)^2 \right] \frac{\partial \psi_i^{(2)}}{\partial x} \frac{\partial \psi_j^{(2)}}{\partial x} \right.$$
$$+ \left[A_{66} \left(\frac{\partial w}{\partial x} \right)^2 + A_{22} \left(\frac{\partial w}{\partial y} \right)^2 \right] \frac{\partial \psi_i^{(2)}}{\partial y} \frac{\partial \psi_j^{(2)}}{\partial x}$$
$$\left. + \left(A_{12} + A_{66} \right) \frac{\partial w}{\partial x} \frac{\partial w}{\partial y} \left(\frac{\partial \varphi_i}{\partial x} \frac{\partial \varphi_j}{\partial y} + \frac{\partial \psi_i^{(2)}}{\partial y} \frac{\partial \psi_j^{(2)}}{\partial x} \right) \right\} dxdy$$

$$
\begin{aligned}
K_{ij}^{34} &= K_{ji}^{43} = \int_{\Omega^e} A_{55} \frac{\partial \psi_i^{(2)}}{\partial x} \psi_j^{(3)} dxdy \\
K_{ij}^{35} &= K_{ji}^{53} = \int_{\Omega^e} A_{44} \frac{\partial \psi_i^{(2)}}{\partial y} \psi_j^{(3)} dxdy \\
K_{ij}^{44} &= \int_{\Omega^e} \left(D_{11} \frac{\partial \psi_i^{(3)}}{\partial x} \frac{\partial \psi_j^{(3)}}{\partial x} + D_{66} \frac{\partial \psi_i^{(3)}}{\partial y} \frac{\partial \psi_j^{(3)}}{\partial y} + A_{55} \psi_i^{(3)} \psi_j^{(3)} \right) dxdy \\
K_{ij}^{45} &= K_{ij}^{54} = \int_{\Omega^e} \left(D_{12} \frac{\partial \psi_i^{(3)}}{\partial x} \frac{\partial \psi_j^{(3)}}{\partial y} + D_{66} \frac{\partial \psi_i^{(3)}}{\partial y} \frac{\partial \psi_j^{(3)}}{\partial x} \right) dxdy \\
K_{ij}^{55} &= \int_{\Omega^e} \left(D_{66} \frac{\partial \psi_i^{(3)}}{\partial x} \frac{\partial \psi_i^{(3)}}{\partial x} + D_{22} \frac{\partial \psi_i^{(3)}}{\partial y} \frac{\partial \psi_i^{(3)}}{\partial y} + A_{44} \psi_i^{(3)} \psi_j^{(3)} \right) dxdy
\end{aligned} \tag{3.49}
$$

$$
q_i^3 = \int_{\Omega_e} p \psi_i^{(2)} dxdy \tag{3.50}
$$

In Eq. (3.47), $\mathbf{F}^i$ are the generalized nodal force vectors. The general form of q_i^3 in Eq. (3.50) will be presented in Sub-section 3.3.4.2.

3.3.2.3 The RSDT

In order to conduct finite element formulation, we use the following approximations for the primary variables of RSDT, which are u, v, w, ϕ_x, and ϕ_y

$$\begin{aligned}
u(x,y,t) &\approx \sum_{j=1}^{n} U_j(t)\psi_j^{(1)}(x,y) \\
v(x,y,t) &\approx \sum_{j=1}^{n} V_j(t)\psi_j^{(1)}(x,y) \\
w(x,y,t) &\approx \sum_{j=1}^{n} \bar{\Delta}_j(t)\varphi_j(x,y) \\
\phi_x(x,y,t) &\approx \sum_{j=1}^{n} \Phi_j^x(t)\psi_j^{(2)}(x,y) \\
\phi_y(x,y,t) &\approx \sum_{j=1}^{n} \Phi_j^y(t)\psi_j^{(2)}(x,y)
\end{aligned} \tag{3.51}$$

In the above approximation, u, v, ϕ_x, and ϕ_y are interpolated using Lagrange family of approximation, while we use the Hermite family of approximation in interpolating w. Generally, it is not necessary to use the same degree of interpolation for (u, v) and (ϕ_x, ϕ_y), however we consider the same interpolation function for all of them.

Substituting the approximations in the governing equation results in the following finite element equations

$$\mathbf{M}\ddot{\mathbf{\Delta}} + \mathbf{K}\mathbf{\Delta} = \mathbf{F} \tag{3.52}$$

or in matrix form, we have

$$\begin{bmatrix} \mathbf{M^{11}} & \mathbf{M^{12}} & \mathbf{M^{13}} & \mathbf{M^{14}} & \mathbf{M^{15}} \\ \mathbf{M^{21}} & \mathbf{M^{22}} & \mathbf{M^{23}} & \mathbf{M^{24}} & \mathbf{M^{25}} \\ \mathbf{M^{31}} & \mathbf{M^{32}} & \mathbf{M^{33}} & \mathbf{M^{34}} & \mathbf{M^{35}} \\ \mathbf{M^{41}} & \mathbf{M^{42}} & \mathbf{M^{43}} & \mathbf{M^{44}} & \mathbf{M^{45}} \\ \mathbf{M^{51}} & \mathbf{M^{52}} & \mathbf{M^{53}} & \mathbf{M^{45}} & \mathbf{M^{55}} \end{bmatrix} \begin{Bmatrix} \ddot{\mathbf{U}} \\ \ddot{\mathbf{V}} \\ \ddot{\mathbf{\Delta}} \\ \ddot{\mathbf{\Phi}}_x \\ \ddot{\mathbf{\Phi}}_y \end{Bmatrix}$$

$$+ \begin{bmatrix} \mathbf{K^{11}} & \mathbf{K^{12}} & \mathbf{K^{13}} & \mathbf{K^{14}} & \mathbf{K^{15}} \\ \mathbf{K^{21}} & \mathbf{K^{22}} & \mathbf{K^{23}} & \mathbf{K^{24}} & \mathbf{K^{25}} \\ \mathbf{K^{31}} & \mathbf{K^{32}} & \mathbf{K^{33}} & \mathbf{K^{34}} & \mathbf{K^{35}} \\ \mathbf{K^{41}} & \mathbf{K^{42}} & \mathbf{K^{43}} & \mathbf{K^{44}} & \mathbf{K^{45}} \\ \mathbf{K^{51}} & \mathbf{K^{52}} & \mathbf{K^{53}} & \mathbf{K^{45}} & \mathbf{K^{55}} \end{bmatrix} \begin{Bmatrix} \mathbf{U} \\ \mathbf{V} \\ \mathbf{\Delta} \\ \mathbf{\Phi_x} \\ \mathbf{\Phi_y} \end{Bmatrix} = \begin{Bmatrix} \mathbf{q^1} \\ \mathbf{q^2} \\ \mathbf{q^3} \\ \mathbf{q^4} \\ \mathbf{q^5} \end{Bmatrix} + \begin{Bmatrix} \mathbf{F^1} \\ \mathbf{F^2} \\ \mathbf{F^3} \\ \mathbf{F^4} \\ \mathbf{F^5} \end{Bmatrix} \tag{3.53}$$

where the nonzero elements of mass matrices $\mathbf{M}^{\alpha\beta}$, stiffness matrices $\mathbf{K}^{\alpha\beta}$ and force vectors $\mathbf{q}^{\alpha}$ can be obtained using the following integrals:

$$\begin{aligned} M_{ij}^{11} &= M_{ij}^{22} = \int_{\Omega_e} I_0 \psi_i^{(1)} \psi_j^{(1)} dxdy \\ M_{ij}^{33} &= \int_{\Omega_e} I_0 \varphi_i \varphi_j + c_1^2 I_6 \left(\frac{\partial \varphi_i}{\partial x} \frac{\partial \varphi_j}{\partial x} + \frac{\partial \varphi_i}{\partial y} \frac{\partial \varphi_j}{\partial y} \right) dxdy \\ M_{ij}^{34} &= M_{ji}^{43} = -c_1 I_4 \int_{\Omega_e} \frac{\partial \varphi_i}{\partial x} \psi_j^{(2)} \\ M_{ij}^{35} &= M_{ji}^{53} = -c_1 I_4 \int_{\Omega_e} \frac{\partial \varphi_i}{\partial y} \psi_j^{(2)} \\ M_{ij}^{44} &= M_{ij}^{55} = \int_{\Omega_e} \hat{I}_2 \psi_i^{(2)} \psi_j^{(2)} dxdy \end{aligned} \tag{3.54}$$

$$K_{ij}^{11} = \int_{\Omega^e} \left(A_{11} \frac{\partial \psi_i^{(1)}}{\partial x} \frac{\partial \psi_i^{(1)}}{\partial x} + A_{66} \frac{\partial \psi_i^{(1)}}{\partial y} \frac{\partial \psi_i^{(1)}}{\partial y} \right) dxdy$$

$$K_{ij}^{12} = K_{ji}^{21} = \int_{\Omega^e} \left(A_{12} \frac{\partial \psi_i^{(1)}}{\partial x} \frac{\partial \psi_i^{(1)}}{\partial y} + A_{66} \frac{\partial \psi_i^{(1)}}{\partial y} \frac{\partial \psi_i^{(1)}}{\partial x} \right) dxdy$$

$$K_{ij}^{13} = \frac{1}{2} \int_{\Omega^e} \left[\frac{\partial \psi_i^{(1)}}{\partial x} \left(A_{11} \frac{\partial w}{\partial x} \frac{\partial \varphi_j}{\partial x} + A_{12} \frac{\partial w}{\partial y} \frac{\partial \varphi_j}{\partial y} \right) \right.$$
$$\left. + A_{66} \frac{\partial \psi_i^{(1)}}{\partial y} \left(\frac{\partial w}{\partial x} \frac{\partial \varphi_j}{\partial y} + \frac{\partial w}{\partial y} \frac{\partial \varphi_j}{\partial x} \right) \right] dxdy$$

$$K_{ij}^{22} = \int_{\Omega^e} \left(A_{66} \frac{\partial \psi_i^{(1)}}{\partial x} \frac{\partial \psi_i^{(1)}}{\partial x} + A_{22} \frac{\partial \psi_i^{(1)}}{\partial y} \frac{\partial \psi_i^{(1)}}{\partial y} \right) dxdy$$

$$K_{ij}^{23} = \frac{1}{2} \int_{\Omega^e} \left[\frac{\partial \psi_i^{(1)}}{\partial y} \left(A_{12} \frac{\partial w}{\partial x} \frac{\partial \varphi_j}{\partial x} + A_{22} \frac{\partial w}{\partial y} \frac{\partial \varphi_j}{\partial y} \right) \right.$$
$$\left. + A_{66} \frac{\partial \psi_i^{(1)}}{\partial x} \left(\frac{\partial w}{\partial x} \frac{\partial \varphi_j}{\partial y} + \frac{\partial w}{\partial y} \frac{\partial \varphi_j}{\partial x} \right) \right] dxdy$$

$$K_{ij}^{31} = \int_{\Omega^e} \left[\frac{\partial \varphi_i}{\partial x} \left(A_{11} \frac{\partial w}{\partial x} \frac{\partial \psi_j^{(1)}}{\partial x} + A_{66} \frac{\partial w}{\partial y} \frac{\partial \psi_j^{(1)}}{\partial y} \right) \right.$$
$$\left. + \frac{\partial \varphi_i}{\partial y} \left(A_{66} \frac{\partial w}{\partial x} \frac{\partial \psi_j^{(1)}}{\partial y} + A_{12} \frac{\partial w}{\partial y} \frac{\psi_j^{(1)}}{\partial x} \right) \right] dxdy$$

$$K_{ij}^{32} = \int_{\Omega^e} \left[\frac{\partial \varphi_i}{\partial x} \left(A_{12} \frac{\partial w}{\partial x} \frac{\partial \psi_j^{(1)}}{\partial y} + A_{66} \frac{\partial w}{\partial y} \frac{\partial \psi_j^{(1)}}{\partial x} \right) + \right.$$
$$\left. \frac{\partial \varphi_i}{\partial y} \left(A_{66} \frac{\partial w}{\partial x} \frac{\partial \psi_j^{(1)}}{\partial x} + A_{22} \frac{\partial w}{\partial y} \frac{\psi_j^{(1)}}{\partial y} \right) \right] dxdy$$

$$
\begin{aligned}
K_{ij}^{33} &= c^2 \int_{\Omega^e} \left[H_{11} \frac{\partial^2 \varphi_i}{\partial x^2} \frac{\partial^2 \varphi_j}{\partial x^2} + 2H_{12} \left(\frac{\partial^2 \varphi_i}{\partial x^2} \frac{\partial^2 \varphi_j}{\partial y^2} + \frac{\partial^2 \varphi_i}{\partial y^2} \frac{\partial^2 \varphi_j}{\partial x^2} \right) \right. \\
&\quad \left. + H_{22} \frac{\partial^2 \varphi_i}{\partial y^2} \frac{\partial^2 \varphi_j}{\partial y^2} + 4H_{66} \frac{\partial^2 \varphi_i}{\partial x \partial y} \frac{\partial^2 \varphi_j}{\partial x \partial y} \right] dxdy \\
&\quad + \frac{1}{2} \int_{\Omega^e} \left\{ \left[A_{11} \left(\frac{\partial w}{\partial x} \right)^2 + A_{66} \left(\frac{\partial w}{\partial y} \right)^2 \right] \frac{\partial \varphi_i}{\partial x} \frac{\partial \varphi_j}{\partial x} \right. \\
&\quad + \left[A_{66} \left(\frac{\partial w}{\partial x} \right)^2 + A_{22} \left(\frac{\partial w}{\partial y} \right)^2 \right] \frac{\partial \varphi_i}{\partial y} \frac{\partial \varphi_j}{\partial x} \\
&\quad \left. + \left(A_{12} + A_{66} \right) \frac{\partial w}{\partial x} \frac{\partial w}{\partial y} \left(\frac{\partial \varphi_i}{\partial x} \frac{\partial \varphi_j}{\partial y} + \frac{\partial \varphi_i}{\partial y} \frac{\partial \varphi_j}{\partial x} \right) \right\} dxdy \\
&\quad + \int_{\Omega^e} \hat{A}_{44} \left(\frac{\partial \varphi_i}{\partial x} \frac{\partial \varphi_j}{\partial x} + \frac{\partial \varphi_i}{\partial y} \frac{\partial \varphi_j}{\partial y} \right) dxdy \\
K_{ij}^{34} &= K_{ji}^{43} = \int_{\Omega^e} \left[-c \left(\bar{F}_{11} \frac{\partial^2 \varphi_i}{\partial x^2} \frac{\partial \psi_j^{(2)}}{\partial x} + 2\bar{F}_{66} \frac{\partial^2 \varphi_i}{\partial x \partial y} \frac{\partial \psi_j^{(2)}}{\partial y} + \bar{F}_{12} \frac{\partial^2 \varphi_i}{\partial y^2} \frac{\partial \psi_j^{(2)}}{\partial x} \right) \right. \\
&\quad \left. + \hat{A}_{44} \frac{\partial \varphi_i}{\partial x} \psi_j^{(2)} \right] dxdy \\
K_{ij}^{35} &= K_{ji}^{53} = \int_{\Omega^e} \left[-c \left(\bar{F}_{12} \frac{\partial^2 \varphi_i}{\partial x^2} \frac{\partial \psi_j^{(2)}}{\partial y} + 2\bar{F}_{66} \frac{\partial^2 \varphi_i}{\partial x \partial y} \frac{\partial \psi_j^{(2)}}{\partial x} + \bar{F}_{22} \frac{\partial^2 \varphi_i}{\partial y^2} \frac{\partial \psi_j^{(2)}}{\partial y} \right) \right. \\
&\quad \left. + \hat{A}_{44} \frac{\partial \varphi_i}{\partial y} \psi_j^{(2)} \right] dxdy \\
K_{ij}^{44} &= \int_{\Omega^e} \left(\hat{D}_{11} \frac{\partial \psi_i^{(2)}}{\partial x} \frac{\partial \psi_j^{(2)}}{\partial x} + \hat{D}_{66} \frac{\partial \psi_i^{(2)}}{\partial y} \frac{\partial \psi_j^{(2)}}{\partial y} + \hat{A}_{44} \psi_i^{(2)} \psi_j^{(2)} \right) dxdy \\
K_{ij}^{45} &= K_{ij}^{54} = \int_{\Omega^e} \left(\hat{D}_{12} \frac{\partial \psi_i^{(2)}}{\partial x} \frac{\partial \psi_j^{(2)}}{\partial y} + \hat{D}_{66} \frac{\partial \psi_i^{(2)}}{\partial y} \frac{\partial \psi_j^{(2)}}{\partial x} \right) dxdy \\
K_{ij}^{55} &= \int_{\Omega^e} \left(\hat{D}_{66} \frac{\partial \psi_i^{(2)}}{\partial x} \frac{\partial \psi_i^{(2)}}{\partial x} + \hat{D}_{22} \frac{\partial \psi_i^{(2)}}{\partial y} \frac{\partial \psi_i^{(2)}}{\partial y} + \hat{A}_{44} \psi_i^{(2)} \psi_j^{(2)} \right) dxdy
\end{aligned} \tag{3.55}
$$

$$
q_i^3 = \int_{\Omega_e} p \varphi_i dxdy \tag{3.56}
$$

In Eq. (3.53), $\mathbf{F}^i$ are the generalized nodal force vectors. The general form of q_i^3 in Eq. (3.56) will be presented in Sub-section 3.3.4.3.

3.3.3 Interface Connecting Fluid and Solid Regions

The finite element model for the coupling between the fluid and solid can be obtained considering that the fluid and solid finite element models are coupled in the respective force vectors of each model. The most common approach to solve such coupled equations is to assume a solution for structure regime (or fluid regime) and use this assumed solution as an input for solving the fluid regime (or solid regimes). Obtained solutions can be used repeatedly as an input for solving the other regime equations. This loop will be stopped when a desirable convergence of solutions in both regimes is achieved. However, formulating the equations using the appropriate displacements fields [see Eqs. (3.35), (3.39), (3.45), and (3.51)] in the evaluation of $\mathbf{F}$ and $\mathbf{q}$ is much more direct. Following this approach, the finite element equations for the fluid domain can be expressed as

$$\mathbf{CP} = \hat{\mathbf{f}} + \rho_f \mathbf{S}\ddot{\mathbf{\Delta}} + \mathbf{Q} \tag{3.57}$$

where $\mathbf{S}$ is known as the solid-fluid coupling matrix and $\hat{\mathbf{f}}$ is a gravity force vector in the fluid medium. Equation (3.57) is accurate for all three plate models considered in the present study. However, it will shortly be presented that the specific form of $\mathbf{S}$ is defined by the chosen plate theory model; therefore, one can describe $\mathbf{S}$ and $\hat{\mathbf{f}}$ as

$$\begin{aligned} S_{ij} &= \int_{y_a}^{y_b} \int_{x_a}^{x_b} \psi_i \chi_j dx dy \\ \hat{f}_i &= \int_{y_a}^{y_b} \int_{x_a}^{x_b} \rho_f g \psi_i dx dy \end{aligned} \tag{3.58}$$

In Eq. (3.58), $\chi_j = \varphi_j$ for the CPT and RSDT. In the case of the FSDT, $\chi_j = \psi_j^{(1)}$.

3.3.4 Condensing out Pressure Degrees of Freedom

Condensing out the pressure degrees of freedom seems to be impossible in the most general case. This is due to the coupling between the fluid and structure equations. Consequently, determining the response of one domain independently from that of the other can not be achieved. However, our model is formulated such that there is only one row of fluid elements above the plate. Considering the specified pressure along the top of each fluid element (i.e., $P_5^e = P_6^e = P_7^e = P_8^e = 0$), it is possible to condense out the pressure degrees of freedom in the finite element model. Therefore, we describe the following equation for pressure in order to condense out the additional pressure degrees of freedom:

$$\mathbf{P} = \bar{\mathbf{C}}^{-1}\left(\hat{\mathbf{f}} + \rho_f \mathbf{S}\ddot{\mathbf{\Delta}} + \mathbf{Q}\right) \tag{3.59}$$

Equation (3.59) can be used along with any plate theory to express the global finite element equations of the system in terms of the generalized structure displacements.

3.3.4.1 Classical Plate Formulation

Condensing out pressure degree of freedom, the finite element equations for the CPT can be expressed as

$$\begin{bmatrix} \mathbf{M}^{11} & 0 & 0 \\ 0 & \mathbf{M}^{22} & 0 \\ 0 & 0 & \mathbf{M}^{33} \end{bmatrix} \begin{Bmatrix} \ddot{\mathbf{U}} \\ \ddot{\mathbf{V}} \\ \ddot{\mathbf{\Delta}} \end{Bmatrix} + \begin{bmatrix} \mathbf{K}^{11} & \mathbf{K}^{12} & \mathbf{K}^{13} \\ \mathbf{K}^{21} & \mathbf{K}^{22} & \mathbf{K}^{23} \\ \mathbf{K}^{31} & \mathbf{K}^{32} & \mathbf{K}^{33} \end{bmatrix} \begin{Bmatrix} \mathbf{U} \\ \mathbf{V} \\ \mathbf{\Delta} \end{Bmatrix} = \begin{Bmatrix} 0 \\ 0 \\ -\mathbf{S}^T\mathbf{P} \end{Bmatrix} + \begin{Bmatrix} \mathbf{F}^1 \\ \mathbf{F}^2 \\ \mathbf{F}^3 \end{Bmatrix} \tag{3.60}$$

Using Eq. (3.59), one can describe Eq. (3.60) as

$$\begin{bmatrix} \mathbf{M}^{11} & 0 & 0 \\ 0 & \mathbf{M}^{22} & 0 \\ 0 & 0 & \bar{\mathbf{M}}^{33} \end{bmatrix} \begin{Bmatrix} \ddot{\mathbf{U}} \\ \ddot{\mathbf{V}} \\ \ddot{\mathbf{\Delta}} \end{Bmatrix} + \begin{bmatrix} \mathbf{K}^{11} & \mathbf{K}^{12} & \mathbf{K}^{13} \\ \mathbf{K}^{21} & \mathbf{K}^{22} & \mathbf{K}^{23} \\ \mathbf{K}^{31} & \mathbf{K}^{32} & \mathbf{K}^{33} \end{bmatrix} \begin{Bmatrix} \mathbf{U} \\ \mathbf{V} \\ \mathbf{\Delta} \end{Bmatrix} = \begin{Bmatrix} 0 \\ 0 \\ -\mathbf{S}^T \bar{\mathbf{C}}^{-1} \left(\hat{\mathbf{f}} + \mathbf{Q} \right) \end{Bmatrix} + \begin{Bmatrix} \mathbf{F}^1 \\ \mathbf{F}^2 \\ \mathbf{F}^3 \end{Bmatrix} \tag{3.61}$$

where the added mass is $\rho_f \mathbf{S}^T \bar{\mathbf{C}}^{-1} \mathbf{S}$, therefore, we have

$$\bar{\mathbf{M}}^{33} = \mathbf{M}^{33} + \rho_f \mathbf{S}^T \bar{\mathbf{C}}^{-1} \mathbf{S} \tag{3.62}$$

3.3.4.2 First-order Shear Deformation Formulation

Similarly, the finite element equations for the FSDT can be described as

$$\begin{bmatrix} \mathbf{M^{11}} & 0 & 0 & 0 & 0 \\ 0 & \mathbf{M^{22}} & 0 & 0 & 0 \\ 0 & 0 & \mathbf{M^{33}} & 0 & 0 \\ 0 & 0 & 0 & \mathbf{M^{44}} & 0 \\ 0 & 0 & 0 & 0 & \mathbf{M^{55}} \end{bmatrix} \begin{Bmatrix} \ddot{\mathbf{U}} \\ \ddot{\mathbf{V}} \\ \ddot{\mathbf{W}} \\ \ddot{\mathbf{\Phi}}_x \\ \ddot{\mathbf{\Phi}}_y \end{Bmatrix} + \begin{bmatrix} \mathbf{K^{11}} & \mathbf{K^{12}} & \mathbf{K^{13}} & \mathbf{K^{14}} & \mathbf{K^{15}} \\ \mathbf{K^{21}} & \mathbf{K^{22}} & \mathbf{K^{23}} & \mathbf{K^{24}} & \mathbf{K^{25}} \\ \mathbf{K^{31}} & \mathbf{K^{32}} & \mathbf{K^{33}} & \mathbf{K^{34}} & \mathbf{K^{35}} \\ \mathbf{K^{41}} & \mathbf{K^{42}} & \mathbf{K^{43}} & \mathbf{K^{44}} & \mathbf{K^{45}} \\ \mathbf{K^{51}} & \mathbf{K^{52}} & \mathbf{K^{53}} & \mathbf{K^{45}} & \mathbf{K^{55}} \end{bmatrix} \begin{Bmatrix} \mathbf{U} \\ \mathbf{V} \\ \mathbf{W} \\ \mathbf{\Phi_x} \\ \mathbf{\Phi_y} \end{Bmatrix} = \begin{Bmatrix} 0 \\ 0 \\ -\mathbf{S}^T \mathbf{P} \\ 0 \\ 0 \end{Bmatrix} + \begin{Bmatrix} \mathbf{F^1} \\ \mathbf{F^2} \\ \mathbf{F^3} \\ \mathbf{F^4} \\ \mathbf{F^5} \end{Bmatrix} \tag{3.63}$$

Using Eq. (3.59) allows Eq. (3.63) to be expressed as

$$\begin{bmatrix} \mathbf{M^{11}} & 0 & 0 & 0 & 0 \\ 0 & \mathbf{M^{22}} & 0 & 0 & 0 \\ 0 & 0 & \bar{\mathbf{M}}^{33} & 0 & 0 \\ 0 & 0 & 0 & \mathbf{M^{44}} & 0 \\ 0 & 0 & 0 & 0 & \mathbf{M^{55}} \end{bmatrix} \begin{Bmatrix} \ddot{\mathbf{U}} \\ \ddot{\mathbf{V}} \\ \ddot{\mathbf{W}} \\ \ddot{\mathbf{\Phi}}_x \\ \ddot{\mathbf{\Phi}}_y \end{Bmatrix}$$

$$+ \begin{bmatrix} \mathbf{K^{11}} & \mathbf{K^{12}} & \mathbf{K^{13}} & \mathbf{K^{14}} & \mathbf{K^{15}} \\ \mathbf{K^{21}} & \mathbf{K^{22}} & \mathbf{K^{23}} & \mathbf{K^{24}} & \mathbf{K^{25}} \\ \mathbf{K^{31}} & \mathbf{K^{32}} & \mathbf{K^{33}} & \mathbf{K^{34}} & \mathbf{K^{35}} \\ \mathbf{K^{41}} & \mathbf{K^{42}} & \mathbf{K^{43}} & \mathbf{K^{44}} & \mathbf{K^{45}} \\ \mathbf{K^{51}} & \mathbf{K^{52}} & \mathbf{K^{53}} & \mathbf{K^{45}} & \mathbf{K^{55}} \end{bmatrix} \begin{Bmatrix} \mathbf{U} \\ \mathbf{V} \\ \mathbf{W} \\ \mathbf{\Phi_x} \\ \mathbf{\Phi_y} \end{Bmatrix} = \begin{Bmatrix} 0 \\ 0 \\ -\mathbf{S}^T \bar{\mathbf{C}}^{-1} \left(\hat{\mathbf{f}} + \mathbf{Q} \right) \\ 0 \\ 0 \end{Bmatrix} + \begin{Bmatrix} \mathbf{F^1} \\ \mathbf{F^2} \\ \mathbf{F^3} \\ \mathbf{F^4} \\ \mathbf{F^5} \end{Bmatrix} \tag{3.64}$$

where

$$\bar{\mathbf{M}}^{33} = \mathbf{M}^{33} + \rho_f \mathbf{S}^T \bar{\mathbf{C}}^{-1} \mathbf{S} \tag{3.65}$$

3.3.4.3 Reddy Third-order Shear Deformation Formulation

And finally, the finite element equations for the RSDT will be

$$\begin{bmatrix} \mathbf{M^{11}} & 0 & 0 & 0 & 0 \\ 0 & \mathbf{M^{22}} & 0 & 0 & 0 \\ 0 & 0 & \mathbf{M^{33}} & \mathbf{M^{34}} & \mathbf{M^{35}} \\ 0 & 0 & \mathbf{M^{43}} & \mathbf{M^{44}} & 0 \\ 0 & 0 & \mathbf{M^{53}} & 0 & \mathbf{M^{55}} \end{bmatrix} \begin{Bmatrix} \ddot{\mathbf{U}} \\ \ddot{\mathbf{V}} \\ \ddot{\mathbf{\Delta}} \\ \ddot{\mathbf{\Phi}}_x \\ \ddot{\mathbf{\Phi}}_y \end{Bmatrix}$$

$$+ \begin{bmatrix} \mathbf{K^{11}} & \mathbf{K^{12}} & \mathbf{K^{13}} & \mathbf{K^{14}} & \mathbf{K^{15}} \\ \mathbf{K^{21}} & \mathbf{K^{22}} & \mathbf{K^{23}} & \mathbf{K^{24}} & \mathbf{K^{25}} \\ \mathbf{K^{31}} & \mathbf{K^{32}} & \mathbf{K^{33}} & \mathbf{K^{34}} & \mathbf{K^{35}} \\ \mathbf{K^{41}} & \mathbf{K^{42}} & \mathbf{K^{43}} & \mathbf{K^{44}} & \mathbf{K^{45}} \\ \mathbf{K^{51}} & \mathbf{K^{52}} & \mathbf{K^{53}} & \mathbf{K^{45}} & \mathbf{K^{55}} \end{bmatrix} \begin{Bmatrix} \mathbf{U} \\ \mathbf{V} \\ \mathbf{\Delta} \\ \mathbf{\Phi_x} \\ \mathbf{\Phi_y} \end{Bmatrix} = \begin{Bmatrix} 0 \\ 0 \\ -\mathbf{S}^T\mathbf{P} \\ 0 \\ 0 \end{Bmatrix} + \begin{Bmatrix} \mathbf{F^1} \\ \mathbf{F^2} \\ \mathbf{F^3} \\ \mathbf{F^4} \\ \mathbf{F^5} \end{Bmatrix} \quad (3.66)$$

We can use Eq. (3.59) to represent Eq. (3.63) as

$$\begin{bmatrix} \mathbf{M^{11}} & 0 & 0 & 0 & 0 \\ 0 & \mathbf{M^{22}} & 0 & 0 & 0 \\ 0 & 0 & \bar{\mathbf{M}}^{33} & \mathbf{M^{34}} & \mathbf{M^{35}} \\ 0 & 0 & \mathbf{M^{43}} & \mathbf{M^{44}} & 0 \\ 0 & 0 & \mathbf{M^{53}} & 0 & \mathbf{M^{55}} \end{bmatrix} \begin{Bmatrix} \ddot{\mathbf{U}} \\ \ddot{\mathbf{V}} \\ \ddot{\mathbf{\Delta}} \\ \ddot{\mathbf{\Phi}}_x \\ \ddot{\mathbf{\Phi}}_y \end{Bmatrix}$$
$$+ \begin{bmatrix} \mathbf{K^{11}} & \mathbf{K^{12}} & \mathbf{K^{13}} & \mathbf{K^{14}} & \mathbf{K^{15}} \\ \mathbf{K^{21}} & \mathbf{K^{22}} & \mathbf{K^{23}} & \mathbf{K^{24}} & \mathbf{K^{25}} \\ \mathbf{K^{31}} & \mathbf{K^{32}} & \mathbf{K^{33}} & \mathbf{K^{34}} & \mathbf{K^{35}} \\ \mathbf{K^{41}} & \mathbf{K^{42}} & \mathbf{K^{43}} & \mathbf{K^{44}} & \mathbf{K^{45}} \\ \mathbf{K^{51}} & \mathbf{K^{52}} & \mathbf{K^{53}} & \mathbf{K^{45}} & \mathbf{K^{55}} \end{bmatrix} \begin{Bmatrix} \mathbf{U} \\ \mathbf{V} \\ \mathbf{\Delta} \\ \mathbf{\Phi_x} \\ \mathbf{\Phi_y} \end{Bmatrix} = \begin{Bmatrix} 0 \\ 0 \\ -\mathbf{S}^T \bar{\mathbf{C}}^{-1} \left(\hat{\mathbf{f}} + \mathbf{Q} \right) \\ 0 \\ 0 \end{Bmatrix} + \begin{Bmatrix} \mathbf{F^1} \\ \mathbf{F^2} \\ \mathbf{F^3} \\ \mathbf{F^4} \\ \mathbf{F^5} \end{Bmatrix} \tag{3.67}$$

In Eq. (3.67), $\bar{\mathbf{M}}^{33}$ is

$$\bar{\mathbf{M}}^{33} = \mathbf{M}^{33} + \rho_f \mathbf{S}^T \bar{\mathbf{C}}^{-1} \mathbf{S} \tag{3.68}$$

3.4 Solution Methods

3.4.1 Newmark's Scheme; Fully Discretized Equations

Using the standard global finite element assembly procedure, one can assemble the global finite element equations into the form

$$\mathbf{M}\ddot{\mathbf{\Delta}} + \mathbf{K}\mathbf{\Delta} = \mathbf{F} \tag{3.69}$$

The equation of motion given by Eq. (3.69) can be solved for transient response. This is especially meaningful if the structure is placed in a vertical column of fluid and excited by some external transient force. The fully discretized finite element equations can be expressed incrementally using the Newmark's scheme for numerical time integration. The Newmark scheme leads to the following set of equations

$$\hat{\mathbf{K}}^{n+1}\boldsymbol{\Delta}^{n+1} = \hat{\mathbf{F}}^{n,n+1} \tag{3.70}$$

where

$$\begin{aligned}
\hat{\mathbf{K}}^{n+1} &= \mathbf{K}^{n+1} + a_3\mathbf{M}^{n+1} \\
\hat{\mathbf{F}}^{n,n+1} &= \mathbf{F}^{n+1} + \mathbf{M}^{n+1}\left(a_3\boldsymbol{\Delta}^{n} + a_4\dot{\boldsymbol{\Delta}}^{n} + a_5\ddot{\boldsymbol{\Delta}}^{n}\right)
\end{aligned} \tag{3.71}$$

At the end of each time step, the new acceleration and velocity vectors are calculated as

$$\begin{aligned}
\ddot{\boldsymbol{\Delta}}^{n+1} &= a_3\left(\boldsymbol{\Delta}^{n+1} - \boldsymbol{\Delta}^{n}\right) - a_4\dot{\boldsymbol{\Delta}}^{n} - a_5\ddot{\boldsymbol{\Delta}}^{n} \\
\dot{\boldsymbol{\Delta}}^{n+1} &= \dot{\boldsymbol{\Delta}}^{n} + a_2\ddot{\boldsymbol{\Delta}}^{n} + a_1\ddot{\boldsymbol{\Delta}}^{n+1}
\end{aligned} \tag{3.72}$$

In addition, the constants a_j per Eqs. (3.71) and (3.72) are defined as

$$a_1 = \alpha\Delta t, \quad a_2 = (1-\alpha)\,\Delta t, \quad a_3 = \frac{1}{\beta(\Delta t)^2}, \quad a_4 = a_3\Delta t, \quad a_5 = \frac{1}{\gamma} - 1, \quad \beta = \frac{1}{2}\gamma \tag{3.73}$$

Therefore, we obtained a system of algebraic equations by using a time-integration method. Now we must solve this system of nonlinear equation iteratively using iteration methods available in literature.

3.4.2 Newtonian Iteration Method; Tangent Matrices

The system of algebraic equations obtained in the previous sub-section includes nonlinear terms which necessitate linearizing these equations for the incremental solution at the $(r+1)$st iteration. Herein, we use the Newtonian iteration method where we have to calculate tangent stiffness matrices for the corresponding stiffness matrices associated with all three plate theories. Newtonian iteration method involves solving the following form of the equations

$$\hat{\mathbf{T}}\left(\boldsymbol{\Delta}_{s+1}^{r}\right)\delta\boldsymbol{\Delta} = -\mathbf{R}_{s+1}^{r} \tag{3.74}$$

where $\delta\boldsymbol{\Delta}$ is the incremental solution. Moreover, tangent stiffness matrices $\mathbf{T}$ and residual vectors $\mathbf{R}$ have the following definitions

$$\begin{aligned}
\hat{\mathbf{T}}\left(\boldsymbol{\Delta}_{s+1}^{r}\right) &\equiv \left[\frac{\partial \mathbf{R}}{\partial \boldsymbol{\Delta}}\right]_{s+1}^{r} \\
\mathbf{R}_{s+1}^{r} &= \hat{\mathbf{K}}\left(\Delta_{s+1}^{r}\right)\boldsymbol{\Delta}_{s+1}^{r} - \hat{\mathbf{F}}_{s+1}^{r}
\end{aligned} \tag{3.75}$$

Therefore, the total solution will be obtained from

$$\boldsymbol{\Delta}_{s+1}^{r+1} = \boldsymbol{\Delta}_{s+1}^{r} + \delta\boldsymbol{\Delta} \tag{3.76}$$

Using the definitions provided in Eq. (3.75), one can calculate the tangent stiffness matrices as

$$\begin{aligned}
T_{ij}^{\alpha\beta} \equiv \frac{\partial R_i^{\alpha}}{\partial \Delta_j^{\beta}} &= \frac{\partial}{\partial \Delta_j^{\beta}}\left(\sum_{\gamma=1}^{5}\sum_{k=1}^{n_\gamma} K_{ik}^{\alpha\gamma}\Delta_k^{\gamma} - F_i^{\alpha}\right) \\
&= K_{ij}^{\alpha\beta} + \sum_{k=1}^{n_\gamma}\frac{\partial K_{ik}^{\alpha\gamma}}{\partial \Delta_j^{\beta}}\Delta_k^{\gamma} - \frac{\partial F_i^{\alpha}}{\partial \Delta_j^{\beta}}
\end{aligned} \tag{3.77}$$

In order to compute tangent stiffness matrices, we are interested in the stiffness matrices which depend on the solution. Otherwise, the tangent matrix is the same as the corresponding stiffness matrix. The only solution that appears in the stiffness matrices is w.

It worth mentioning that the matrices $\hat{\mathbf{K}}^r_{s+1}$, $\hat{\mathbf{T}}^r_{s+1}$, and force vector $\mathbf{R}^r_{s+1}$ are updated at each iteration using the most recent solution $\boldsymbol{\Delta}^r_{s+1}$.

3.4.2.1 CPT

For CPT, we have the same tangent stiffness definition as for the stiffness coefficient for the following submatrices

$$\begin{aligned} T_{ij}^{\alpha 1} &= K_{ij}^{\alpha 1}, \quad T_{ij}^{1\alpha} = K_{ij}^{1\alpha} \\ T_{ij}^{\alpha 2} &= K_{ij}^{\alpha 2}, \quad T_{ij}^{2\alpha} = K_{ij}^{2\alpha} \end{aligned} \tag{3.78}$$

Therefore, we have to calculate T_{ij}^{13}, T_{ij}^{23}, and T_{ij}^{33}. After eliminating the terms that are independent of w, we have

$$\begin{aligned} T_{ij}^{13} &= K_{ij}^{13} + \sum_{k=1}^{n} \frac{\partial K_{ik}^{13}}{\partial w_j} w_k \\ &= K_{ij}^{13} + \frac{1}{2} \int_{\Omega^e} \left[\frac{\partial \psi_i}{\partial x} \left(A_{11} \frac{\partial w}{\partial x} \frac{\partial \varphi_j}{\partial x} + A_{12} \frac{\partial w}{\partial y} \frac{\partial \varphi_j}{\partial y} \right) \right. \\ &\qquad \left. + A_{66} \frac{\partial \psi_i}{\partial y} \left(\frac{\partial w}{\partial x} \frac{\partial \varphi_j}{\partial y} + \frac{\partial w}{\partial y} \frac{\partial \varphi_j}{\partial x} \right) \right] dxdy \end{aligned}$$

$$
\begin{aligned}
T_{ij}^{23} &= K_{ij}^{23} + \sum_{k=1}^{n} \frac{\partial K_{ik}^{23}}{\partial w_j} w_k \\
&= K_{ij}^{23} + \frac{1}{2} \int\limits_{\Omega^e} \left[\frac{\partial \psi_i}{\partial y} \left(A_{12} \frac{\partial w}{\partial x} \frac{\partial \varphi_j}{\partial x} + A_{11} \frac{\partial w}{\partial y} \frac{\partial \varphi_j}{\partial y} \right) \right. \\
&\qquad \left. + A_{66} \frac{\partial \psi_i}{\partial x} \left(\frac{\partial w}{\partial x} \frac{\partial \varphi_j}{\partial y} + \frac{\partial w}{\partial y} \frac{\partial \varphi_j}{\partial x} \right) \right] dxdy \\
T_{ij}^{33} &= K_{ij}^{33} + \sum_{k=1}^{n} \left(\frac{\partial K_{ik}^{31}}{\partial w_j} u_k + \frac{\partial K_{ik}^{32}}{\partial w_j} v_k + \frac{\partial K_{ik}^{33}}{\partial w_j} w_k \right) \\
&= K_{ij}^{33} + \int\limits_{\Omega^e} \left[\frac{\partial \varphi_i}{\partial x} \left(A_{11} \frac{\partial u}{\partial x} \frac{\partial \varphi_j}{\partial x} + A_{66} \frac{\partial u}{\partial y} \frac{\partial \varphi_j}{\partial y} \right) \right. \\
&\qquad \left. + \frac{\partial \varphi_i}{\partial y} \left(A_{66} \frac{\partial u}{\partial y} \frac{\partial \varphi_j}{\partial x} + A_{12} \frac{\partial u}{\partial x} \frac{\partial \varphi_j}{\partial y} \right) \right] dxdy \\
&\qquad + \int\limits_{\Omega^e} \left[\frac{\partial \varphi_i}{\partial x} \left(A_{12} \frac{\partial v}{\partial y} \frac{\partial \varphi_j}{\partial x} + A_{66} \frac{\partial v}{\partial x} \frac{\partial \varphi_j}{\partial y} \right) \right. \\
&\qquad \left. + \frac{\partial \varphi_i}{\partial y} \left(A_{66} \frac{\partial v}{\partial x} \frac{\partial \varphi_j}{\partial x} + A_{11} \frac{\partial v}{\partial y} \frac{\partial \varphi_j}{\partial y} \right) \right] dxdy \\
&\qquad + \int\limits_{\Omega^e} \left[\left(A_{11} \left(\frac{\partial w}{\partial x} \right)^2 + \frac{A_{12} + A_{66}}{2} \left(\frac{\partial w}{\partial y} \right)^2 \right) \frac{\partial \varphi_i}{\partial x} \frac{\partial \varphi_j}{\partial x} \right. \\
&\qquad + \left(\frac{A_{12} + A_{66}}{2} \left(\frac{\partial w}{\partial x} \right)^2 + A_{11} \left(\frac{\partial w}{\partial y} \right)^2 \right) \frac{\partial \varphi_i}{\partial y} \frac{\partial \varphi_j}{\partial y} \\
&\qquad \left. + \left(\frac{A_{12} + 3A_{66}}{2} \right) \frac{\partial w}{\partial x} \frac{\partial w}{\partial y} \left(\frac{\partial \varphi_i}{\partial x} \frac{\partial \varphi_j}{\partial y} + \frac{\partial \varphi_i}{\partial y} \frac{\partial \varphi_j}{\partial x} \right) \right] dxdy \qquad (3.79)
\end{aligned}
$$

3.4.2.2 FSDT

For FSDT, we have the same tangent stiffness definition as for the stiffness coefficient for the following submatrices

$$\begin{aligned} T_{ij}^{\alpha 1} &= K_{ij}^{\alpha 1}, \quad T_{ij}^{1\alpha} = K_{ij}^{1\alpha} \\ T_{ij}^{\alpha 2} &= K_{ij}^{\alpha 2}, \quad T_{ij}^{2\alpha} = K_{ij}^{2\alpha} \\ T_{ij}^{\alpha 4} &= K_{ij}^{\alpha 4}, \quad T_{ij}^{4\alpha} = K_{ij}^{4\alpha} \\ T_{ij}^{\alpha 5} &= K_{ij}^{\alpha 5}, \quad T_{ij}^{5\alpha} = K_{ij}^{5\alpha} \end{aligned} \tag{3.80}$$

Therefore, we have to calculate T_{ij}^{13}, T_{ij}^{23}, and T_{ij}^{33}. After eliminating the terms that are independent of w, we have:

$$\begin{aligned} T_{ij}^{13} &= K_{ij}^{13} + \sum_{k=1}^{n} \frac{\partial K_{ik}^{13}}{\partial w_j} w_k \\ &= K_{ij}^{13} + \frac{1}{2} \int_{\Omega^e} \left[\frac{\partial \psi_i^{(1)}}{\partial x} \left(A_{11} \frac{\partial w}{\partial x} \frac{\partial \psi_j^{(2)}}{\partial x} + A_{12} \frac{\partial w}{\partial y} \frac{\partial \psi_j^{(2)}}{\partial y} \right) \right. \\ &\qquad \left. + A_{66} \frac{\partial \psi_i^{(1)}}{\partial y} \left(\frac{\partial w}{\partial x} \frac{\partial \psi_j^{(2)}}{\partial y} + \frac{\partial w}{\partial y} \frac{\partial \psi_j^{(2)}}{\partial x} \right) \right] dxdy \\ T_{ij}^{23} &= K_{ij}^{23} + \sum_{k=1}^{n} \frac{\partial K_{ik}^{23}}{\partial w_j} w_k \\ &= K_{ij}^{23} + \frac{1}{2} \int_{\Omega^e} \left[\frac{\partial \psi_i^{(1)}}{\partial y} \left(A_{12} \frac{\partial w}{\partial x} \frac{\partial \psi_j^{(2)}}{\partial x} + A_{22} \frac{\partial w}{\partial y} \frac{\partial \psi_j^{(2)}}{\partial y} \right) \right. \\ &\qquad \left. + A_{66} \frac{\partial \psi_i^{(1)}}{\partial x} \left(\frac{\partial w}{\partial x} \frac{\partial \psi_j^{(2)}}{\partial y} + \frac{\partial w}{\partial y} \frac{\partial \psi_j^{(2)}}{\partial x} \right) \right] dxdy \end{aligned}$$

$$
\begin{aligned}
T_{ij}^{33} &= K_{ij}^{33} + \sum_{k=1}^{n} \left(\frac{\partial K_{ik}^{31}}{\partial w_j} u_k + \frac{\partial K_{ik}^{32}}{\partial w_j} v_k + \frac{\partial K_{ik}^{33}}{\partial w_j} w_k \right) \\
&= K_{ij}^{33} + \int_{\Omega^e} \left[\frac{\partial \psi_i^{(2)}}{\partial x} \left(A_{11} \frac{\partial u}{\partial x} \frac{\partial \psi_j^{(2)}}{\partial x} + A_{66} \frac{\partial u}{\partial y} \frac{\partial \psi_j^{(2)}}{\partial y} \right) \right. \\
&\quad \left. + \frac{\partial \psi_i^{(2)}}{\partial y} \left(A_{66} \frac{\partial u}{\partial y} \frac{\partial \psi_j^{(2)}}{\partial x} + A_{12} \frac{\partial u}{\partial x} \frac{\partial \psi_j^{(2)}}{\partial y} \right) \right] dxdy \\
&\quad + \int_{\Omega^e} \left[\frac{\partial \psi_i^{(2)}}{\partial x} \left(A_{12} \frac{\partial v}{\partial y} \frac{\partial \psi_j^{(2)}}{\partial x} + A_{66} \frac{\partial v}{\partial x} \frac{\partial \psi_j^{(2)}}{\partial y} \right) \right. \\
&\quad \left. + \frac{\partial \psi_i^{(2)}}{\partial y} \left(A_{66} \frac{\partial v}{\partial x} \frac{\partial \psi_j^{(2)}}{\partial x} + A_{11} \frac{\partial v}{\partial y} \frac{\partial \psi_j^{(2)}}{\partial y} \right) \right] dxdy \\
&\quad + \int_{\Omega^e} \left[\left(A_{11} \left(\frac{\partial w}{\partial x} \right)^2 + \frac{A_{12} + A_{66}}{2} \left(\frac{\partial w}{\partial y} \right)^2 \right) \frac{\partial \psi_i^{(2)}}{\partial x} \frac{\partial \psi_j^{(2)}}{\partial x} \right. \\
&\quad + \left(\frac{A_{12} + A_{66}}{2} \left(\frac{\partial w}{\partial x} \right)^2 + A_{11} \left(\frac{\partial w}{\partial y} \right)^2 \right) \frac{\partial \psi_i^{(2)}}{\partial y} \frac{\partial \psi_j^{(2)}}{\partial y} \\
&\quad \left. + \left(\frac{A_{12} + 3A_{66}}{2} \right) \frac{\partial w}{\partial x} \frac{\partial w}{\partial y} \left(\frac{\partial \psi_i^{(2)}}{\partial x} \frac{\partial \psi_j^{(2)}}{\partial y} + \frac{\partial \psi_i^{(2)}}{\partial y} \frac{\partial \psi_j^{(2)}}{\partial x} \right) \right] dxdy
\end{aligned} \tag{3.81}
$$

3.4.2.3 RSDT

For RSDT, we have the same tangent stiffness definition as for the stiffness coefficient for the following submatrices

$$
\begin{aligned}
T_{ij}^{\alpha 1} &= K_{ij}^{\alpha 1}, \quad T_{ij}^{1\alpha} = K_{ij}^{1\alpha} \\
T_{ij}^{\alpha 2} &= K_{ij}^{\alpha 2}, \quad T_{ij}^{2\alpha} = K_{ij}^{2\alpha} \\
T_{ij}^{\alpha 4} &= K_{ij}^{\alpha 4}, \quad T_{ij}^{4\alpha} = K_{ij}^{4\alpha} \\
T_{ij}^{\alpha 5} &= K_{ij}^{\alpha 5}, \quad T_{ij}^{5\alpha} = K_{ij}^{5\alpha}
\end{aligned} \tag{3.82}
$$

Therefore, we have to calculate T_{ij}^{13}, T_{ij}^{23}, and T_{ij}^{33}. After eliminating the terms that are independent of w, we have:

$$
\begin{aligned}
T_{ij}^{13} &= K_{ij}^{13} + \sum_{k=1}^{n} \frac{\partial K_{ik}^{13}}{\partial w_j} w_k \\
&= K_{ij}^{13} + \frac{1}{2} \int_{\Omega^e} \left[\frac{\partial \psi_i^{(1)}}{\partial x} \left(A_{11} \frac{\partial w}{\partial x} \frac{\partial \varphi_j}{\partial x} + A_{12} \frac{\partial w}{\partial y} \frac{\partial \varphi_j}{\partial y} \right) \right. \\
&\qquad \left. + A_{66} \frac{\partial \psi_i^{(1)}}{\partial y} \left(\frac{\partial w}{\partial x} \frac{\partial \varphi_j}{\partial y} + \frac{\partial w}{\partial y} \frac{\partial \varphi_j}{\partial x} \right) \right] dxdy \\
T_{ij}^{23} &= K_{ij}^{23} + \sum_{k=1}^{n} \frac{\partial K_{ik}^{23}}{\partial w_j} w_k \\
&= K_{ij}^{23} + \frac{1}{2} \int_{\Omega^e} \left[\frac{\partial \psi_i^{(1)}}{\partial y} \left(A_{12} \frac{\partial w}{\partial x} \frac{\partial \varphi_j}{\partial x} + A_{11} \frac{\partial w}{\partial y} \frac{\partial \varphi_j}{\partial y} \right) \right. \\
&\qquad \left. + A_{66} \frac{\partial \psi_i^{(1)}}{\partial x} \left(\frac{\partial w}{\partial x} \frac{\partial \varphi_j}{\partial y} + \frac{\partial w}{\partial y} \frac{\partial \varphi_j}{\partial x} \right) \right] dxdy \\
T_{ij}^{33} &= K_{ij}^{33} + \sum_{k=1}^{n} \left(\frac{\partial K_{ik}^{31}}{\partial w_j} u_k + \frac{\partial K_{ik}^{32}}{\partial w_j} v_k + \frac{\partial K_{ik}^{33}}{\partial w_j} w_k \right) \\
&= K_{ij}^{33} + \int_{\Omega^e} \left[\frac{\partial \varphi_i}{\partial x} \left(A_{11} \frac{\partial u}{\partial x} \frac{\partial \varphi_j}{\partial x} + A_{66} \frac{\partial u}{\partial y} \frac{\partial \varphi_j}{\partial y} \right) \right. \\
&\qquad \left. + \frac{\partial \varphi_i}{\partial y} \left(A_{66} \frac{\partial u}{\partial y} \frac{\partial \varphi_j}{\partial x} + A_{12} \frac{\partial u}{\partial x} \frac{\partial \varphi_j}{\partial y} \right) \right] dxdy \\
&\qquad + \int_{\Omega^e} \left[\frac{\partial \varphi_i}{\partial x} \left(A_{12} \frac{\partial v}{\partial y} \frac{\partial \varphi_j}{\partial x} + A_{66} \frac{\partial v}{\partial x} \frac{\partial \varphi_j}{\partial y} \right) \right. \\
&\qquad \left. + \frac{\partial \varphi_i}{\partial y} \left(A_{66} \frac{\partial v}{\partial x} \frac{\partial \varphi_j}{\partial x} + A_{11} \frac{\partial v}{\partial y} \frac{\partial \varphi_j}{\partial y} \right) \right] dxdy \\
&\qquad + \int_{\Omega^e} \left[\left(A_{11} \left(\frac{\partial w}{\partial x} \right)^2 + \frac{A_{12} + A_{66}}{2} \left(\frac{\partial w}{\partial y} \right)^2 \right) \frac{\partial \varphi_i}{\partial x} \frac{\partial \varphi_j}{\partial x} \right. \\
&\qquad + \left(\frac{A_{12} + A_{66}}{2} \left(\frac{\partial w}{\partial x} \right)^2 + A_{11} \left(\frac{\partial w}{\partial y} \right)^2 \right) \frac{\partial \varphi_i}{\partial y} \frac{\partial \varphi_j}{\partial y} \\
&\qquad \left. + \left(\frac{A_{12} + 3A_{66}}{2} \right) \frac{\partial w}{\partial x} \frac{\partial w}{\partial y} \left(\frac{\partial \varphi_i}{\partial x} \frac{\partial \varphi_j}{\partial y} + \frac{\partial \varphi_i}{\partial y} \frac{\partial \varphi_j}{\partial x} \right) \right] dxdy
\end{aligned}
\tag{3.83}
$$

Despite the nonlinear nature of the stiffness matrices, the tangent matrices for the all three considered plate theories are symmetric.

3.5 Numerical Results

Numerical results are presented to investigate the effect of the fluid-structure interaction on transient response of rectangular plates using the proposed models. In the numerical calculations, we used the following parameters:

$$E = 200 \text{ GPa}, \quad \nu = 0.25, \quad \rho_s = 5000 \text{ kg}/m^3$$
$$L_x = L_y = L = 1 \text{ m}, \quad h_z = 0.2 \text{ m}, \quad \beta = \frac{\rho_f}{\rho_s}, \quad f = 10^5 \text{ N}/m^2$$

and we consider H and ρ_f to be varied for different cases. The transverse deflection of the plate is presented in the following nondimensional form

$$\bar{w} = 100w\left(0, 0, t\right) \frac{Eh^3}{fL^4} \tag{3.84}$$

Here, we consider two boundary conditions for the rectangular plate; a plate with all edges clamped (CCCC) and a plate with all edges simply supported (SSSS). Numerical simulations are performed for three different fluid densities; $\beta = 0$ (corresponding to the case where the plate is not in contact with fluid), $\beta = 0.04$, and $\beta = 0.08$. For each β value, two different plate thickness ratios, $L/H = 10$ and $L/H = 100$, are considered. In all cases, the mesh used is 20×20 elements. This mesh is arrived after a number of convergence studies to make sure that the results are independent of mesh.

The variation of the nondimensionalized transverse deflection for different β values and L/H ratios are summarized in Table 3.1 for CCCC, and in Table 3.2 for SSSS. The transient behavior of the plate for the aforementioned cases followed the

trend expected from previous studies; it is influenced by the immersion depth h_z and fluid density ρ_f. For instance, increasing h_z (or correspondingly increasing ρ_f) increases the added mass and consequently increases or decreases the transverse deflection depending on the direction of the external mechanical load applied. Moreover, changing L/H ratio results in different variation of transverse deflection to the presence of the fluid medium.

From the results in Tables 3.1 and 3.2, it can be concluded that the effect of the added mass is considerable for thin plate limit. Furthermore, increasing β (or h_z) will decrease transverse deflection in our simulations, since both external load and fluid interactions are applied in the opposite directions. For higher β values (more dense fluids), the transverse deflection will be less affected if one changes the fluid density ρ_f.

The other point worth mentioning is that the results for higher L/H ratios converge for all three plate theories; i.e. in the thin plate limits, we can use any of three plate theories. However, for the lower L/H ratios, since the normality assumption is not valid, CPT does not converge to the final solution.

Figures 3.2 and 3.5 represents the transverse deflection of a plate in contact with an inviscid incompressible fluid medium for CCCC and SSSS, respectivley. These plots are provided for $L/H = 10$ and $\beta = 0.08$ based on the RSDT. For clamped boundary condition, Figs. 3.3 and 3.4 compare nondimensional transverse deflection of a plate in an inviscid incompressible fluid medium versus time for $L/H = 10$ and $L/H = 100$, respectively. The effect of the fluid presence is to reduce the amplitude and increase the period of the transverse deflection and this effect is more considerable in the thin plate limit. Corresponding results are depicted in Figs. 3.6 and 3.7 for a plate with simply supported boundary condition.

Table 3.1: Comparison of nondimonsional transverse deflection of a CCCC plate in contact with a fluid medium using CPT, FSDT and RSDT with 20×20 elements.

L/H	β	CPT	FSDT	RSDT
	0.00	1.3953	1.5428	1.5412
10	0.04	1.3856	1.5346	1.5311
	0.08	1.3739	1.5291	1.5273
	0.00	1.3955	1.3987	1.3964
100	0.04	1.3864	1.3897	1.3886
	0.08	1.3752	1.3779	1.3771

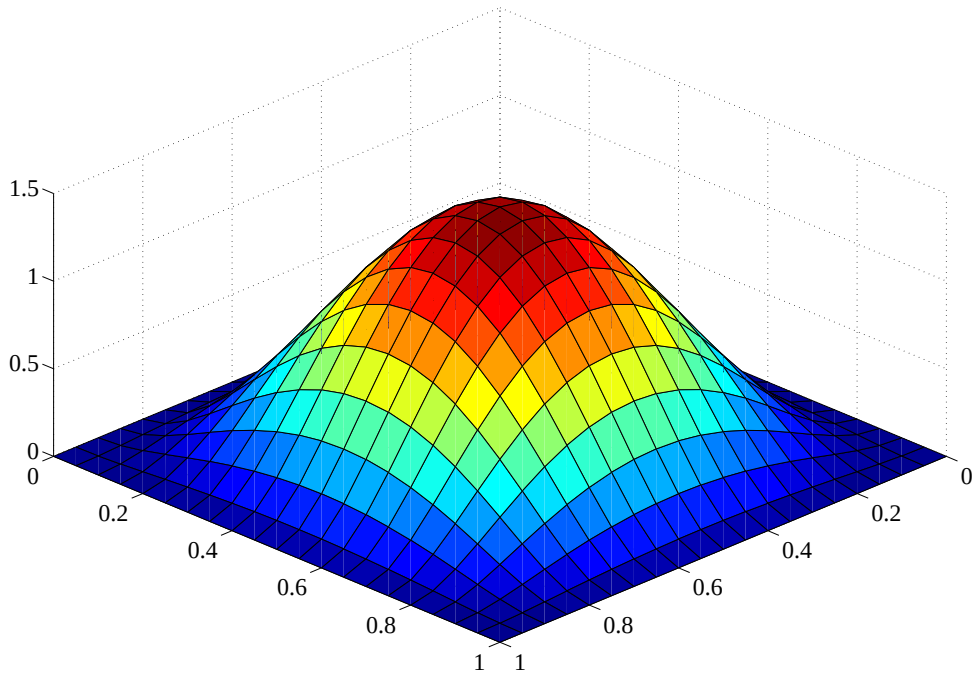

Figure 3.2: Transverse deflection of a CCCC plate in an inviscid incompressible fluid medium for $L/H = 100$ and $\beta = 0.08$.

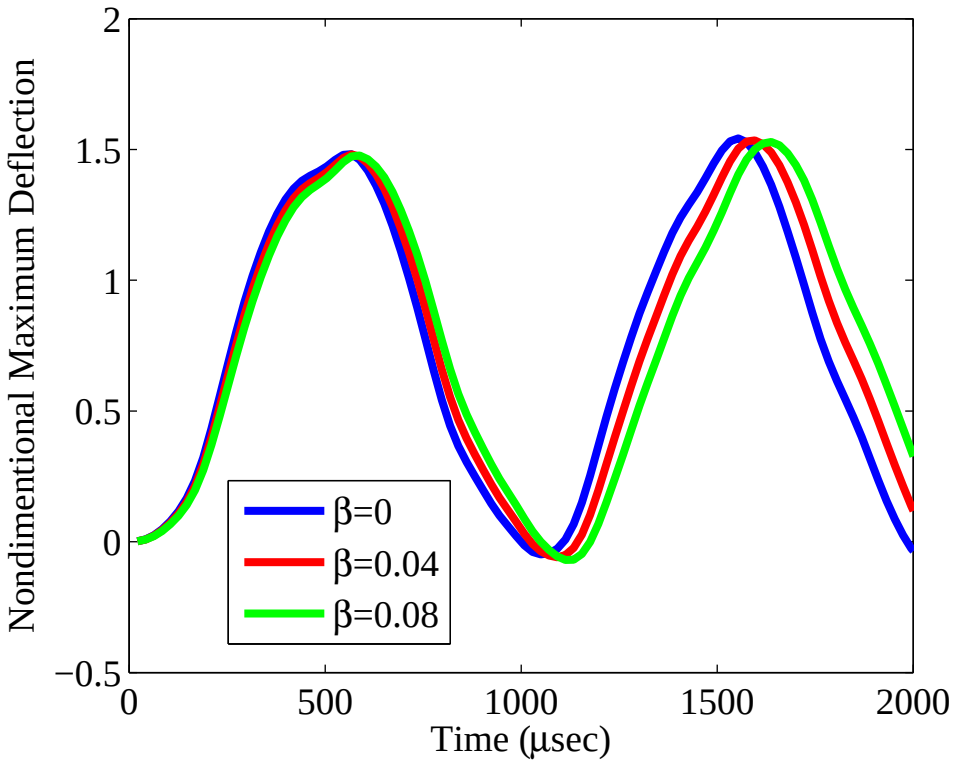

Figure 3.3: Nondimensional transverse deflection of a CCCC plate in an inviscid incompressible fluid medium versus time for $L/H = 10$.

Table 3.2: Comparison of nondimonsional transverse deflection of a SSSS plate in contact with a fluid medium using CPT, FSDT and RSDT with 20×20 elements.

L/H	β	CPT	FSDT	RSDT
	0.00	4.5600	4.7826	4.7805
10	0.04	4.5545	4.7745	4.7718
	0.08	4.5496	4.7678	4.7661
	0.00	4.5603	4.5628	4.5615
100	0.04	4.5548	4.5561	4.5553
	0.08	4.5497	4.5523	4.5514

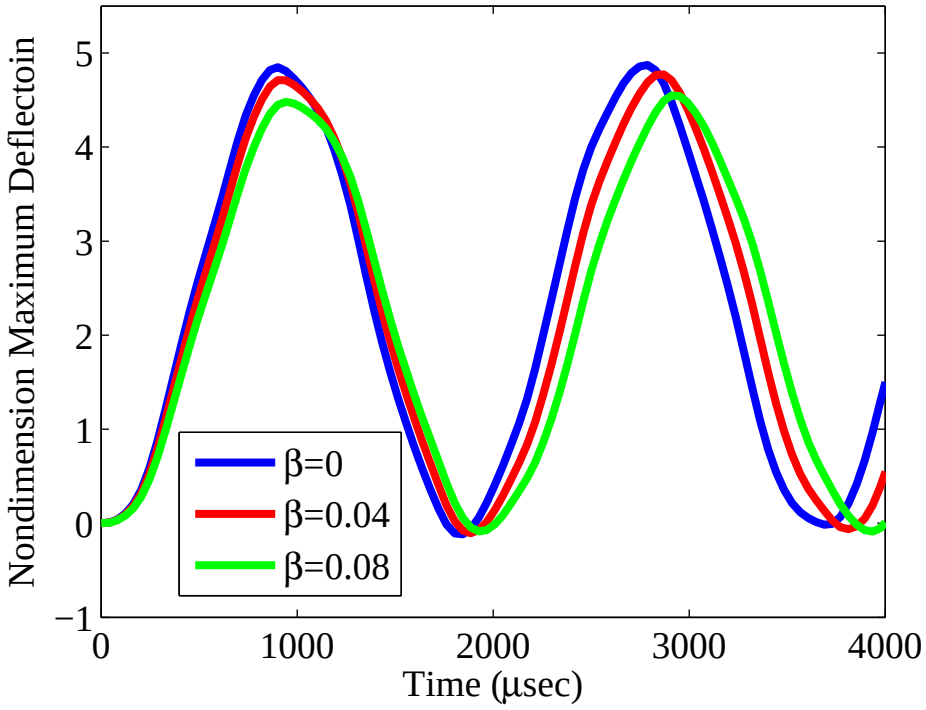

Figure 3.4: Nondimensional transverse deflection of a CCCC plate in an inviscid incompressible fluid medium versus time for $L/H = 100$.

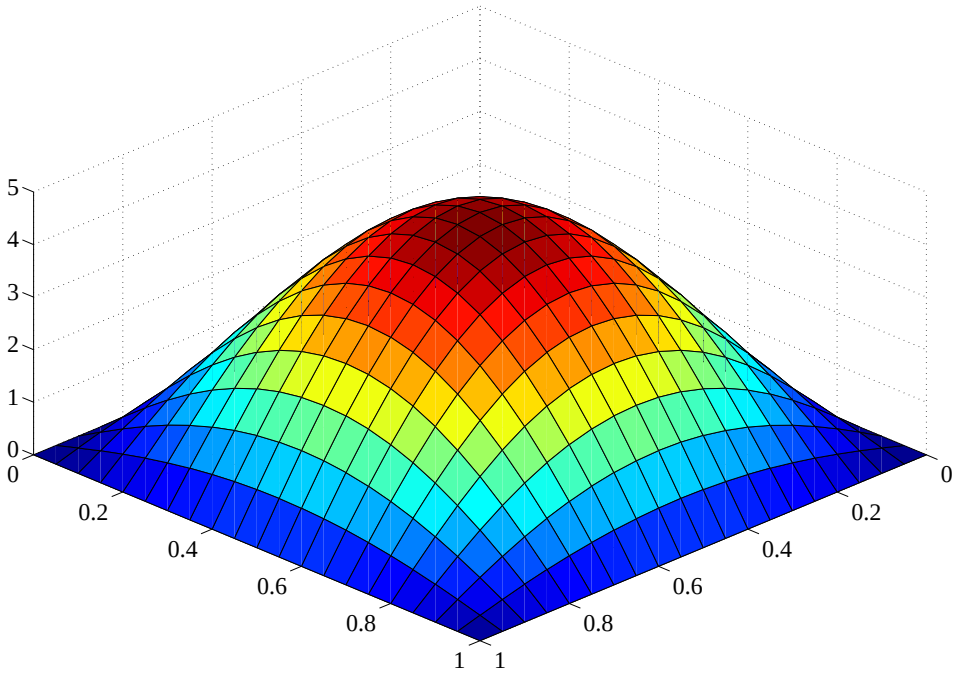

Figure 3.5: Transverse deflection of a SSSS plate in an inviscid incompressible fluid medium for $L/H = 100$ and $\beta = 0.08$.

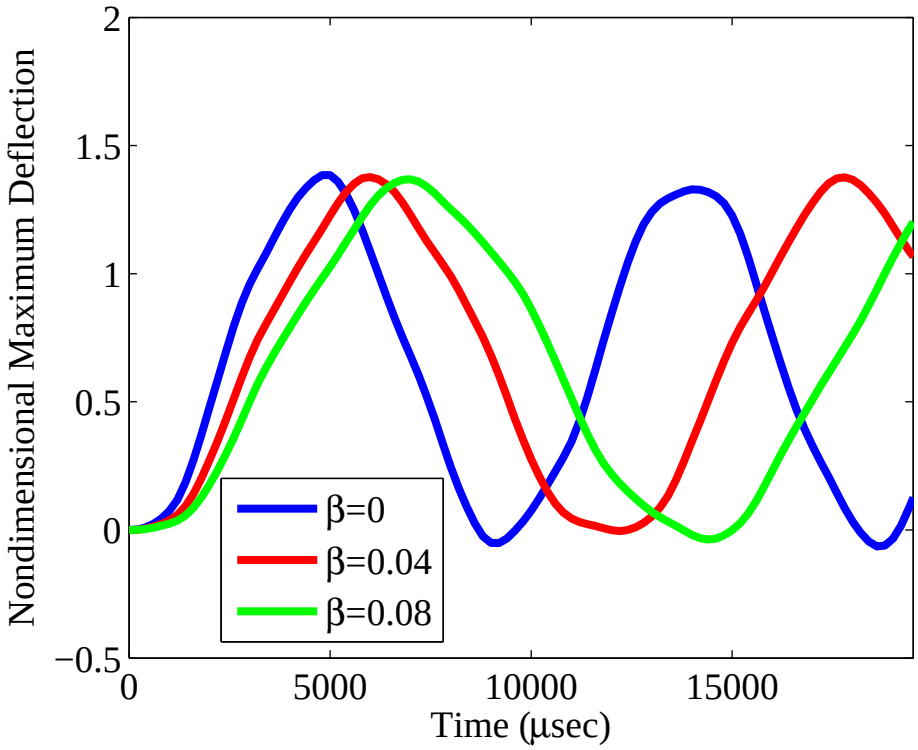

Figure 3.6: Nondimensional transverse deflection of a CCCC plate in an inviscid incompressible fluid medium versus time for $L/H = 10$.

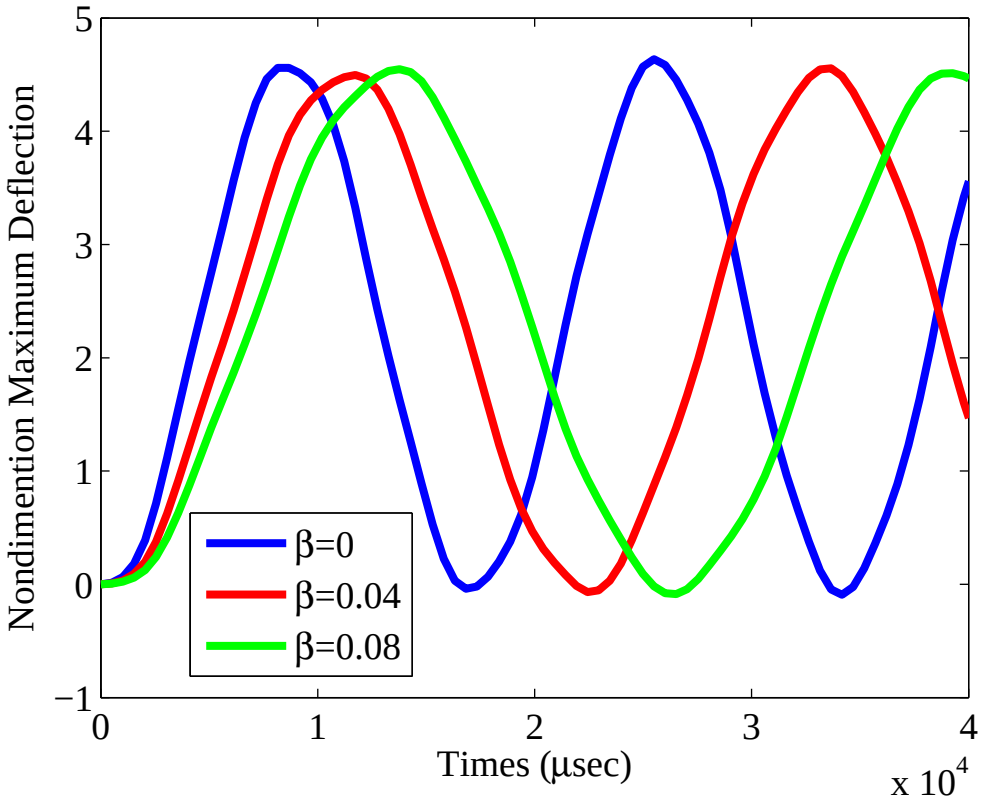

Figure 3.7: Nondimensional transverse deflection of a CCCC plate in an inviscid incompressible fluid medium versus time for $L/H = 100$.

3.6 Concluding Remarks

In this section, we studied the transient analysis of the plate fluid-structure interaction problem considering geometry nonlinearity. In our study, we considered the classical, first-order and the Reddy third-order plate theories, and an comprehensive study was conducted independent of the plate geometry. The effect of fluid medium was introduced as an added mass through the mass matrix of the system of equations. The effect of various parameters, such as fluid density and geometric dimensions, on the transverse deflection of the CCCC and SSSS plate structure were investigated through numerical simulations. The obtained numerical results are in good agreement with the results available in literature.

4. BLOOD FLOW THROUGH LARGE ARTERIES

4.1 Introduction

In order to understand the behavior of human vascular system, detailed knowledge of the response of the blood vessels and blood flow is of significant importance. Having a deep insight of this response provides getting the idea on connection between blood flow and the development of diseases. It also may help improving medical device design such as heart valves, artificial heart, and so on. The problem of blood flow through human arteries is one of the representative applications of the flow of a viscous incompressible fluid through a tube. Corresponding to all FSI problems, deformability of the blood vessel influences velocity and pressure of blood in arteries and vice versa. Conducting a study on this problem requires developing a model and simulating the blood flow which describes this influence. In general, the blood flow in human arteries is too sophisticated to be solved analytically, however, several simplifications can be made in order to ease the calculations. For instance, although arterial walls are composed of anisotropic and heterogeneous layers with completely different biomechanical properties, there are several methods which describe them with average-value properties so that arterial walls can be considered as a homogeneous layer with nonlinear elastic behavior. Moreover, although this problem is a complicated 3D problem, simplifying it to the 1D problem provides a reasonable insight into the most general case of blood flow. In the analysis of blood flow, it is common to treat the blood as a single homogeneous Newtonian fluid rather than considering two-phase fluid with varying properties. In other word, one can approximate blood properties by averaging properties determined from measurements in whole blood. Dynamics of the blood flow is basically governed by the continuity and

conservation of linear momentum principles. Using these principles does not get the idea of how the constraint of blood vessels may affect the flow. Therefore, another constitutive equation is required to show this interaction.

The approach that we are studying in this section is based on the fact that the blood flow is generally a three dimensional motion. Then considering the asymmetric nature of the problem along with the appropriate boundary conditions, we can simplify the governing equations to the one dimensional problem. Moreover, we assume the pressure to be constant over the cross-sectional area at any distance x form the origin of the coordinate system. In addition, the impermeability of the vessel is assumed. We will discuss more about the assumptions throughout the section.

Herein, we develop a finite element approach in order to solve transient FSI problems involving moving boundaries; the problems that arise in modeling blood flow through arteries. Depending on the characteristics of the blood flow and arteries, several formulations can be derived. Regardless of the formulation categories, since FSI problems are dealing with the strong coupling between fluid and solid behavior, solving such problems requires numerical methods. In case of nonlinearity, the least-squares finite element formulation has the capability to solve these problems using a single variational approach. Fluid flow in our model, is derived by two-dimensional incompressible Navier-Stokes equations, while we take the advantage of axisymmetric flow for building the linear elastic model. The structure and fluid medium are fully coupled by means of describing fluid pressure as a function of artery cross-sectional area which makes sense in explaining the blood flow through arteries problem.

4.2 Mathematical Models of Blood Flow

4.2.1 Blood Flow

In order to study the blood flow, several models has been used based on different types of simplifications. The most complicated one belongs to the 3D fluid-structure interaction which requires the accurate information about the vessel geometry and material properties of several branches. The blood flow mathematical formulation is too complex and, therefore, a numerical model is needed for solving the governing equations. In analyzing blood flow, an Eulerian description of blood fluid motion will be used in the field equations (fluids elements are assumed to be fixed in space). The following types of flow can be considered in analyzing the blood flow:

1. Laminar or turbulent

   The blood flow is generally laminar except under the disease condition and in large arteries at branch points which is turbulent. When we are dealing with laminar flow, i.e. the Reynolds number is very low, the inertial terms is negligible, therefore, we do not have any nonlinear terms. The low Reynolds number corresponds to high velocity or low viscosity flow.

2. Newtonian or non-Newtonian

   In analyzing the blood flow, it is important to have a good understanding of blood viscosity. The main factors that affect blood viscosity are plasma viscosity, volume fraction of particles which red blood cells (RBCs) are their main constitutive, mechanical properties of RBCs, i.e. their deformability and aggregation, and also temperature. Viscosity of blood, and in general any fluids, decreases with increasing temperature. Among all of the mentioned factors, the volume fraction of RBCs has the most significant affect on blood viscosity.

The flow can obey linear or nonlinear constitutive behavior. In latter case, the viscosity depends on the shear rate and there exist several models formulating this dependency, such as the power-law fluid relation. The point worth mentioning is that blood viscosity strongly depends on the shear rate. The higher the shear rate is, the less viscous the blood becomes. Because of this property of blood, it can be considered as a shear-thinning or pseudoplastic fluid. For this reason, the blood behaves as a Newtonian fluid at high shear rate ($\frac{\partial u}{\partial y}$). At lower shear rate the RBCs aggregate and the viscosity will be increased.

For those categories of blood flows that are classifed into shear-thinning (non-Newtonian) fluids, their behavior can be demonstrated by several theories, e.g. Cassons equation which describes the nonlinear relation between shear stress and strain and it is valid for the shear rates above $1s^{-1}$. Our research here is focused on large vessels and veins whose characteristic dimensions is not comparable with the characteristic size of the blood cells, and, therefore, blood behaves as an isotropic, Newtonian and incompressible fluids. Otherwise it behaves as a non-Newtonian one.

3. Steady or unsteady

   The unsteady blood flow is called the pulsatile blood flow. In this kind of flow, the flow velocity and wall shear stress during the pulse cycle are of great importance. And the most complex part of study goes to the study of branching regions and sharp curvature parts of the vessel. Flow separation, flow recirculation, and low wall shear stress are observed in this kind of flow. Womersley parameter used for unsteady flow ($\alpha = R\sqrt{\frac{\omega\rho}{\mu}}$ with ω being the angular velocity of a given harmonic) is corresponding to Reynolds number for steady flow ($\mathrm{Re} = \frac{\rho u D}{\mu}$). For $\alpha < 10$ the flow is assumed to be steady. The term

viscous resistance is introduced through Poiseuille law which is valid for fully developed (there is no variation in the direction of the flow for velocity, $\frac{\partial u}{\partial x} = 0$) and steady flow ($\frac{\partial u}{\partial t} = 0$), keeping in mind that for most of the arteries, the flow is considered to be laminar.

4.2.2 Arterial Walls

In order to simulate the blood flow in arteries, we need to model the arterial wall which seems to be sophisticated. Arterial walls are composed of anisotropic and heterogeneous layers with completely different biomechanical properties. Tunica Intima, Tunica Media, and Tunica Adventitia are the main three layers of the arteries. However, there are several methods which describe them with average-value properties so that arterial walls can be considered as a homogeneous layer with nonlinear elastic behavior. So we need to make some assumptions in order to make the calculations possible. One of the simple assumptions is converting the 3D problem to 2D problem by eliminating the variation in the third dimension. In other words, we can consider the material with small deformation and small deformation gradient as linearly elastic material. Since the thickness of the blood vessel wall is negligible in comparison to two other dimensions, we can treat it as a 2D problem. Furthermore we can reduce the mentioned model to a 1D model considering the axial symmetry nature of the applied loading of the blood flow to the vessel walls. The other useful assumption is to use the cylindrical shell models due to cylindrical geometry of an artery section. And if we have the possibility to neglect the bending rigidity of the arteries, we can use the membrane models instead.

According to the above discussions, it is a good idea to investigate the blood flow characteristics in large arteries with simple geometry. Therefore, we are dealing with the unsteady laminar flow of a Newtonian incompressible viscous fluid through a

longitudinally tethered vessel without any branch. The most important assumption in our study of blood flow in arteries is that there is no flow through any solid surface, i.e. the impermeability property of the vessel should be held.

4.3 Theoretical Formulations

One dimensional models provide a simplified description of the fluid flow in arteries and its interaction with the vessel wall displacement. Although being inappropriate to provide details on the flow field (such as recirculation or oscillating shear stresses), they can however effectively describe the propagation phenomena due to the wall compliance. The mass conservation and the linear momentum conservation equation are the equations governing the blood flow. Considering the flow to be laminar, the only velocity exist in the axial direction, i.e. the flow is such that there are some laminates moving parallel to each other.

The following assumptions have been made during our investigations:

- The arterial curvature is neglected, i.e. it is assumed to be a straight tube with circular cross-sectional area.
- Wall inertia and wall viscosity are assumed to be small, so we consider thin, homogeneous, incompressible and elastic arterial walls.
- The structural arterial properties are constant over a cross-sectional area.
- Since we consider reasonably large arteries, the blood is considered as an incompressible and Newtonian fluid, i.e. the density ρ and viscosity μ are constant variables.
- The flow is considered to be laminar, i.e. the Reynolds number is lower than 2000 in arteries.

- The effect of red blood cells are negligible in large arteries unless the shear rate is very low.
- The no-slip boundary condition near the arterial wall is assumed.

In order to predict the blood flow and corresponding pressure profile in large arteries, we start with the continuity equation and linear momentum equation which ensure the conservation of mass and momentum, respectively.

4.3.1 Continuity Equation

The continuity equation for the incompressible flow takes the following form [52]

$$\nabla.\mathbf{u} = 0 \tag{4.1}$$

where $\mathbf{u} = \mathbf{u}(u_r, u_\theta, u_x)$ is the velocity vector with the component in radial, tangential and axial direction, respectively. An appropriate model that can describe blood flow in large vessels is achieved by assuming the vessel is an elastic cylindrical structure. So the above-mentioned equation is valid on a cylindrical domain which changes in time because of the flow induced wall movement. Therefore, for cylindrical coordinate, Eq. (4.1) can be expressed as

$$\frac{1}{r}\frac{\partial}{\partial r}(ru_r) + \frac{1}{r}\frac{\partial u_\theta}{\partial \theta} + \frac{\partial u_x}{\partial x} = 0 \tag{4.2}$$

Considering the blood flow in arteries being an axisymmetric flow, we have no dependency on θ. Therefore, one can write Eq. (4.2) as

$$\frac{1}{r}\frac{\partial}{\partial r}(ru_r) + \frac{\partial u_x}{\partial x} = 0 \tag{4.3}$$

where $u_r = u_r(r,x,t)$ and $u_x = u_x(r,x,t)$. Assuming that the vessel undergoes radial motion only, i.e. the vessels are longitudinally tethered (Fig. 4.1), we have $R = R(x,t)$ and, hence, the vessel cross-sectional area is $A = A(x,t) = \pi R^2(x,t)$.

Integrating Eq. (4.3) over the cross-sectional area and taking the advantage of

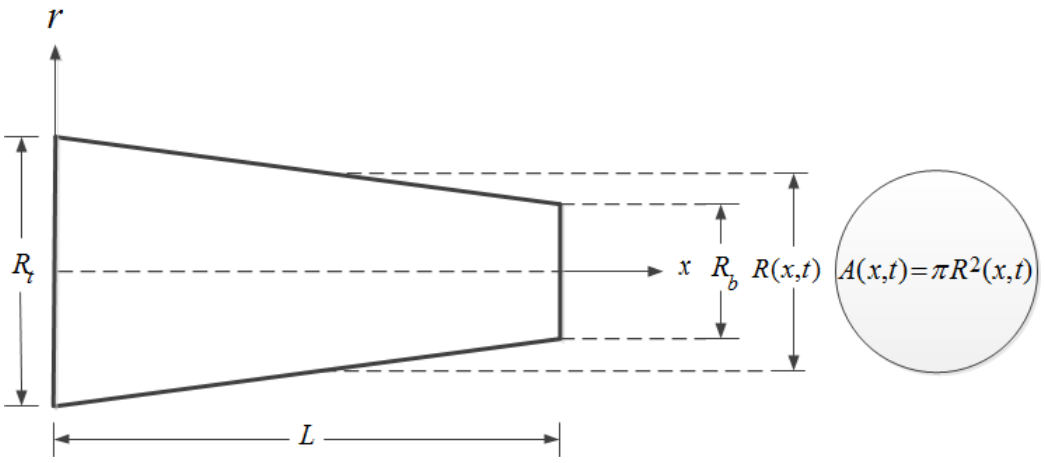

Figure 4.1: Geometry of longitudinally tethered blood vessel

Leibniz integral rule, we have

$$\begin{aligned} &2\pi \int_0^R \left[\frac{1}{r}\frac{\partial}{\partial r}(ru_r) + \frac{\partial u_x}{\partial x}\right] r dr \\ &= 2\pi \frac{\partial}{\partial x}\int_0^R u_x r dr - 2\pi \frac{\partial R}{\partial x}[ru_x]_R + 2\pi [ru_r]_R = 0 \end{aligned} \tag{4.4}$$

where $[u_x]_R = 0$ due to no-slip boundary condition. Moreover, since the blood vessel undergoes radial motion only, i.e. $[u_r]_R = \frac{\partial R}{\partial t}$, the last term of Eq. (4.4) takes the following form

$$2\pi [ru_r]_R = 2\pi R \frac{\partial R}{\partial t} = \frac{\partial A}{\partial t} \tag{4.5}$$

Keeping in mind that the volume flow rate is defined as volume change per time, we have

$$Q = 2\pi \int_0^R u_x r dr \tag{4.6}$$

So the continuity equation for the one-dimensional flow at hand will be described as

$$\frac{\partial Q}{\partial x} + \frac{\partial A}{\partial t} = 0 \tag{4.7}$$

4.3.2 Linear Momentum Equation

The linear momentum equation can be defined as

$$\frac{\partial \mathbf{u}}{\partial t} + (\mathbf{u}.\nabla)\,\mathbf{u} + \frac{1}{\rho}\nabla.\mathbf{P} = \frac{\mu}{\rho}\nabla^2\mathbf{u} \tag{4.8}$$

where for the axisymmetric one-dimesional flow, the linear momentum equation consists of only one equation in the direction of flow, which takes the form

$$\rho\frac{\partial u_x}{\partial t} + \rho u_x\frac{\partial u_x}{\partial x} + \rho u_r\frac{\partial u_x}{\partial r} + \frac{\partial P}{\partial x} = \mu\left[\frac{\partial^2 u_x}{\partial x^2} + \frac{1}{r}\frac{\partial}{\partial r}\left(r\frac{\partial u_x}{\partial r}\right)\right] \tag{4.9}$$

where ρ and μ are fluid density and viscosity, respectively. Since blood vessel is generally long compared to its radius, the longitudinal viscous term in small in comparison with the radial viscous term, and therefore, we neglect the first term in the right side of Eq. (4.9). Also for modeling the blood flow through large arteries, forces acting on the fluid are due to the pressure and viscosity. Integrating Eq. (4.9)

over the cross-sectional area results in:

$$2\pi\rho\int_{o}^{R}\frac{\partial u_x}{\partial t}rdr+2\pi\rho\int_{0}^{R}\left(u_x\frac{\partial u_x}{\partial x}+u_r\frac{\partial u_x}{\partial r}\right)rdr+A\frac{\partial P}{\partial x}=2\pi\mu\left[r\frac{\partial u_x}{\partial r}\right]_R \tag{4.10}$$

using the same procedure as for the continuity equation, we have

$$\begin{aligned}&\frac{\partial}{\partial t}\left(2\pi\int_{0}^{R}u_x rdr\right)-2\pi\frac{\partial R}{\partial t}[ru_x]_R\\&=2\pi\int_{0}^{R}\left(ru_x\frac{\partial u_x}{\partial x}-u_x\frac{\partial\left(ru_r\right)}{\partial r}\right)dr+\frac{A}{\rho}\frac{\partial P}{\partial x}=2\pi\frac{\mu}{\rho}\left[r\frac{\partial u_x}{\partial r}\right]_R\end{aligned} \tag{4.11}$$

Since we can consider flat velocity profile for the blood flow in large artery region except for the boundary layer where the velocity profile should satisfy the no-slip condition at the arterial walls, the one-dimensional linear moment equation can be described as:

$$\frac{\partial Q}{\partial t}+\frac{\partial}{\partial x}\left(\frac{Q^2}{A}\right)+\frac{A}{\rho}\frac{\partial P}{\partial x}=-\frac{2\pi\mu R}{\delta}\frac{Q}{A} \tag{4.12}$$

where δ is the overall thickness of the boundary layer. Lighthill [53] estimated the value of δ to be 0.1 cm for blood flow in large arteries. Having continuity and linear momentum conservation equation, there exist a set of two equations and three unknowns; Q, A, and P. Therefore, the third equation needed to solve for these three unknown is the relation between cross-sectional area and pressure, i.e. the FSI issue.

4.3.3 Pressure-Area Equation

So far, we have two differential partial equations which are presented as Eqs. (4.7) and (4.12) with three primary variables Q, A, and P. Therefore, one more equation is required so that the system of equations can be solved. Since the obtained equations

are the equations governing the fluid domain, it seems that third equation may relate cross-sectional area with pressure, therefore, it may describe the FSI nature of the problem at hand.

Vessel walls are made of anisotropic and viscoelastic material and are not perfectly cylindrical. Therefore, the pressure is not only the function of area, but also the function of its derivative. However, since the effect of area derivative is negligible in comparison to area, we ignored the functionality of pressure to area derivatives. There exists several pressure-area relations used in the literature. Among all of proposed model; i.e. the linear elastic, nonlinear elastic, viscoelastic and so on, the viscoelastic models are the most complete and most complicated as well. If we ignore the effect of wall viscosity, which is a reasonable assumption, we can use nonlinear elastic relation. So the model proposed by Olufsen [54] will be considered

$$P = P_0 + \beta \left(\sqrt{A} - \sqrt{A_0} \right) \tag{4.13}$$

where P_0 is the pressure exerting form surrounding tissues, and A_0 is the cross-sectional area when the only pressure is P_0. In Eq. (4.13), β is the parameter describes the material properties of the elastic blood vessel.

$$\beta = \frac{\sqrt{\pi} h E}{A_0 \left(1 - \nu^2\right)} \tag{4.14}$$

In this equation, h is the vessel thickness, E is the Youngs modulus of elasticity, and ν is the Poissons ratio which is considered to be 0.5 since the vessel walls are assumed to be incompressible. This set of three nonlinear equations and three unknowns along with appropriate boundary and initial conditions can be solved to yield values of cross-sectional area, volume flow rate, and pressure as functions of time and arterial

position x.

4.3.4 Least-Squares Formulations

The least-squares approach has been a useful method for the approximate solution of first-order systems of partial differential equations. A least-squares functional can be set up by summing up the squares of the residuals of all partial differential equations which can be stated as

$$\mathcal{J}(Q, A, P) = \|E_1\|_0^2 + \|E_2\|_0^2 + \|E_3\|_0^2 \tag{4.15}$$

which in the integral form can be written as follows

$$\mathcal{J}(Q, A, P) = \int_\Omega |E_1|^2 d\Omega + \int_\Omega |E_2|^2 d\Omega + \int_\Omega |E_3|^2 d\Omega \tag{4.16}$$

Substituting E_1, E_2 and E_3 form Eqs. (4.7), (4.12) and (4.13) into Eqs. (4.15) and (4.16), we have

$$\begin{aligned}
\mathcal{J}(Q, A, P) &= \left\| \frac{\partial Q}{\partial x} + \frac{\partial A}{\partial t} \right\|_0^2 + \left\| \frac{\partial Q}{\partial t} + \frac{\partial}{\partial x}\left(\frac{Q^2}{A}\right) + \frac{A}{\rho}\frac{\partial P}{\partial x} + \frac{2\sqrt{\pi}\mu}{\delta}\frac{Q}{\sqrt{A}} \right\|_0^2 \\
&\quad + \left\| P - P_0 - \beta\left(\sqrt{A} - \sqrt{A_0}\right) \right\|_0^2 \\
&= \int_\Omega \left| \frac{\partial Q}{\partial x} + \frac{\partial A}{\partial t} \right|^2 d\Omega + \int_\Omega \left| \frac{\partial Q}{\partial t} + \frac{\partial}{\partial x}\left(\frac{Q^2}{A}\right) + \frac{A}{\rho}\frac{\partial P}{\partial x} + \frac{2\sqrt{\pi}\mu}{\delta}\frac{Q}{\sqrt{A}} \right|^2 d\Omega \\
&\quad + \int_\Omega \left| P - P_0 - \beta\left(\sqrt{A} - \sqrt{A_0}\right) \right|^2 d\Omega
\end{aligned} \tag{4.17}$$

Keeping in mind that the above-mentioned functional includes the products of at most first derivatives. Therefore, the least-squares principle can be presented as:

Find (Q, A, P) which minimizes $\mathcal{J}$ over an appropriate class of $\mathcal{V}$. Here the

function class $\mathcal{V}$ consists of $H^1(\Omega)$ flux rate, cross-sectional area and pressure field, constrained by boundary conditions. Minimization of $\mathcal{J}$ requires the following equation in the integral form

$$\delta\mathcal{J} = \frac{\partial\mathcal{J}}{\partial\Delta_j} = 2\int_{\Omega}\left(E_i\frac{\partial E_i}{\partial\Delta_j}\right)d\Omega = 2\int_{\Omega}\left(E_i.\delta E_{ij}\right)d\Omega = 0 \tag{4.18}$$

which Δ_j is the solution vector ($j = Q, P, andA$), E_i are the i^{th} equations, while δE_{ij} are their first variation with respect to the dependent variables. Therefore, we are seeking the solution vector Δ which satisfies Eq. (4.18). With the specification of problem at hand, the first governing equation and its first derivative with respect to three primary variables Q, A, and P are as follows

$$\begin{aligned}
&E_1 : \frac{\partial Q}{\partial x} + \frac{\partial A}{\partial t} = 0\\
&\delta E_{1Q} : \frac{\partial \delta Q}{\partial x}\\
&\delta E_{1A} : \frac{\partial \delta A}{\partial t}\\
&\delta E_{1P} : 0
\end{aligned}$$

The second governing equation and its first derivative with respect to three primary

variables Q, A, and P can be describes as

$$
\begin{aligned}
E_2 &: \frac{\partial Q}{\partial t} + \frac{\partial}{\partial x}\left(\frac{Q^2}{A}\right) + \frac{A}{\rho}\frac{\partial P}{\partial x} + \frac{2\sqrt{\pi}\mu}{\delta}\frac{Q}{\sqrt{A}} = 0 \\
&= \frac{\partial Q}{\partial t} + \frac{2Q}{A}\frac{\partial Q}{\partial x} - \frac{Q^2}{A^2}\frac{\partial A}{\partial x} + \frac{A}{\rho}\frac{\partial P}{\partial x} + \frac{2\sqrt{\pi}\mu}{\delta}\frac{Q}{\sqrt{A}} = 0 \\
\delta E_{2Q} &: \frac{\partial \delta Q}{\partial t} + \frac{2}{A}\frac{\partial Q}{\partial x}\delta Q + \frac{2Q}{A}\frac{\partial \delta Q}{\partial x} - \frac{2Q}{A^2}\frac{\partial A}{\partial x}\delta Q + \frac{2\sqrt{\pi}\mu}{\delta\sqrt{A}}\delta Q \\
\delta E_{2A} &: -\frac{2Q}{A^2}\frac{\partial Q}{\partial x}\delta A + \frac{2Q^2}{A^3}\frac{\partial A}{\partial x}\delta A - \frac{Q^2}{A^2}\frac{\partial \delta A}{\partial x} \\
&\qquad + \frac{1}{\rho}\frac{\partial P}{\partial x}\delta A - \frac{2\sqrt{\pi}\mu Q}{A\sqrt{A}}\delta A \\
\delta E_{2P} &: \frac{A}{\rho}\frac{\partial \delta P}{\partial x}
\end{aligned}
$$

And finally, the third governing equation and its first derivative with respect to three primary variables Q, A, and P are

$$
\begin{aligned}
E_3 &: P - P_0 - \beta\left(\sqrt{A} - \sqrt{A_0}\right) = 0 \\
\delta E_{3Q} &: 0 \\
\delta E_{3A} &: \frac{\beta \delta A}{2\sqrt{A}} \\
\delta E_{3P} &: \delta P
\end{aligned}
$$

As the above equations indicated, $\delta\mathcal{J}$ is a nonlinear function of Δ_j which necessitate using iterative method in order to solve the least-squares formulation.

4.4 Finite Element Formulations

Since we can treat variable t as a single variable in the finite element approximation, we assume the following interpolating of the flow rate Q, cross-sectional area

A, and pressure P over each element

$$
\begin{aligned}
Q(x,t) &= \sum_{j=1}^{n} Q_j \psi_j^{(1)}(x,t) \\
A(x,t) &= \sum_{j=1}^{n} A_j \psi_j^{(2)}(x,t) \\
P(x,t) &= \sum_{j=1}^{n} P_j \psi_j^{(3)}(x,t)
\end{aligned} \tag{4.19}
$$

where $\psi_j^{(\alpha)}(\alpha = 1,2,3)$ are Lagrange family interpolation functions, while Q_j, A_j, and P_j are the nodal values. In other word, we consider t as the second coordinate. This assumption converts the time-dependent 1D problem to the steady state 2D problem. Therefore, for the present study, we utilize two dimensional linear rectangular elements in x and t directions. Generally, it is not necessary to use the same degree of interpolation for Q, A, and P, however, we consider the same interpolation function for all of them. Substituting the approximations (4.19) in the obtained least-squares formulations Eq. (4.18), we have the following finite element model in the matrix form

$$
\begin{bmatrix}
\mathbf{K}^{11} & \mathbf{K}^{12} & \mathbf{K}^{13} \\
\mathbf{K}^{21} & \mathbf{K}^{22} & \mathbf{K}^{23} \\
\mathbf{K}^{31} & \mathbf{K}^{32} & \mathbf{K}^{33}
\end{bmatrix}
\begin{Bmatrix}
\mathbf{Q} \\ \mathbf{A} \\ \mathbf{P}
\end{Bmatrix}
=
\begin{Bmatrix}
\mathbf{F}^1 \\ \mathbf{F}^2 \\ \mathbf{F}^3
\end{Bmatrix} \tag{4.20}
$$

where the nonzero components of the stiffness matrices $\mathbf{K}^{\alpha\beta}$ and force vectors $\mathbf{F}^{\alpha}$ defined as

$$
\begin{aligned}
K_{ij}^{11} &= \int_{\Omega^e} \left[\frac{\partial \psi_i}{\partial x}\frac{\partial \psi_j}{\partial x} + \left(\frac{\partial \psi_i}{\partial t} + \frac{2}{A}\frac{\partial Q}{\partial x}\psi_i + \frac{2Q}{A}\frac{\partial \psi_i}{\partial x} - \frac{2Q}{A^2}\frac{\partial A}{\partial x}\psi_i + \frac{\alpha}{\sqrt{A}}\psi_i \right) \right. \\
&\quad \left. \left(\frac{\partial \psi_j}{\partial t} + \frac{2Q}{A}\frac{\partial \psi_j}{\partial x} + \frac{\alpha}{\sqrt{A}}\psi_j \right) \right] dxdt \\
K_{ij}^{12} &= \int_{\Omega^e} \left[\frac{\partial \psi_i}{\partial x}\frac{\partial \psi_j}{\partial t} + \left(\frac{\partial \psi_i}{\partial t} + \frac{2}{A}\frac{\partial Q}{\partial x}\psi_i + \frac{2Q}{A}\frac{\partial \psi_i}{\partial x} - \frac{2Q}{A^2}\frac{\partial A}{\partial x}\psi_i + \frac{\alpha}{\sqrt{A}}\psi_i \right) \right. \\
&\quad \left. \left(-\frac{Q^2}{A^2}\frac{\partial \psi_j}{\partial x} \right) \right] dxdt \\
K_{ij}^{13} &= \int_{\Omega^e} \left(\frac{\partial \psi_i}{\partial t} + \frac{2}{A}\frac{\partial Q}{\partial x}\psi_i + \frac{2Q}{A}\frac{\partial \psi_i}{\partial x} - \frac{2Q}{A^2}\frac{\partial A}{\partial x}\psi_i + \frac{\alpha}{\sqrt{A}}\psi_i \right) \left(\frac{A}{\rho}\frac{\partial \psi_j}{\partial x} \right) dxdt \\
K_{ij}^{21} &= \int_{\Omega^e} \left[\frac{\partial \psi_i}{\partial t}\frac{\partial \psi_j}{\partial x} + \left(-\frac{2Q}{A^2}\frac{\partial Q}{\partial x}\psi_i + \frac{2Q^2}{A^3}\frac{\partial A}{\partial x}\psi_i - \frac{Q^2}{A^2}\frac{\partial \psi_i}{\partial x} + \frac{1}{\rho}\frac{\partial P}{\partial x}\psi_i - \frac{\alpha Q}{2A\sqrt{A}}\psi_i \right) \right. \\
&\quad \left. \left(\frac{\partial \psi_j}{\partial t} + \frac{2Q}{A}\frac{\partial \psi_j}{\partial x} + \frac{\alpha}{\sqrt{A}}\psi_j \right) \right] dxdt \\
K_{ij}^{22} &= \int_{\Omega^e} \left[\frac{\partial \psi_i}{\partial t}\frac{\partial \psi_j}{\partial t} + \left(-\frac{2Q}{A^2}\frac{\partial Q}{\partial x}\psi_i + \frac{2Q^2}{A^3}\frac{\partial A}{\partial x}\psi_i - \frac{Q^2}{A^2}\frac{\partial \psi_i}{\partial x} + \frac{1}{\rho}\frac{\partial P}{\partial x}\psi_i - \frac{\alpha Q}{2A\sqrt{A}}\psi_i \right) \right. \\
&\quad \left. \left(-\frac{Q^2}{A^2}\frac{\partial \psi_j}{\partial x} \right) \right] dxdt \\
K_{ij}^{23} &= \int_{\Omega^e} \left[\left(-\frac{2Q}{A^2}\frac{\partial Q}{\partial x}\psi_i + \frac{2Q^2}{A^3}\frac{\partial A}{\partial x}\psi_i - \frac{Q^2}{A^2}\frac{\partial \psi_i}{\partial x} + \frac{1}{\rho}\frac{\partial P}{\partial x}\psi_i - \frac{\alpha Q}{2A\sqrt{A}}\psi_i \right) \left(\frac{A}{\rho}\frac{\partial \psi_j}{\partial x} \right) \right. \\
&\quad \left. -\frac{\beta}{\sqrt{A}}\psi_i\psi_j \right] dxdt \\
K_{ij}^{31} &= \int_{\Omega^e} \left(\frac{A}{\rho}\frac{\partial \psi_i}{\partial x} \right) \left(\frac{\partial \psi_j}{\partial t} + \frac{2Q}{A}\frac{\partial \psi_j}{\partial x} + \frac{\alpha}{\sqrt{A}}\psi_j \right) dxdt \\
K_{ij}^{32} &= \int_{\Omega^e} \frac{-Q^2}{A\rho}\frac{\partial \psi_i}{\partial x}\frac{\partial \psi_j}{\partial x} dxdt \\
K_{ij}^{33} &= \int_{\Omega^e} \left(\frac{A^2}{\rho^2}\frac{\partial \psi_i}{\partial x}\frac{\partial \psi_j}{\partial x} + \psi_i\psi_j \right) dxdt
\end{aligned}
\tag{4.21}
$$

$$F_i^2 = \int_{\Omega^e} -\frac{\beta}{2\sqrt{A}} \left[P_0 + \beta\left(\sqrt{A} - \sqrt{A_0}\right)\right] \psi_i dxdt$$
$$F_i^3 = \int_{\Omega^e} \left[P_0 + \beta\left(\sqrt{A} - \sqrt{A_0}\right)\right] \psi_i dxdt \tag{4.22}$$

where α is defined as $\frac{2\sqrt{\pi}\mu}{\delta}$. Since the above matrices and vectors are nonlinear functions of primary variables Q, A, P, and their first derivatives, it requires an initial guess in ordered to be solved numerically.

4.5 Numerical Results

The following parameters are used in the 1-D blood flow problem:

$E = 1$ MPa, $\quad \nu = 0.5$, $\quad \rho = 1056$ kg/m^3, $\quad \mu = 3.5 \times 10^{-3}$ Pa.s

$R_t = 0.5$ cm, $\quad R_b = 0.7$ cm, $\quad \delta = 0.05$ cm, $\quad L = 20$ cm, $\quad h = 0.1$ cm

$P_0 = 0.012$ MPa

Moreover, for numerical simulation, we need appropriate boundary conditions. One of the boundary conditions is flow rate Q at the inlet of the blood vessel. This data can be specified using a magnetic resonance measurement of the flow in arteries. Since our main concern here is to develop a formulation, we extracted this data from one of the studies in the literature ([54]). Figure 4.2 represents the initial flow rate at the inlet of artery. Other boundary condition can be considered for the cross-sectional area A. According to Fig. 4.1, we can calculate A at $t = 0$ using the following equation which can be obtained easily based on the geometry.

$$A = \left(\frac{L - x}{L}\right) A_t + \left(\frac{x}{L}\right) A_b \tag{4.23}$$

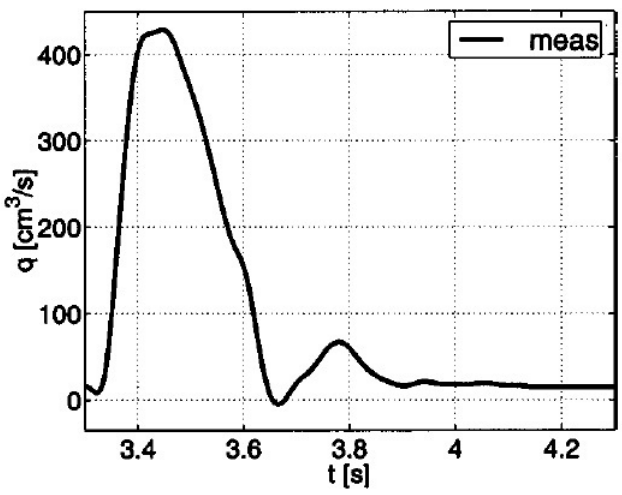

Figure 4.2: The initial flow rate at the inlet of artery (Extracted from [54])

And finally the prescribed boundary condition for P at $t = 0$ can be obtained based on Eq. (4.13) by setting $A = A_0$, i.e. $P = P_0$ at $t = 0$.

Solving obtained finite element model of Eq. (4.20) for the prescribed boundary conditions, Figs. 4.3 and 4.4 represent the variation of cross-sectional area and pressure along the blood vessel at $t = 1.5\ s$, respectively. It is evident that there exists pressure drop through the arteries. Similarly, Figs. 4.5 and 4.6 indicate the result for the variation of cross-sectional area and pressure at a location of $x = L/2$ for a time interval of 1 second, respectively. It can be observed that there is an increase in pressure as the flow rate increases, and for the case where the flow rate is decreased, we can see the pressure drop. Comparing the obtained results with the results available in literature validates the efficiency of the proposed finite element model.

Figure 4.7 shows the linear relation between pressure and cross-sectional area at $x = \frac{L}{2}$. It indicates that although we considered a nonlinear elastic model as a

constitutive equation describing P as a function of A, variation of P with respect to A at a specific location in arteries is linear. This linearity can be interpreted due to the small variation of cross-sectional area at certain location. However, the assumption of linearity is not valid along the artery, as Fig. 4.8 does not represent linear relation. The obtained nonlinearity is due to the fact that the variables in the formulation which affect the dependency.

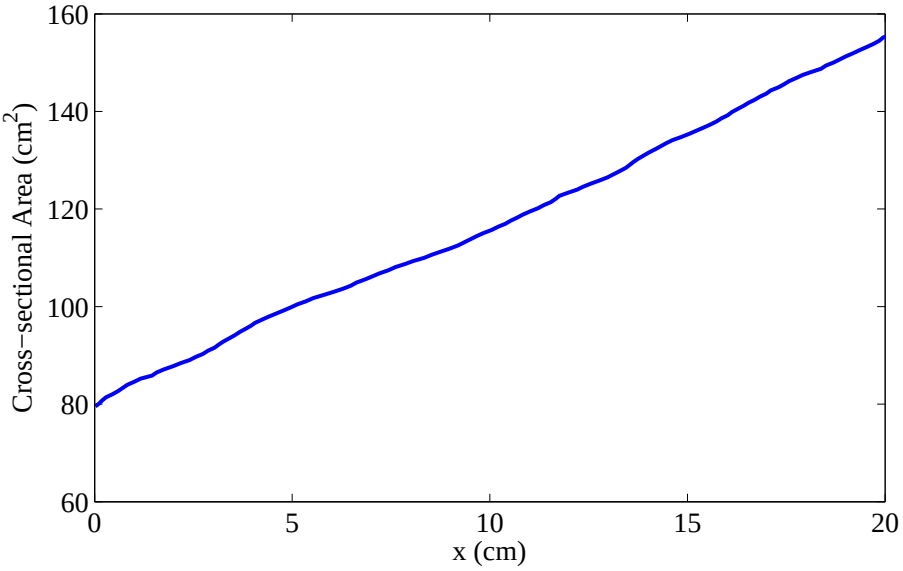

Figure 4.3: The cross-sectional area along the artery at $t = 1.5\ s$

4.6 Concluding Remarks

A finite element model of the fluid-structure interaction of blood flow through large arteries was developed. The problem contains large nonlinearity that makes it quite impossible to solve it analytically. Since the obtained system of equations contains primary variables and their first derivatives, a least-squares formulation is adopted to construct the finite element model. Several assumptions were made in

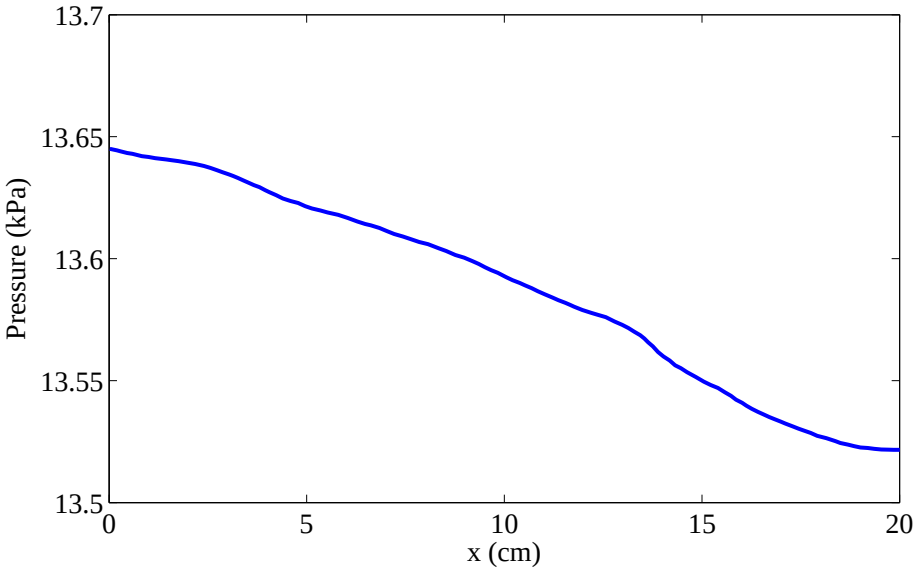

Figure 4.4: The pressure along the artery at $t = 1.5\ s$

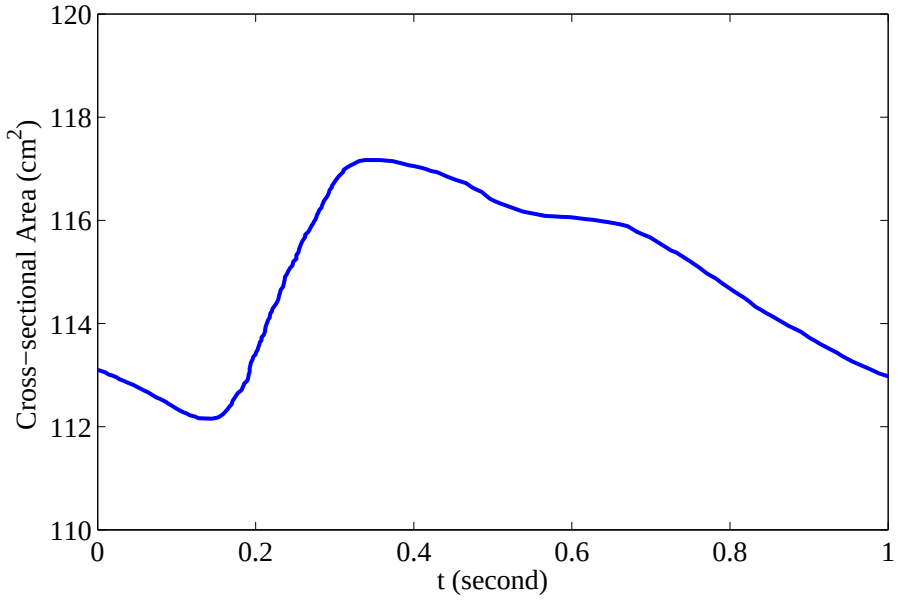

Figure 4.5: The artery cross-sectional area at $x = \frac{L}{2}$ versus time

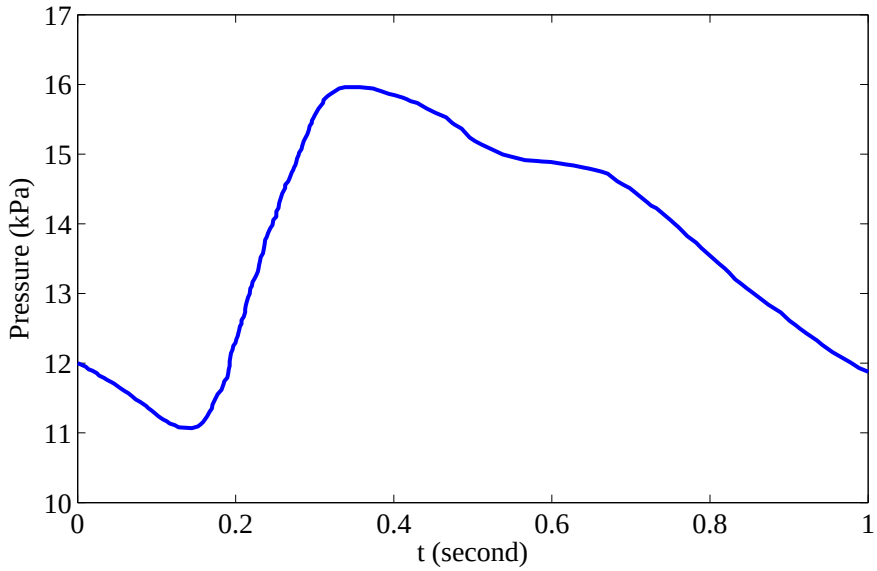

Figure 4.6: The artery pressure at $x = \frac{L}{2}$ versus time

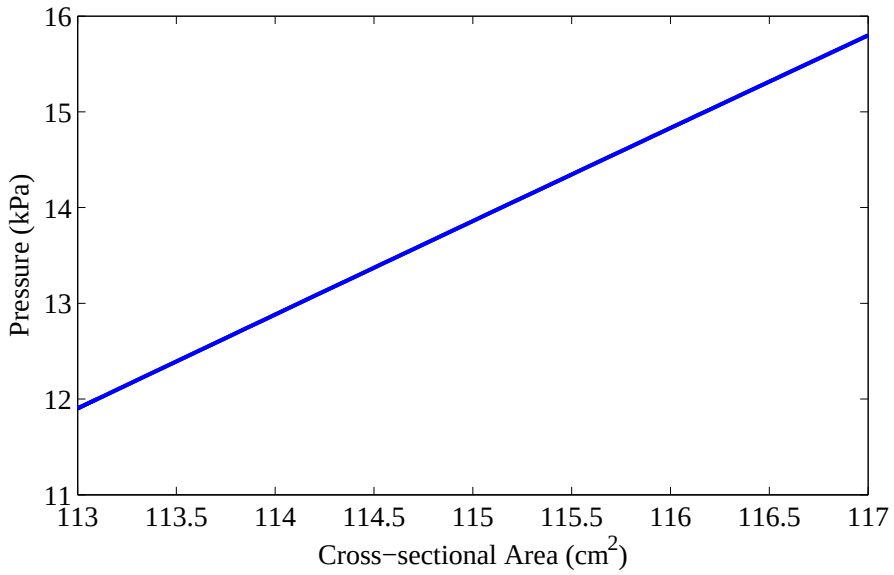

Figure 4.7: Variation of artery pressure versus cross-sectional area at $x = \frac{L}{2}$

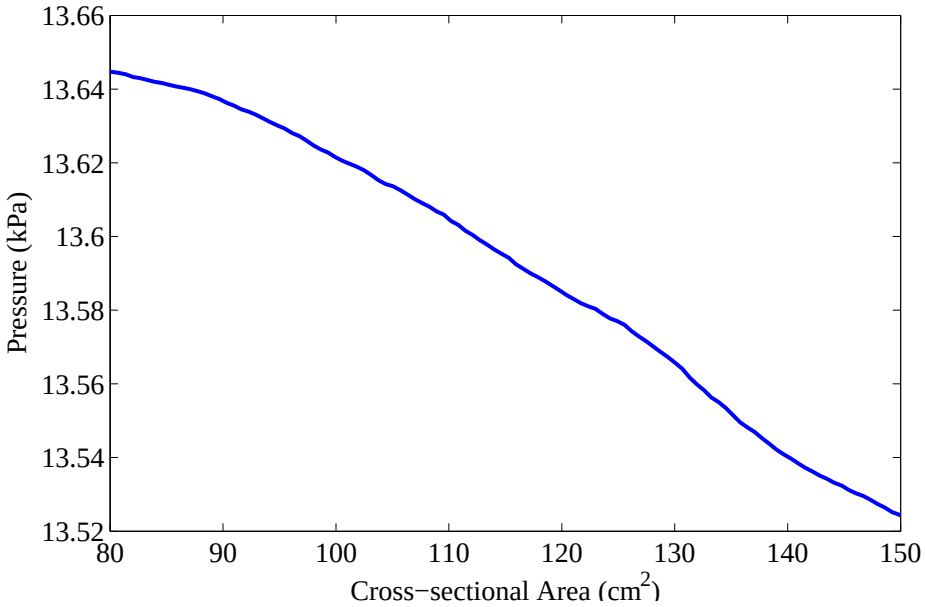

Figure 4.8: Variation of artery pressure through the artery versus cross-sectional area at $t = 1.5\ s$

order to simplify the problem. Even though blood flow through large arteries is treated as a 1D problem, a good insight of the blood flow behavior is obtained. Such understanding of the blood flow characteristics by considering FSI can be used to improve medical care.

5. CONCLUSIONS

This dissertation proposed finite element formulations to study the dynamics of Fluid-Structure Interaction (FSI) systems with applications to a wide range of engineering and science problems including blood flow through large arteries.

In Section 2, we developed a finite element model characterizing the free vibration of elastic beams and plates in the presence of an inviscid fluid medium. We introduced an "added mass" phenomena in our formulations in order to investigate the effect of the fluid pressure on the natural frequencies and modeshapes of the solid structure. Through numerical simulations, we studied the effect of various parameters, such as fluid density and structure thickness, on the structure's modal response. In order to validate our method, we used several theories in the literature for structural domain. In our analysis throughout this section, we assumed small deflections and rotations. The numerical results indicate that the presence of fluid has significant effect on the dynamic behavior of the structure. Generally, FSI decreases the corresponding natural frequencies. For the beam problems, EBT and RBT converged to final values with fewer number of elements rather than TBT, while for the plate structures, CPT and RSDT showed similar trend compared to FSDT. Furthermore, for the thin structure limit, all of the theories are in good agreement with each other, however, for the thick structure limit, EBT and CPT, as expected, converge to different final values because they do not take the shearing effect into the account. Finally, by increasing the length-to-height ratio, geometrically translated to making the structure thinner, the effect of the fluid medium on the free vibration becomes more considerable.

In Section 3, we extended the formulation developed in Section 2 for the plate

structures to a nonlinear case, by assuming small deflections and moderate rotations for the structural domain, to study the transient response of the structure. As a result, our finite element formulation embraces nonlinear terms which necessitates the linearization of the equations through an iteration method. In our numerical examples, we used the Newtonian iteration method calculating the tangent matrices and residual vectors. Considering all the plate theories, namely CPT, FSDT, and RSDT, we found that the FSI affects the transverse deflection of the plate. Furthermore, CPT and RSDT converged to the final solution with fewer number of elements compared to FSDT. For the thin plate limit, all theories agree with each other, but for the thick plate limit, CPT, as anticipated, does not converge to the final solution as it does not consider the shearing effect. Similar to the free vibration case, making the structure thinner, the fluid medium effect on the transverse deflection of the structure is proved to be more significant.

Eventually, in Section 4, a finite element formulation was presented for solving an unsteady FSI problem involving moving boundaries which has important applications to the modeling of blood flow through large arteries. The governing equations for the blood flow domain are the well-known Navier-Stokes equations including nonlinear terms recommending the use of iteration methods for linearization purposes. Since the obtained equations have only first derivative terms, a least-squares approach is employed. Our numerical simulations show consistency to the results available in the literature. We made a set of reasonable assumptions to simplify the governing equations, for instance, considering the blood flow as a one-dimensional fluid flow. However, our results revealed a deep insight into the blood flow behavior even under such assumptions. The proposed approach can be readily extended to higher dimensional geometries.

REFERENCES

[1] R. Shabani, H. Hatami, F.G. Golzar, S. Tariverdilo, and G. Rezazadeh, Coupled vibration of a cantilever micro-beam submerged in a bounded incompressible fluid domain. *Acta Mechanica*, **224**(4): pp. 841–850, 2013.

[2] A.T. Jones, Vibration of beams immersed in a liquid. *Experimental Mechanics*, **10**(2): pp. 84–88, 1970.

[3] M. Aureli, and M. Porfiri, Low frequency and large amplitude oscillations of cantilevers in viscous fluids. *Applied Physics* Letters, **96**(16): pp. 164102, 2010.

[4] D. Sedlar, Z. Lozina, and D. Vucina, Experimental investigation of the added mass of the cantilever beam partially submerged in water. *Tehnicki Vjesnik-Technical Gazette*, **18**(4): pp. 589–594, 2011.

[5] J. Lee, and W.W. Schultz, Eigenvalue analysis of Timoshenko beams and axisymmetric Mindlin plates by the pseudospectral method. *Journal of Sound and Vibration*, **269**(3-5): pp. 609–621, 2004.

[6] H. Lamb, On the vibrations of an elastic plate in contact with water. *Proceedings of the Royal Society of London Series A*, **98**(690): pp. 205–216, 1920.

[7] J.H. Powell, On the frequency of vibration of circular diaphragms. *Proceedings of the Physical Society of London*, **35**: pp. 170–182, 1923.

[8] J. H. Powell and J. H. T. Roberts, On the frequency of vibration of circular diaphragms, *Proceedings of the Physical Society of London*, **35**: pp. 170–182, 1923.

[9] G. Muthuveerappan, N. Ganesan, and M.A. Veluswami, Vibration of a cantilever plate immersed in water. *Journal of Sound and Vibration*, **63**(3): pp. 385–391, 1979.

[10] D.D.K. Lindholm, W.H. Chu, Elastic vibration characteristics of cantilever plates in water. *J. Ship Res.*, **9**(1): pp. 11–22, 1965.

[11] D. Zhou, and Y.K. Cheung, Vibration of vertical rectangular plate in contact with water on one side. *Earthquake Engineering and Structural Dynamics*, **29**(5): pp. 693–710, 2000.

[12] A.L. Facci, and M. Porfiri, Analysis of three-dimensional effects in oscillating cantilevers immersed in viscous fluids. *Journal of Fluids and Structures*, **38**: pp. 205–222, 2013.

[13] K.M. Liew, K.C. Hung, and M.K Lim, Three-dimensional vibration of rectangular plates: effects of thickness and edge constraints, *Journal of Sound and Vibration*, **182**(5): pp. 709–727, 1995.

[14] A.J.M. Ferreira, R.C. Batra, C.M.C.Roque, L.F. Qian, R.M.N. and Jorge, Natural frequencies of functionally graded plates by a meshless method, *Composite Structures*, **75**(1-4): pp 593–600, 2006.

[15] N.J. Robinson, and S.C. Palmer, A modal-analysis of a rectangular plate floating on an incompressible liquid. *Journal of Sound and Vibration*, **142**(3): pp. 453–460, 1990.

[16] Y. Fu, and W.G. Price, Interactions between a partially or totally immersed vibrating cantilever plate and the surrounding fluid, *Journal of Sound and Vibration*, **118**(3): pp 495–513, 1987.

[17] G.C. Volcy, P. Morel, M. Bureau, and K. Tanida, Some studies and researches related to the hydro-elasticity of steel work, *Proceedings of the 122nd Euromech Colloquium on numerical analysis of the dynamics of ship structures*, Ecole Polytechnique, Paris, pp. 403–406, 1979.

[18] Y. Kerboua, A.A. Lakis, M. Thomas, and L. Marcouiller, Vibration analysis of rectangular plates coupled with fluid, *Applied Mathematical Modelling*, **32**(12): pp. 2570–2586, 2008.

[19] M.R. Haddara, and S. Cao, A study of the dynamic response of submerged rectangular flat plates, *Marine Structures*, **9**(10): pp. 913–933, 1996.

[20] Sh. Hosseini-Hashemia, M. Karimia, and H. Roknia, Natural frequencies of rectangular Mindlin plates coupled with stationary fluid, *Applied Mathematical Modelling*, **36**(2): pp. 764–778, 2013.

[21] A. Ergin, and B. Ugurlu, Linear vibration analysis of cantilever plates partially submerged in fluid. *Journal of Fluids and Structures*, **17**(7): pp. 927–939, 2013.

[22] Y. Yadykin, V. Tenetov, and D. Levin, The added mass of a flexible plate oscillating in a fluid, *Journal of Fluids and Structures*, **17**(1): pp. 115-123, 2003.

[23] C.C. Liang, C.C. Liao, Y.S. Tai, and W.H. Lai, The free vibration analysis of submerged cantilever plates. *Ocean Engineering*, **28**(9): pp. 1225–1245, 2001.

[24] M.K. Kwak, Hydroelastic vibration of rectangular plates. *Journal of Applied Mechanics*, **63**: pp. 110–115, 1996.

[25] T. Brugo, R. Panciroli, G. Minak, Study of the dynamic behavior of plates immersed in a fluid. IMEKO TC15 - *Experimental Mechanics* (Proceedings of the 11th Youth Symposium on Experimental Solid Mechanics, Brasov, Romina), pp. 34–39, 2012.

[26] G. Muthuveerappan, N. Ganesan, and M.A. Veluswami, Influence of fluid added mass on the vibration characteristics of plates under various boundary-conditions. *Journal of Sound and Vibration*, **69**(4): pp. 612–615, 1980.

[27] L. Qiu, Modeling and simulation of transient responses of a flexible beam floating in finite depth water under moving loads. *Applied Mathematical Modelling*, **33**(3): pp. 1620–1632, 2009.

[28] L. Qiu, H. Liu, Three-dimensional time-domain analysis of very large oating structures subjected to unsteady external loading. *J. Offshore Mech. Arct. Eng.*, **129**(1): pp. 21–28, 2006.

[29] I. V. Sturova, Unsteady behavior of an elastic beam floating in shallow water under external loading. *Journal of Applied Mechanics and Technical Physics*, **43**(3): pp. 415–423, 2002.

[30] I. V. Sturova, The action of an unsteady external load on a circular elastic plate floating in shallow water, *Applied Mathematics and Mechanics*, **67**(3): pp. 407–416, 2003.

[31] A. A. Korobkin, Unsteady hydroelasticity of floating plates. *Journal of Fluids and Structures*, **14**(7): pp. 971–991, 2000.

[32] M.H. Meylana, I.V. Sturova, Time-dependent motion of a two-dimensional floating elastic plate. *Journal of Fluids and Structures*, **25**(3): pp. 445–460, 2009.

[33] J.Z. Jin, J.T. Xing, Transient dynamic analysis of a floating beamwater interaction system excited by the impact of a landing beam. *Journal of Sound and Vibration*, **303**(1-2): pp. 371–390, 2007.

[34] C.S. Konig, C. Clark, M.R. Mokhtarzadeh-Dehghan, Comparison of fluid in numerical and physical models of a ventricular assist device using low and high-

viscosity fluids. *Journal of Biomedical Engineering*, **116**(1-2): pp. 294–301, 1999.

[35] N. Stergiopulos, D.F. Young, and T.R. Rogge, Computer simulation of arterial flow with applications to arterial and aortic stenoses. *Journal of Biomechanics*, **25**(12): pp. 1477–1488, 1992.

[36] M. Bathe and R.D. Kamm, A fluid-structure interaction finite element analysis of pulsatile blood flow through a compliant stenotic artery. *Journal of Biomechanical Engineering*, **121**: pp. 361–369, 1999.

[37] S.J. Sherwin, L. Formaggia, J. Peiro, and V. Franke, Computational modeling of 1D blood flow with variable mechanical properties and its application to the simulation of wave propagation in the human arterial system. *International Journal for Numerical Methods in Fluids,* **43**(6-7): pp. 673–700, 2003.

[38] J. Wan, B. Steele, S.A. Spicer, S. Strohband, G.R. Feijoo, T.J.R. Hughes, and C.A. Taylor, A one-dimensional finite element method for simulation-based medical planning for cardiovascular disease. *Computer Methods in Biomechanics and Biomedical Engineering*, **5**(3): pp. 195–206, 2002.

[39] I. Larrabide, P.J. Blanco, S.A. Urquiza, E.A. Dari, M.J. Venere, N.A. de Souza e Silva, R.A. Feijo, HeMoLab–Hemodynamics Modelling Laboratory: an application for modelling the human cardiovascular system. *Computers in Biology and Medicine*, **42**(10): pp. 993–1004, 2012.

[40] G. Porenta, D.F. Young, and T.R. Rogge, A finite-element model of blood flow in arteries including taper, branches, and obstructions. *Journal of Biomechanical Engineering*, **108**(2): pp. 161–167, 1986.

[41] F.J.H. Gijsen, F.N. van de Vosse, and J.D. Janssen, The influence of the non-Newtonian properties of blood on the flow in large arteries: steady flow in a

carotid bifurcation model, *Journal of Biomechanics*, **32**(6): pp. 601–608, 1999.

[42] K. Perktold, M. Resch, H. Florian, Pulsatile non-Newtonian flow characteristics in a three-dimensional human carotid bifurcation model. *Journal of Biomedical Engineering (ASME)*, **113**: pp. 464–475, 1991.

[43] K. Perktold, RO. Peter, M. Resch, and G. Langs, Pulsatile non-Newtonian flow in three-dimensional carotid bifurcation models: a numerical study of flow phenomena under different bifurcation angles. *Journal of Biomechanical Engineering (ASME)*, **113**: pp. 507–515, 1991.

[44] A. Avolio, Multi-branched model of the human arterial system. *Medical and Biological Engineering and Computing*, **18**(6): pp. 709–718, 1980.

[45] G.A. Holzapfel , T.C. Gasser, and M. Stadler, A structural model for the viscoelastic behavior of arterial walls: Continuum formulation and finite element analysis. *European Journal of Mechanics-A/Solids*, **21**(3): pp. 441–463, 2002.

[46] C.M Wang, J.N. Reddy, and K.H. Lee, *Shear Deformation Theories of Beams and Plates. Relationships with Classical Solution*, Elsevier, U.K., 2000.

[47] J.N. Reddy, *Energy Principles and Variational Methods in Applied Mechanics*, 2nd ed., John Wiley and Sons, New York, 2002.

[48] J.N. Reddy, *Mechanics of Laminated Composite Plates and Shells*, 2nd ed., CRC Press, Boca Raton, FL, 2004.

[49] J.N. Reddy. *An Introduction to Nonlinear Finite Element Analysis*, 2nd ed., Oxford University Press, UK, 2015.

[50] J.N. Reddy, *An Introduction to Continuum Mechanics*, 2nd ed., Cambridge University Press, New York, 2013.

[51] J.N. Reddy. *An Introduction to the Finite Element Method*, 3rd ed., McGraw-Hill, New York, 2006.

[52] J.N. Reddy, D.K. Gartling, *The Finite Elemet Method in Heat Transfer and Fluid Dynamics*, 3rd ed., CRC Press, FL, 2010.

[53] J. Lighthill, *Mathematical Biofluiddynamics*, 3rd ed., Philadelphia: Society for Industrial and Applied Mathematics, pp. 227–253, 1989.

[54] M.S. Olufsen, C.S. Peskin, W.Y. Kim, E.M. Pedersen, A. Nadim, and J. Larsen, Numerical simulation and experimental validation of blood flow in arteries with structured-tree outflow conditions. *Annals of Biomedical Engineering*, **28**: pp. 1281–1299, 2000.